Alma Mater Studiorum – Università di Bologna

DOTTORATO DI RICERCA IN CHIMICA

Ciclo XXXI

Settore Concorsuale: 03C2

Settore Scientifico Disciplinare: CHIM/04

MICRO-NANOSTRUCTURED POLYMERIC MATERIALS WITH SPECIFIC FUNCTIONALITIES FOR ADVANCED BIOMEDICAL APPLICATIONS

Presentata da: Andrea Merlettini

Coordinatore Dottorato

Prof. Aldo Roda

Supervisore

Prof.ssa Maria Letizia Focarete

Co-supervisori

Dr. Chiara Gualandi

Dr. Luisa Stella Dolci

Esame finale anno 2019

To my mother

Abstract

The possibility to tune material properties up to nanoscale represents a great opportunity for the scientific community to obtain devices capable to fulfill the always new medical demands. During this Thesis project micro and nano-structured polymeric materials have been used in the field of drug delivery and tissue engineering. In particular, three different research lines have been explored, as reported in the following scheme: (i) the use of polymeric fibrous systems as drug and nanoparticles carriers, (ii) design and evaluation of novel shape memory polymers to produce shape memory scaffolds and (iii) development of smart affinity membranes.

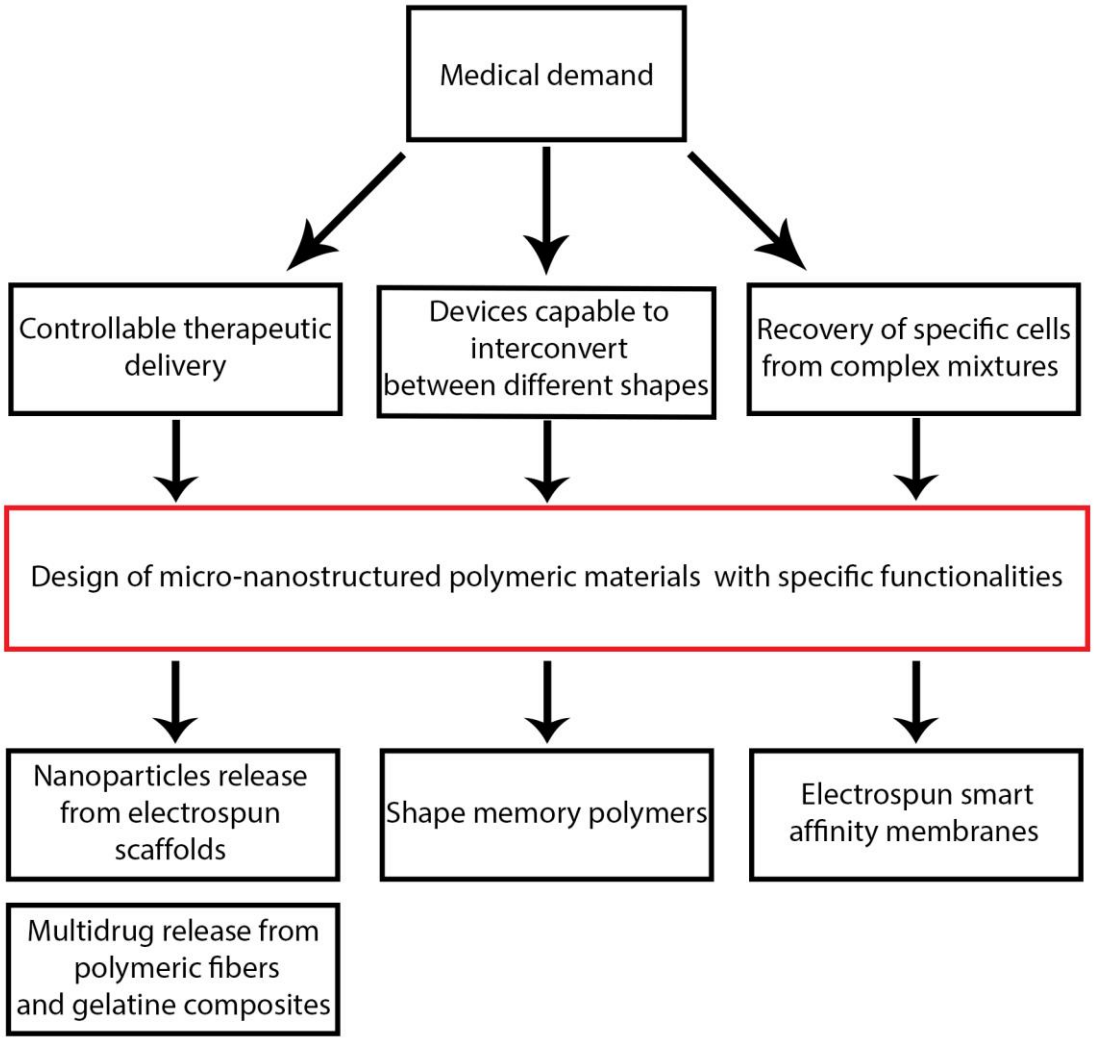

Electrospinning outstanding properties were exploited to obtain polymeric fibrous carriers made of different biodegradable and bioresorbable polymers, such us Poly(lactic-acid) and Poly(lactic-co-glycolic) copolymers. The obtained biodegradable electrospun carriers have been exploited to achieve controllable particles release as well as, in combination with natural polymer, to obtain composites capable to deliver two drugs simultaneously with controllable and predictable kinetics.

The possibility to obtain electrospun scaffolds capable of interconverting between a temporary and a permanent shape with the application of a thermal stimulus was explored. In this context, two polymers have been designed to behave as shape memory materials in the range of human body temperature by following two different approaches. In the first case a new linear triblock copolymer was specifically designed, synthesized and electrospun to gain a biodegradable and biocompatible scaffold showing a thermally induced shape memory effect around 40°C. In the second case, a crosslinked α,ω-triethoxysilane-terminated Polycaprolactone was used to obtain an electrospun scaffold with excellent shape memory properties.

Finally smart affinity membranes have been studied. This kind of materials are capable to detect specific molecules or biomacromolecules from complex mixtures, finding useful applications in the biomedical field as diagnostic and therapeutic devices. Smart affinity membranes might be used for example to detect specific kind of cells by exploiting the binding interaction between an antibody and cell receptors. During this thesis project poly(L-lactic acid) electrospun scaffolds conjugated with antibodies have been produced and the efficacy of different functionalization methods to generate the –COOH group necessary to perform the antibodies conjugation was investigated.

In the course of this Thesis, knowledge of structure-properties relations in polymeric materials was crucial in order to always find the best match between the physico-chemical polymeric characteristics and the specific final applications.

1 Introduction

1.1 Micro and nanostructured polymeric materials for advanced biomedical applications

With the raise of new biomedical applications like tissue engineering and controlled drug delivery, the need for specific polymeric biomaterials with adjustable chemical-physical properties is more than ever a hot topic. A biomaterial is defined as any natural or synthetic substance engineered to interact with biological systems in order to direct medical treatment (1). A biomaterial can be a ceramic, a metal alloy, a polymer or a composite made with the previous mentioned materials. Even though the specific properties of different materials should be carefully evaluated in order to match the specific applications, there are some requirements that are mandatory to consider a material a promising biomaterial (2). Generally speaking, a material in order to be used as a biomaterial should be biocompatible and bioactive, i.e. should be able to induce a non-toxic physiological response that is supportive of the biomaterial's function. Among the above-mentioned materials probably the most promising ones belong to the class of polymeric materials, and in particular biodegradable polymeric materials. In fact biodegradable polymers are usually biocompatible, are easily metabolized and cleared from the body once their primary function is accomplished (3) and their chemical physical properties can be ad hoc adjusted to comply with different applications (4). Due to the previously discussed characteristics biodegradable polymers finds their best application in the biomedical field (5,6) where it is possible to successfully employ many natural and synthetic polymers (7-9).

The possibility to control the architecture of materials up to nanoscale is very appealing and in this context polymeric materials are very versatile, allowing to obtain a great variety of dimensions and shapes such as fibers, particles, films, needles and more. This great versatility allows to employ polymeric based devices for many medical applications.

In recent years the scientific community is moving towards new advanced biomedical applications, in which biomaterials are required to interact with different biological environments in a specific way, providing therapeutic stimuli to the surrounding environment or being able to actively respond to particular conditions. Different advanced biomedical applications can be found in literature such as stimuli responsive materials (10), that are capable to respond to endogenous and exogenous stimuli in different ways, for example by releasing specific drugs (11, 12) (Figure 1).

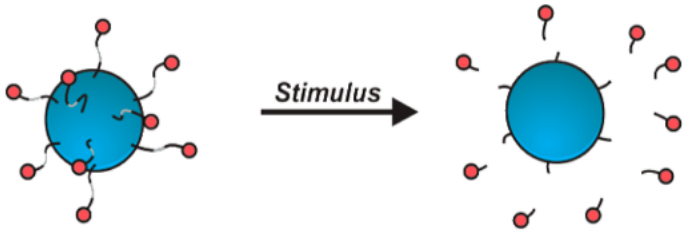

Figure 1. Schematic representation of stimuli responsive biomedical device for drug delivery. Reprinted with permission from J.Am.Chem.Soc.2015, 137, 2140−2154.

It is possible to find application of polymeric fibrous materials to achieve scaffolds capable to closely mimic the micro and nano structure of biological tissue for tissue engineering (13); polymeric particles from micro to nano scale capable to recognize specific tissue (14) or able to deliver drugs in a controlled and predictable way (15).

This thesis work focused on the study of polymeric materials for tissue engineering and drug delivery. In particular three research activities have been conducted: (i) fabrication and characterization of stimuli responsive polymeric fibrous scaffolds obtained with the use of electrospinning technique, (ii) the use of polymeric nanoparticles and fibrous scaffolds as drug delivery carrier and (ii) fabrication and characterization of bioconjugated fibrous matrix as smart affinity membrane. These research activities have been performed paying particular attention to the characterization of the obtained polymeric devices and trying to always find the best match between the applications and the materials to be used.

1.2 Electrospinning: general principles

Electrospinning (ES) is one of the most used techniques to fabricate polymeric fibers (16) as well as particles (17) with diameter ranging from tens of nanometers to microns. ES is very versatile and allows to work with a great variety of polymers; nearly all soluble polymers can be processed into fibers by

electrospinning. The inexpensive nature of the ES basic apparatus and the intrinsic versatility of the technique led to an increasing interest of the scientific community over the years.

ES is influenced by many parameters (18) that can be divided in three main groups (i) environmental parameters (ii) solution parameters and (iii) operative parameters. The environmental parameters are relative humidity (RH) and temperature at which the process takes place (19), solution parameters are related to the used solvent mixture (20) and to the viscosity of the solution, while the operative parameters are related to the applied voltage, needle to collector distance and feed rate of the solution through the metallic needle. Molecular weight of the used polymer and the solution viscosity are probably the most important parameters to take care since the viscosity of the solution is strictly related to the success or failure of the ES process; this is due to the so called physical entanglements (21). Macromolecular chains dissolved into a mixture of solvents arrange into a random coil conformation, the presence of physical interconnections between those random coil structures, i.e. physical entanglements, are mandatory in order to obtain a constant and continuous flow of macromolecules during the ES process allowing to successfully produce fibers (22). However, it is not only a matter of viscosity, the molecular weight of the polymers play a key role in the formation of the entanglements interaction and that's why most of the polymers employed for the ES process are high molecular weight ones, usually way over tens of kilo Daltons.

ES is an electrostatically driven process and it's based on the feeding of a polymeric solution through a capillary tube into a high electric field (Figure 2).

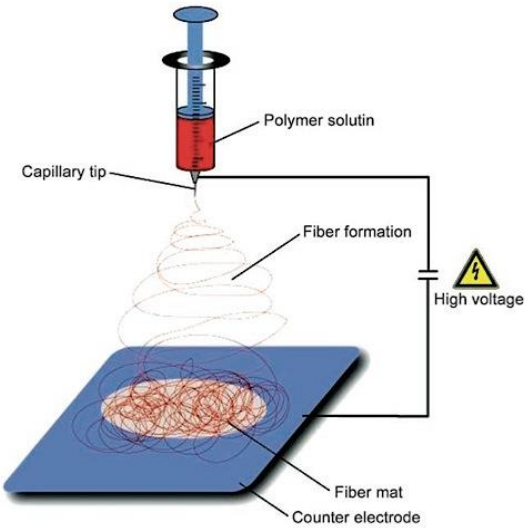

Figure 2. A scheme of an electrospinning laboratory apparatus. Reprinted with permission from Angew. Chem. Int. Ed. 2007, 46, 5670 – 5703.

When the solution reaches the electrified needle it is subject to forces produced by the magnetic field, once these forces overcome the surface tension of the polymeric solution it leads to the formation of the so called Taylor cone. After that a small a thin fluid jet is ejected and the fiber starts forming. The applied voltage leads to a whipping motion that has two main effects: (i) it allows stirring the fibers and in the meantime (ii) promotes solvent evaporation and let the dry fibers to be collected over a grounded collector. It is possible to control not only the fibers dimensions but also their architecture, obtaining fibers as random oriented, aligned, core shell, hallow and even with more complex structures (Figure 3) (23).

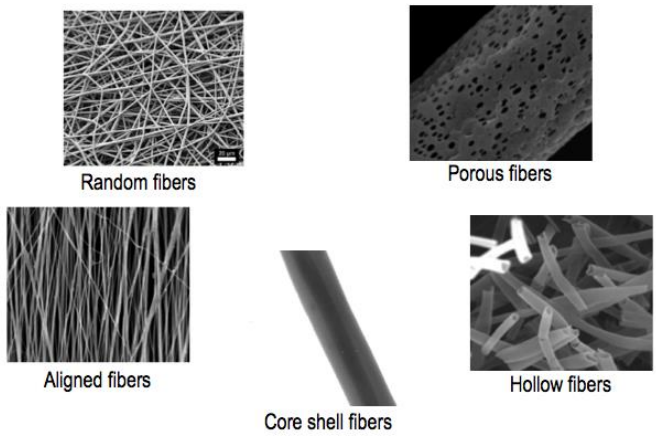

Figure 3. Different obtainable structures by mean of electrospinning technique

Electrospun fibers find application in many fields (Figure 4); for example in combination with conventional textiles to modify their properties (24). The objective can be to increase the wind resistance, to regulate the water-vapor permeability or to optimize the thermal insulation behavior. ES fibers can find application as air (25) or water filters (26), reinforcement of synthetic materials in many technical products (27), as catalyst support making it easy the recycling of the catalyst after the reaction (28) and last but not least in tissue engineering.

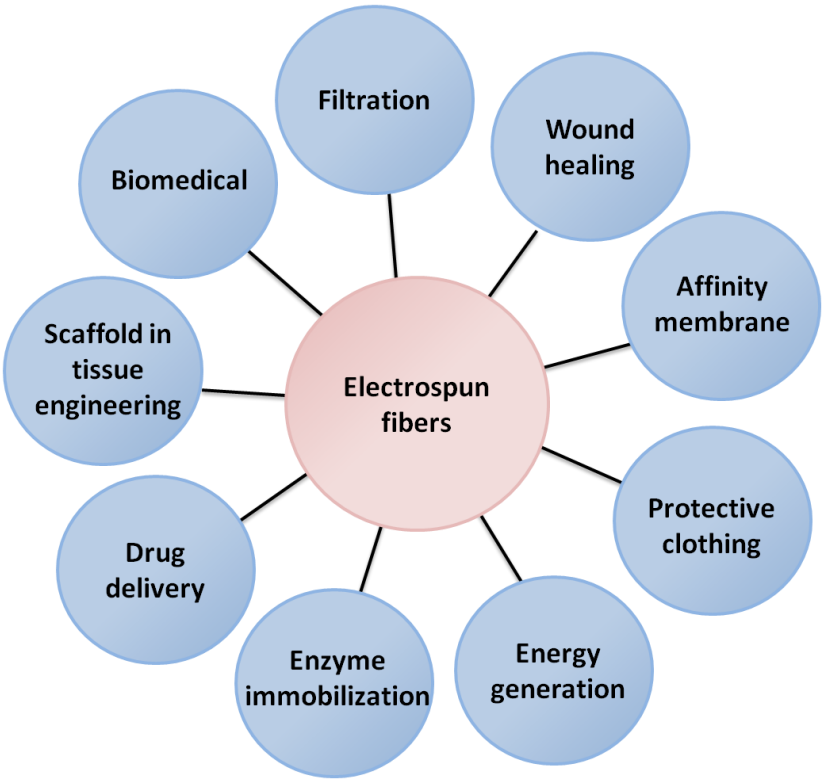

Figure 4. Possible applications of electrospun nanofibers

The latter field represents one of the most interesting one. The 3D structures of the ES fibrous systems, know in tissue engineering as scaffolds, are highly porous made up of fibers with high surface to volume ratio. This allows to greatly mimic the extracellular matrix well-supporting cell activities involved in tissue regeneration processes (29). Coupling this with the possibility to obtain new generations of scaffolds that can act as drug carrier, providing a controlled release of drugs while promoting the tissue regeneration might represent a big step forward in the field of tissue engineering (30,31).

In this context electrospinning can be considered a powerful and versatile tool to be applied to meet all the requirements for advanced medical applications that nowadays are of central interest for the scientific community.

1.3 Stimuli responsive polymers

Polymeric materials capable to respond to specific stimuli while promoting tissue regeneration are of great interest in medicine. Such polymers can be used for many applications like drug delivery, biosensors, biological actuators (32). Sometimes we refer to stimuli responsive materials as “smart”

materials for their capacity to respond to external stimuli in a non-linear way. Many stimuli can be provided to obtain a change in the polymeric behavior but usually all falls within three main classes (i) biological, (ii) chemical and (iii) physical stimuli (Table 1).

Table 1. Examples of stimuli responsive polymers along with their specific trigger and response

Stimulus	Polymer	Response	References
pH	Polyglycerol with a poly(ethylene glycol) shell	Drug release activation	(33)
	Cysteamine modified monomethoxyl poly(ethylene glycol)-b-poly-(allyl ethylene phosphate)	Drug release activation	(34)
	polybutadiene-poly(L-lysine) block copolymer	Morphology switch (rod to sphere transition)	(35)
Redox process	Poly(benzyl carbamate)-poly(N,N-dimethylacrylamide) block copolymer	Disassembly	(36)
	Glutathione sensitive Poly(N-isopropylacrylamide) based particles	Disassembly	(37)
Enzymes	N-(2-hydroxypropyl) methacrylamide (HPMA) copolymer-Gly-Phe-Leu-Gly-doxorubicin conjugate PK1	Drug release activation	(38)
	Conjugated poly N-(2-Hydroxypropyl)methacrylamide	Drug release activation	(39)
	DNA-brush copolymer amphiphiles micelles	Morphology switch	(40)
	Polymer-peptide block copolymer amphiphiles	Morphology switch	(41)
Temperature	Poly(N-isopropylacrylamide-co-propylacrylic acid) copolymers	Change of conformation	(42)
	Acid-labile thermoresponsive block copolymers: PEG-b-PtNEA	Disassembly	(43)
	Chimeric polypeptide–doxorubicin conjugate nanoparticles	Assembly	(44)
	Poly(N-isopropyl acrylamide) based amphiphilic block copolymers	Morphology switch	(45)
Light	Polyethylene glycol (PEG)-branch-azide bivalent-brush polymers	Drug release activation	(46)
	Peptide amphiphile (PA) containing fibronectin epitope Arg-Gly-Asp-Ser (RGDS)	Assembly	(47)
	Star shape poly(e-caprolactone) block poly(ethylene glycol)	Morphology switch	(48)

Biologically activated polymeric materials usually are capable to display a specific response in the presence of enzymes, specific molecules and biomacromolecules. One of the most studied application for this kind of materials is the self-regulated insulin delivery. This kind of devices are capable to deliver insulin just when needed, continuously measuring the glucose concentration over time (50) . Biologically activated materials can be also used to achieve drug delivery devices activated by enzymes, in this case the enzymes can specifically “cut” the covalent linkage created between the polymeric scaffold and the drug leading to a drug release just where needed (51). Even though biologically activated materials are very appealing, in literature there are not as much studies as chemical and physical responsive polymers (49).

There are many different sub-classes of chemical activated polymeric devices and usually the applied stimuli involve pH, ionic strength and specific redox conditions. Among those, the most interesting and studied stimulus is certainly the pH variation. This class of polymer displays a dramatic change in the coil dimension due to protonation and deprotonation events, this behavior can be exploited to obtain a targeted drug delivery device activated by the pH gradient of the different tissues (53). In fact it is well known that different tissues are characterized by different pH. For example, stomach and intestine are characterized by pH ranging from 1-3 and 5-8, respectively, and tumor tissues are well known for their acidity (54). These characteristics can be exploited to obtain polymeric devices capable to act in the presence of specific tissue such as tumor tissues (55) while behave as inert polymers in other region of the body.

Physically activated polymers are those that can display a change over the application of external stimuli, such as temperature. Materials that are capable to respond to temperature variation are well known in literature and are usually characterized by a specific temperature at which above and/or below there is a dramatic change of the properties of the devices. Many examples can be reported, such as the well know poly(N-alkyl substituted acrylamides), like the poly(N-isopropylacrylamide) (PNiPAAm) (56), poly (ethylene oxide)-poly(propylene oxide)-poly (ethylene oxide) (PEO–PPO–PEO) copolymers (57) and poly (N-vinylalkylamides) (58). During this thesis work it was decided to focus over a very interesting class of materials that can respond to temperature variation: the shape memory polymers (SMPs).

1.3.1 Shape memory polymers

SMPs are a class of smart polymers able to interconvert between a temporary shape and a permanent shape upon the application of an external stimulus (59). Many different stimuli can be used to trigger the shape memory effect, such as light irradiation (60), pH change, magnetic field (61) and, of course, temperature (62). The most commonly SMPs belong to the thermally triggered ones, where heating the specimen above a certain temperature is required to recover the permanent initial shape (63,64) (Figure 5).

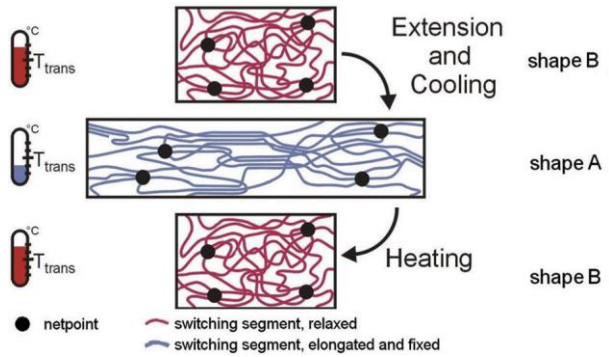

Figure 5. Schematic representation of the shape memory effect. reprinted with permission from Materialstoday Volume 10, Issue 4, April 2007, Pages 20-28.

All SMPs are characterized by a fundamental temperature, the transition temperature (T_{trans}), that defines at which temperature the scaffold is able to switch between the temporary and permanent shape. T_{trans} can be a T_g or a T_m, some examples of SMP investigated in the literature are reported in Table 2, along with their transition temperature.

Table 2. Examples of Shape memory polymers along with their specific transition temperature

Polymer	Transition temperature (°C)	References
Polycaprolactone	54–58	(65)
Polycyclooctene	45	(66)
Polyethylene	110	(67)
Poly(caprolactone-co-n-butyl acrylate) copolymers	45	(68)
Copolyester-Urethane Networks	48-66	(69)
Thermosetting polyurethane	up to 56	(70)
Dehydrochlorinated cross-linked PVC	80	(71)
Polynorbornene	40	(72)
High Mw polymethyl methacrylate	105	(73)
Aramid/PCL crosslinked block copolymer	up to 35	(74)
Poly(lactide-co-poly(glycolide-co-caprolactone) multiblock copolymer	40-50	(75)

Polymer	Transition temperature (°C)	References
Telechelic Polyhedral Oligosilsesquioxane	55	(76)

It is worth mentioning that not all polymers are capable to exhibit a shape memory behavior and a suitable macromolecular network composed by net-points and molecular switches are required (77). A net-point is a chemical (covalent bond) or physical (entanglement or crystal) interaction that is maintained at temperature above the T_{trans}. The net-points are responsible of the recovery of the permanent shape of the object. Molecular switches are defined as the part of the macromolecule capable to respond to the external triggering stimulus and enable to fix the temporary shape. Molecular switches can be an amorphous phase or a crystalline phase, thus identifying the T_{trans} as T_g or T_m, respectively.

SMPs exhibit the shape memory behavior in the course of a thermomechanical cycle (Figure 6). During this cycle the SMP is heated above the T_{trans} and deformed under a constant loading rate at a constant temperature until the desired temporary shape is obtained (Figure 6 from IV to I). Then the cycle proceeds with the cooling step, under constant tensile stress, below the T_{trans}. This step enables to fix the temporary shape (Figure 6 from I to II). Now the applied load can be released and the temporary shape is maintained (Figure 6 from II to III). The polymeric material is now ready to be used for all the different applications and purposes for which it was designed. The shape memory property is displayed when the sample is heated again above T_{trans} where it recovers its permanent shape (Figure 6 from III to IV). Commonly, SMPs are capable of recovering up to 90% of their permanent shape.

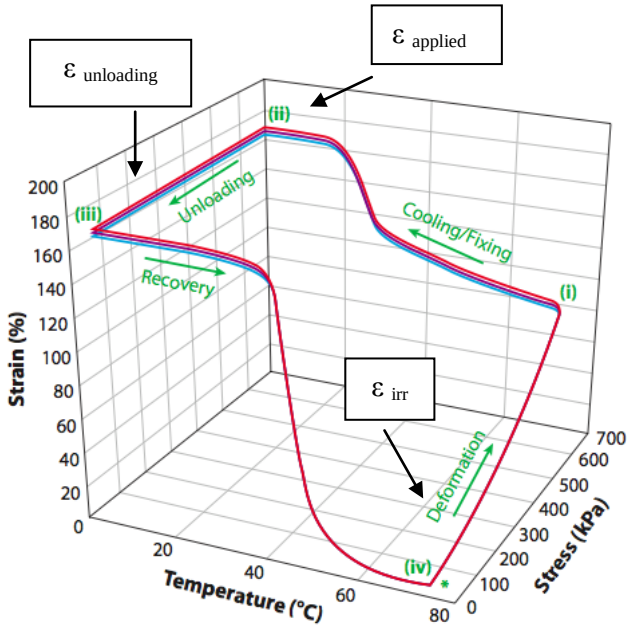

Figure 6. Thermomechanical cycle for a SMP

In order to characterize the properties of a SMP it is very important to define and estimate the shape recovery index (R_r, Equation 1.1) and the shape fixity index (R_f, Equation 1.2). R_r describes the ability of the material to completely recover its permanent shape after a thermomechanical cycle, while R_f describes the ability of the switching segments to fix the temporary shape when the load is released just after the cooling step during the thermomechanical cycle.

$$R_r = \frac{\varepsilon_{unloading} - \varepsilon_{irr}}{\varepsilon_{unloading}} \quad (1.1)$$

$$R_f = \frac{\varepsilon_{unloading}}{\varepsilon_{applied}} \quad (1.2)$$

where, $\varepsilon_{unloading}$, ε_{irr} and $\varepsilon_{applied}$ are the nominal strain measured at unloading, the irreversible strain and the strain at the application of the maximum load, respectively (see Figure 6).

Depending on the values of R_r and R_f, SMPs can be divided in four different groups along with their shape memory behavior (78) (Figure 7). The first graph (a) represents an ideal polymer with a perfect shape memory behavior, inasmuch it shows the complete and instant recover of the permanent shape (R_r=100%) and an excellent capability to fix the temporary shape (R_f=100%). A real SMP typically displays a shape memory behavior similar to those reported in graphs (b), (c) and (d), i.e. (b) SMP with both

excellent shape fixity and shape recovery (R_r=100% and R_f=100%), even if the recovery is not instantaneous; (c) SMP with excellent shape recovery index (R_r=100%) and moderate shape fixity index (R_f<100%); (d) SMP with moderate shape recovery (R_r<100%) associated with excellent shape fixity index (R_f=100%).

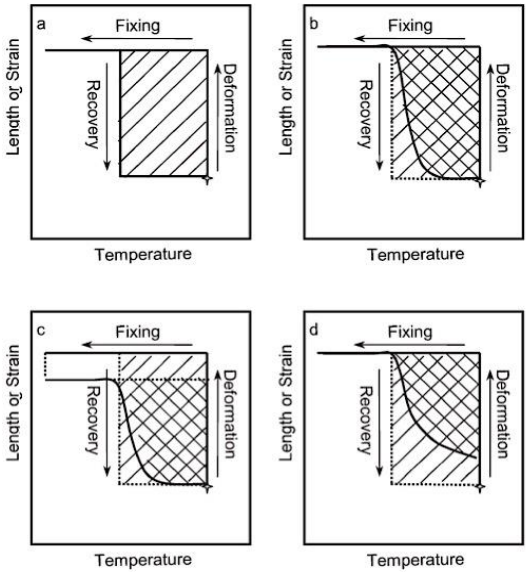

Figure 7. Classifications of SMPs by their shape-fixing and shape-recovery abilities. Reprinted with permission from Mater. Chem., 2007,17, 1543-1558.

SMPs can be applied to many different fields, among those the biomedical represent the most interesting one and, in this respect, SMPs whose transition temperature can be tuned to human body temperature or slightly above can be particularly promising. In this regards Baer et al. (79) successfully fabricated a shape memory polymeric stent prototypes from thermoplastic polyurethane. The obtained stents showed full recovery at temperature around human body temperature, demonstrating that SMP are promising material for the development of neurovascular stents. Another interesting example is reported by Xue et al.(80) that managed to synthesize a series of SMP containing three-arm PCL-based switching segment and poly(3-hydroxybutyrate-co-3-hydroxyvalerate) (PHBV) as hard segment; the authors demonstrated that the block copolymers containing 25 wt% of PHBV were characterized by excellent shape memory behavior with R_f and R_r of 94% and 98% respectively, with a T_{trans} of just 40°C.

Biodegradable SMPs can be used as short term implants, thus avoiding subsequent device removal by surgery. For example, biodegradable intragastric implants for obesity treatment can be produced with this new smart class of materials. Another extremely interesting example is the use of biodegradable

SMPs as intelligent wound closures that are able to close the wound by recalling their permanent shape upon heating (81) (Figure 8).

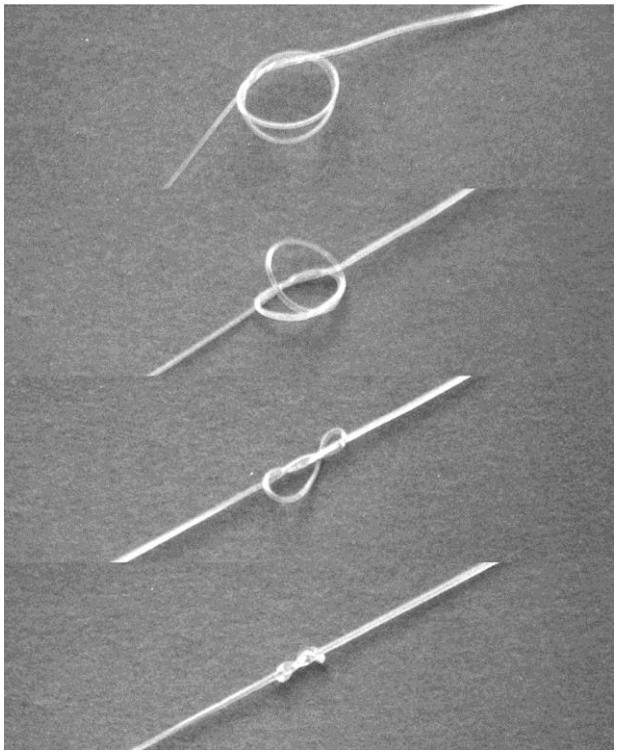

Figure 8. A fiber of a thermoplastic shape-memory polymer was programmed by stretching about 200%. After forming a loose knot, both ends of the suture were fixed. The photo series shows, from top to bottom, how the knot tightened in 20 s when heated to 40°C. Reprinted with permission from Science 296.5573 (2002): 1673-1676.

Another important application in the biomedical area is represented by the possibility to create SMP stents that can be mold in a small temporary shape in order to be implanted in a patient without an invasive surgery operation (82).

It is well known that micro/nano-structure has a dramatic impact on materials properties, offering an alternative way to achieve enhanced properties without changing the chemical composition of the material. SMP non-woven mesh with stable and reversible micro/nano-fibrous structure can be produced by electrospinning starting from a polymers that should satisfy the following conditions: (i) it must be solubilized in order to give an electrospinnable fluid (a sacrificial polymer can also be used to improve electrospinnability) and (ii) upon electrospinning and drying, it must maintain the micro/nano-fibrous structure. When micro/nano-structuring is applied to SMPs, it may result in promoted or amplified functionality and response. Indeed, it was demonstrated that a micro/nano-fibrous mesh had much

better shape recovery sensitivity than the corresponding bulk film (83).

During this thesis work the possibility to obtain SM electrospun devices capable to switch shape within the body temperature range or slightly above was investigated by working with specifically synthesized α-ω-triethoxysilane-terminated poly(ε-caprolactone) and a new triblock copolymer made of poly lactide, sebacic and azelaic acid.

1.4 Polymeric based materials as drug carriers: nanoparticles, fibrous scaffolds and composites

The possibility to obtain devices capable to in-situ release one or multiple drugs with predictable kinetics has attracted considerable attention in the last decades. Those systems can help to overcome the limitation of the most common administration ways that consist of inhalation, oral administration and injections. Usually those approaches can achieve high drug concentration in the blood stream in a relative short span on time but they require multiple dosages over prolonged period in order to maintain the drug concentration within the therapeutic window, i.e. the range of dosage of a drug or of its concentration in a bodily system that provides safe effective therapy (Figure 9). This great limitation is both time and cost consuming and might results to poor treatment efficacy.

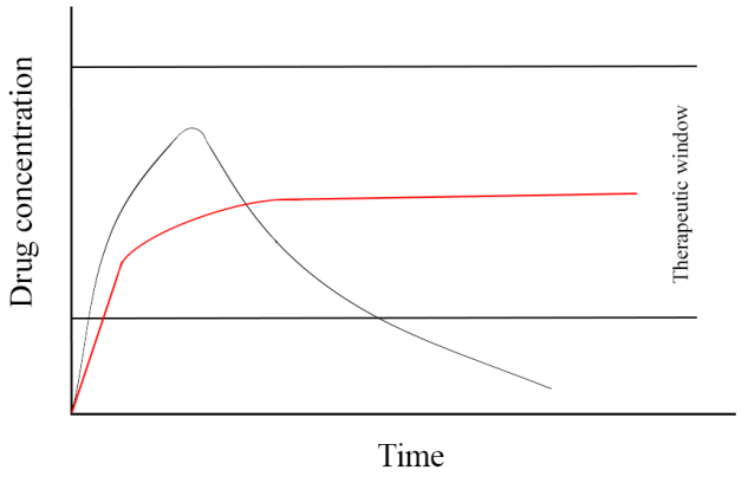

Figure 9. Plasma drug concentration over time for conventional administration (black) and sustained drug delivery device (red)

Conventional therapeutics are usually low molecular weight molecules capable to cross the different body compartments, reaching the therapeutic spot. This peculiar behavior represent simultaneously their best and worst feature, since it can open up to possible side effects and indiscriminate drug distribution.

Modern medicine is trying to overcome the above-mentioned limitation; working together chemist, engineering and pharmaceutical scientist are trying to obtain devices capable to deliver in a controlled, predictable and sustained way one or even more drugs at same time.

In this respect polymers played a key role in the last decades as potential drug carriers. In fact, polymers in different forms can be used as carrier to transport drugs in the site of action, protecting them from the normal clearance mechanism. The use of polymers as carriers might allow overcoming the indiscriminate drug distribution (84) of the commonly used administration ways and furthermore might help to obtain a more sustained drug release over time. In the following paragraphs the possibility to use fibrous scaffolds, composites and nanoparticles as drug delivery systems will be discussed in detail.

1.4.1 Nanoparticles as drug carriers

The most commonly used polymeric drug delivery systems are the polymeric nanoparticles. This system allows transporting one or more drugs both as covalently linked to the particles surface or embedded within it. In particular when the drug is encapsulated into the particles, depending on the method of preparation, it is possible to obtain nanocapsule (reservoir system) or nanosphere (matrix system). In the first case the drug is confined into a cavity surrounded by a uniform polymer membrane while in the second case the drug is uniformly distributed within all nanoparticles volume (Figure 10).

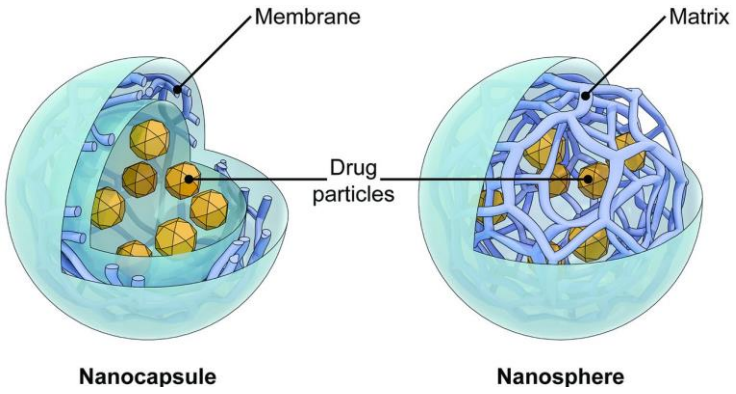

Figure 10. Schematic representation of the structure of a nanocapsule and a nanosphere. The image is in the public domain and credited to the National Institutes of Health/Department of Health and Human Services.

Nanoparticles can be used to delivery many different drugs and ca be made of different materials both natural and synthetic (Table 3), just to mention some: chitosan (85), gelatin (86), poly lactide and glycolide copolymers (87) and polycaprolactone (88) can be used.

Table 3. Examples of particles and nanoparticles used as efficient drug carriers

Polymer	Drug	References
Sodium alginate	Carboplatin	(89)
Chitosan-g-poly(N-vinylcaprolactam)	5-Fluorouracil	(90)
PEGylated PLGA	Doxorubicin	(91)
Chitosan-poly(ethylene oxide-g-acrylamide)	Capecitabine	(92)
Chitosan, Chitosan-PCL, PLL-PCL	Mitomycin C	(93)
Gelatin	Rifampicin	(94)
Poloxamer nanoparticles	Cyclosporine A	(95)
PLA/Chitosan	Lamivudine	(96)
Chitosan	Tacrine	(97)
Ethyl cellulose, poly (ethyleneglycol)-4-methoxycinnamoylphthaloylchitosan	Retinyl acetate	(98)
Polyacrylate	β Lactam analogue	(99)
PLA-co-PLG	Clotrimazole	(100)

NPs can be loaded with drugs basically in two different ways (i) during the NPs fabrication (reservoir and matrix systems) or (ii) after the NPs production by incubating them into the drug solution. It was already demonstrated that the drug incorporation during the fabrication process is far more efficient compared to the post-process adsorption mechanism (101). Another method of drug loading is gaining increasingly attention: drug conjugation over NPs surface. Whit this method it is possible to covalently bind molecules or even biomacromolecules over the surface of the NPs, making them available once the chemical bond brakes down due to enzymatic action. In this case the drug release mechanism from the NPs is no more strictly related to the drug diffusion and particle erosion like it is with reservoir and matrix systems.

Nowadays it is possible to achieve a site-targeted release to obtain a localized drug delivery, not affecting the healthy tissues at all, thus avoiding the undesired aspecific drug release. In order to obtain this result the NPs need to be functionalized and bioconjugated in order to recognize specific tissue, for example with the use of antibodies (103) (Figure 11).

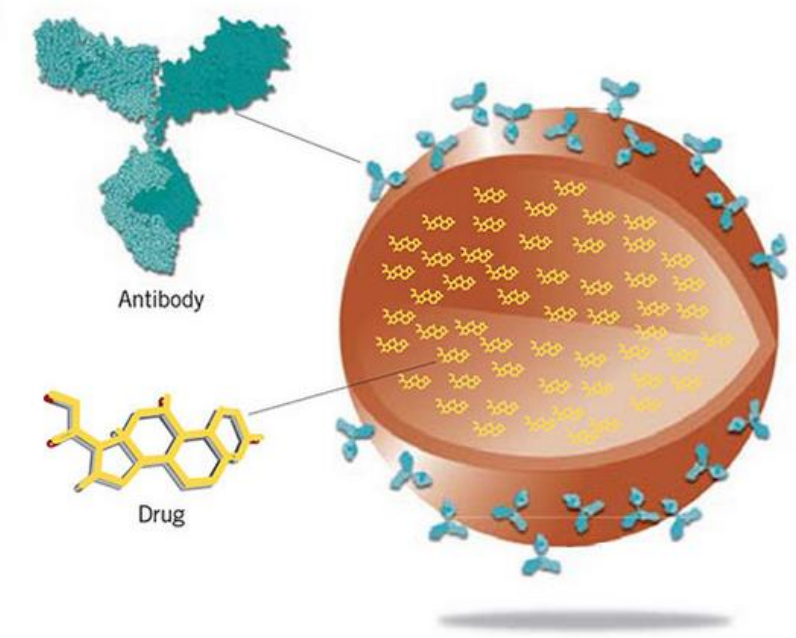

Figure 11. Example of targeted drug loaded NPs obtained conjugating the NPs with a specific antibody. Reprinted from Particle Sciences - Technical Brief 2015 Volume 1, all rights reserved.

Usually targeted NPs are administered through systemic circulation and many examples can be found in literature. One of the most interesting one is the kidney site-targeted drug delivery. This targeted drug delivery allows preventing the formation of excess fibrous to proximal tubular cells avoiding tubular inflammation with the use of targeted drug loaded particles (104).

1.4.2 Electrospun fibers as drug carriers

Another interesting polymeric carrier that might be exploited to obtain controllable drug delivery is the electrospun (ES) fibrous systems (Figure 12).

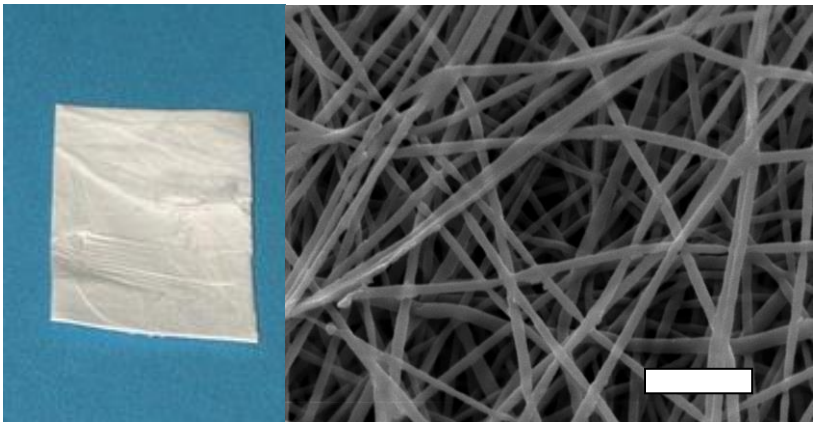

Figure 12. On the left side an electrospun mesh on the right side its SEM images obtained at 4000x that highlight the 3D porous fibrous structure of the material. scale bar 2µm.

ES fibrous systems have demonstrated great potential as drug carrier, enabling the possibility to locally release high concentration of specific molecule by using a small amount of drug loaded fibrous matrix (105). This approach allows to in-situ release the drug in a sustained way over prolonged periods improving the quality life of the patients.

Many studies reported in literature describing the high loading efficacy of ES fibrous system, with values that sometimes reach the 100%. Moreover, by using ES it is possible to modulate the drug release kinetics by carefully choosing the polymer chemical composition and playing with ES solution parameters (106). For example, it is possible to slow down the drug release rate by enhancing the fiber diameter or choosing a hydrophobic polymer to produce the fiber, thus slowing down water permeation.

When designing a drug release from ES fibrous system it is necessary to carefully consider many factor that might influence the final drug release kinetics: (i) the interaction between the fiber and the medium, (ii) the interaction between the fiber and the drug and finally (iii) the interaction between the drug and the medium. By carefully considering and evaluating these factors it is possible to speed up or slow down the release behavior of a desired drug. Drug loaded ES fibers can be successfully obtained by means of many different approaches (Figure 13, Table 4) such as post-fabrication functionalization (107), blending

approach (108), core shell fiber approach (109) and even loading drug loaded micro/nanoparticles inside the fibers mash (110).

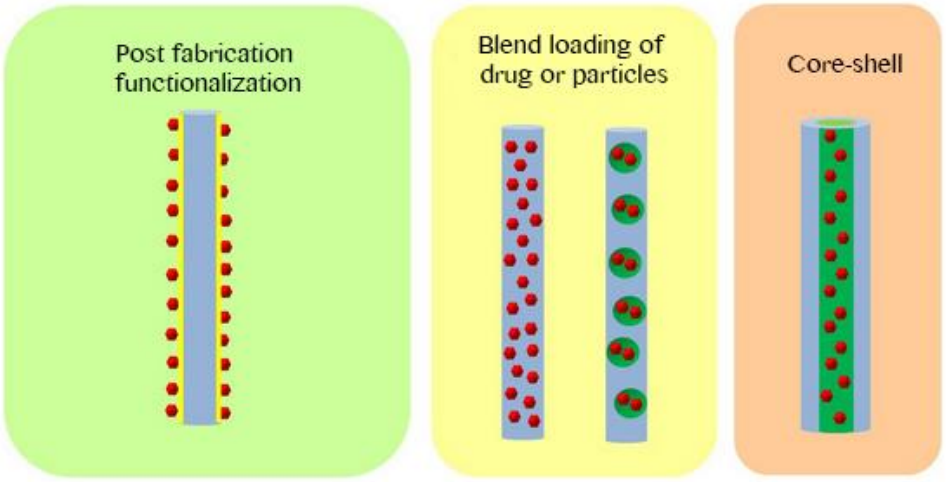

Figure 13. Techniques of drug loading of electrospun fibers.

Table 4. Examples of polymers used as electrospun drug carriers to achieve controlled drug release

Polymer	Loaded drugs	Fabrication tecnique	References
PLA, PEVA and PLA/PEVA	Tetracycline hydrochloride	Blend	(111)
PLA/PCL	Tetracycline hydrochloride	Blend	(112)
PCL	siRNA	Blend	(113)
PLGA	Fusidic acid and rifampicin	Blend	(114)
Ethyl cellulose and polyvinylpyrrolidone	Ketoprofen	Blend	(115)
PLGA poly(ethylene glycol)-g-chitosan	Ibuprofen	Blend	(116)
PLGA	Mefoxin	Blend	(117)
Poly(ethylene oxide)	Bovine serum albumin	Blend	(118)
PEG–PLA	Doxorubicin hydrocloride	Blend	(119)
PLA–PEG and PLGA	DNA	Blend	(120)
PCL/PVA	HRP encapsulated liposomes	Core shell	(121)
PLLA	BSA loaded into chitosan particles	Core shell	(134)
Poly(lactic-co-glycolic acid) 90:10	Rhodamine (B) loaded mesoporous silica nanoparticles	Core shell	(135)
Poly vinyl alcohol	Diclofenac loaded nanoparticles	Core shell	(136)
PLGA	Paclitaxel	Blend	(122)
PLA/PLGA	Cisplatin	Blend	(123)
PLA	Dichloroacetate	Blend	(124)
PEG–PLLA	1,3-Bis(2-chloroethyl)-1-nitrosourea	Core-shell	(125)

Post-fabrication functionalization consists in the covalent link of molecule or biomacromolecules into the surface of the fibers while the blend approach allows obtaining a drug loaded scaffold starting from an electrospinnable blend mixture of polymer and drug. Finally, the use of drug loaded NPs embedded into fibrous system is widely used in order to prevent the drug burst effect during the first release stages.

Nowadays the most studied field of application for drug loaded ES scaffolds is the cancer therapy. In this respect many contribution can be found in literature, like the application of super hydrophobic ES drug loaded scaffolds to obtain a sustained drug release up to 90 days preventing relapse in colon rectal cancer (127), the use of doxorubicin-loaded poly(L-lactic acid) (PLLA) electrospun scaffolds to target hepatic carcinoma in a mice model (128) and many others (129-132).

As previously mentioned coupling, the NPs and ES scaffolds might allow to both overcome the burst release effect, which is typical for monolithic fibers, and to protect the payloads into the particles. In this respect two different strategies are reported in literature, the first one makes it necessary to start from an electrospinnable blend of NPs and polymer (133) while the second one involves the adsorption of NPs on pre-fabricated fibrous system. Indeed the first approach represent the most interesting one allowing to prevent burst release and to obtain a more accurate control on the drugs release, while the second one, due to its peculiar geometry might not help to completely overcome the burst release effect. As reported below, in literature it is possible to find different examples related to the use of drug loaded NPs to achieve mono and multi drug release from electrospun composites. Jiao at al. report the possibility to obtain a dual drug delivery of bovine serum albumin (BSA) and benzoin, used as hydrophilic and hydrophobic model drugs, respectively. BSA was loaded into chitosan particles while benzoin was loaded within an ES matrix of poly (l-lactic acid) (PLLA). The authors reports the fast BSA release and more sustained release of benzoin; furthermore it was demonstrated that the release of the embedded drugs can be even more modified by adding different amount of PVP into the final composites. The modification of the composites hydrophobicity allows to significantly change the BSA and benzoin release kinetics (134). Another interesting approach is proposed by Chang and coworkers that developed an ES/NPs composites made of mesoporous silica nanoparticles (MSNs) and electrospun poly(lactic-co-glycolic acid) 90:10. The study takes advantage of two model drugs, Rhodamine (B) and Fluorescein. The first one was embedded into the particles systems while the second into the ES mats (Figure 14). The study demonstrates the possibility to release two drugs in two distinct way, 90% of the Fluorescein was released up to 300h while just 8–37% of the loaded Rhodamine (B) was released after 324 h (135).

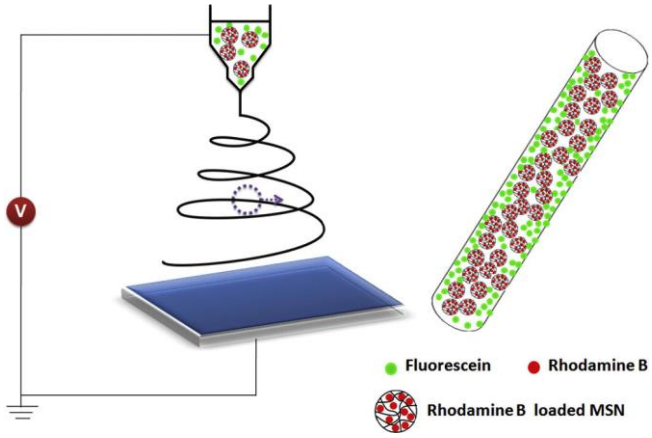

Figure 14. Schematic illustration of the process of fabrication of dual drug-loaded electrospun composite fiber and the position of the two model drugs located in the fiber. Reprinted with permission from Acta Biomaterialia Volume 8, Issue 5, May 2012, Pages 1901-1907

Finally it is possible to report an example of how NPs loaded into an ES matrix can help preventing the burst release effect and to achieve more controlled release kinetics. In this study Galhei et Al. loaded zein NPs with diclofenac (DLF) demonstrating that the formulation of zein:DLF 1:1 exhibited optimum encapsulation efficiency of 47.8%. The release behavior of DLF from the obtained drug loaded NPs was studied, obtaining the release of about 80% of DLF within the first 120h. Release studies revealed that the zein loaded NPs embedded in poly vinyl alcohol (PVA) nanofiber structure could efficiently reduce the burst effect of DLF and also prolong the release period up to 5 days.

1.4.3 Hydrogel and electrospun fiber composite materials for drug delivery

Nowadays, researchers are exploring ways to overcome the limitation of different materials commonly employed in the biomedical field to achieve controlled drug release, combining them creating new composite materials. Polymeric electrospun scaffolds and hydrogels are commonly exploited to produce composites; nevertheless they are characterized by specific drawbacks, such as poor cellular infiltration into electrospun scaffolds (136,137) and hydrogel poor mechanical properties (138-140). Even with these specific drawbacks, electrospun fibers and hydrogels are an excellent starting materials to fabricate composites for drug delivery. As previously reported fibers can be successfully loaded with high amount of drugs due to their high surface to volume ratio (141) but they are often associated with high burst release and drug aggregation problems (142). Even if the electrospun scaffolds can be tailored by controlling fiber diameters and porosity, it is not straightforward to obtain a sustained and linear release kinetics from a

drug loaded electrospun scaffold. Hydrogels are often used as hydrophilic drug delivery system (143,144) and their easy modification of swelling, crosslink density and degradation can be exploited to regulate the embedded drug release kinetics (145), however the difficulty to load hydrophobic drugs restricts their use to a small amount of molecules and highly subjected to burst release effect. By combining hydrogels and electrospun scaffolds it might be possible to obtain composites capable of releasing drugs in a more controlled way compared to the corresponding single components. Different techniques can be employed to combine electrospun fibers and hydrogels to obtain composite materials with the best characteristics of each component. In particular the most known techniques are the lamination, homogenation and micro-integration techniques (146). Laminated composites are obtained by stacking separately made electrospun scaffolds and hydrogel layers obtaining a packed structure with poor connection between the different components (147) (Figure 15).

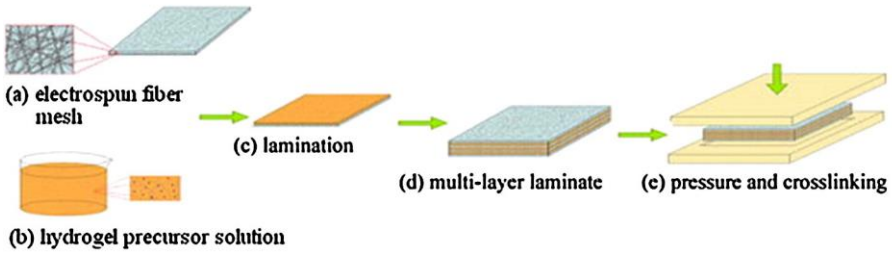

Figure 15. Scheme representing the assembly of electrospun scaffolds and hydrogel to create layer upon layer composite. Adapted with permission from Acta Biomater, 6 (2010), pp. 1992-2002.

Integrated composites are better packed, they are made by electrospinning the polymer and spraying the hydrogel solution simultaneously on the same collector, resulting in composites of hydrogels and electrospun-fibers on microscale (148-150) (Figure 16)].

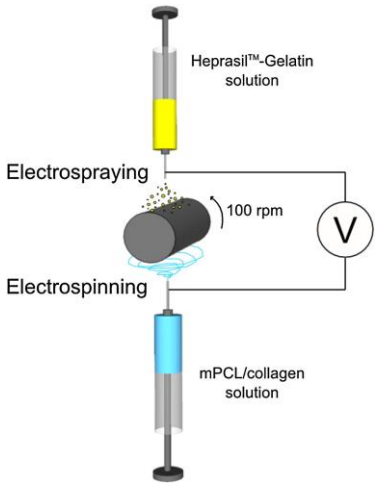

Figure 16. Schematic representation of the fabrication of integrated composites obtained by co-spinning of an electrospun mixture and an hydrogel solution. Reprinted with permission from Biomacromolecules, 9 (8) (2008), pp. 2097-2103.

Finally, homogenous composites are made by adding an electrospun scaffold to a hydrogel solution during the gelation process, obtaining composites in which the electrospun scaffold is completely integrated in the hydrogel matrix (151,152) (Figure 17).

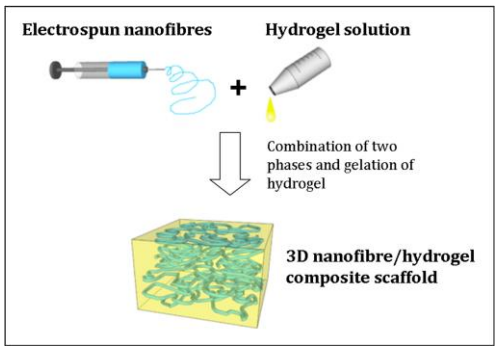

Figure 17. Schematic representation of the process used to obtain homogenous composites. Reprinted with permission from Nanomedicine: Nanotechnology, Biology and Medicine Volume 9, Issue 3, April 2013, Pages 322-335.

Some works are reported in literature demonstrating that combining electrospun scaffolds and hydrogels can be a promising approach to achieve ad-hoc drug delivery. Han et al. have demonstrated the possibility to dramatically reduce the burst release of an hydrophilic model drug (bovine albumin serum, BSA) from a composite made of poly(ε-caprolactone) (PCL) electrospun fiber mats and poly(ethylene glycol)-poly(ε-caprolactone) diacrylate (PEGPCL) hydrogels coupled through photo-polymerization. Furthermore, the authors demonstrated that by combining the electrospun scaffold and the hydrogel it was possible to obtain a near-linear BSA release kinetics of about two months (153). Jong Lee and co-workers also reported the possibility to couple hydrogels and electrospun fibers, in particular PEG hydrogel and BSA loaded PCL electrospun fibers, to control BSA release. They demonstrated the possibility to reduce the initial burst release effect and to promote a more linear and sustained release kinetics by using the composites rather than the BSA loaded scaffolds (154).

In this paragraph the great potential of polymeric based drug delivery carrier to obtain controlled and tunable drug or multi drug delivery was discussed. By carefully choosing the carriers material composition it is possible to impact the drug release behavior, delaying the release or preventing the burst release effect. By coupling different materials it is possible to achieve multi drug delivery

composites and highly tunable in situ release devices. The possibility to couple different materials allows to theoretically obtain the desired carrier for each medical demand and open up to huge medical advancements.

1.5 Electrospun affinity membranes for specific cell recruitment

Usually the separation process of a desired analyte from a complex mixture is performed by means of technologies that exploit the dimension parameter or at best a non-covalent weak interaction between a stationary phase and the analyzed mixture. In the last 30 years are gaining always more interest new ways to perform selective filtration with the use of smart affinity membrane (SAM). In contrast to the previously mentioned set up, SAM can be successfully employed to recognize analytes by means of specific interactions between the membrane and the analyte. SAM allows separating analytes not by dimension but exploiting their peculiar chemical physical properties (155).

The design and fabrication of SAM requires the collaboration of researchers with different backgrounds. It is necessary to wisely choose the right materials to be functionalized and conjugated with the right proteins, antigens, antibodies, nucleotides and enzymes, to gives rise to a unique set of binding domains. The great advancement of SAM is related to the specificity: these kinds of membranes are capable to selectively recognize specific analytes through the ligand-receptor interaction. In fact, it is well known that some biomacromolecules such as antibodies are characterized by the presence of a small domain, well defined from the 3D point of view, known as receptor, capable to recognize a specific ligand domain on the surface of the analyte (Figure 18).

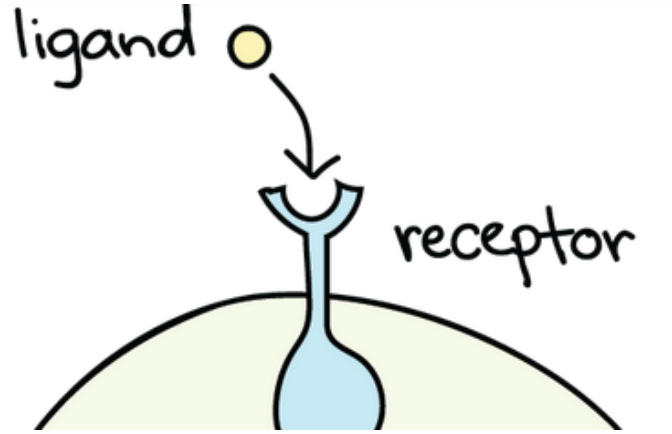

Figure 18. Schematic representation of ligand-receptor interaction

This interaction is very strong and highly specific, thus it is possible to recover just the desired analyte with accuracy and specificity. The affinity method is not restricted to the isolation of proteins: nucleic acids and whole cells can also be separated (156).

Membranes can be classified on the basis of their barrier structure as either non-porous or porous. Porous membranes can be divided into three classes: micro, meso and macro porous membranes. The first ones are characterized by the small porous size of about 2 nm while the second and third ones range from 2-50nm and 50 to 500nm, respectively. Depending on pore size, these membranes can be used to achieve microfiltration (MF), ultrafiltration (UF) and nanofiltration (NF) (157). The architecture of the membrane has a great impact on the method of filtration. Non-porous membranes are capable to separate the analyte from a complex mixture through the interactions between the permeant and the interphase, in contrast to porous membranes, that tend to also exploit the size of the analyte to achieve the separation.

From the technological point of view, SAM can be used as self-standing sheet or as membrane modules. Membrane modules are highly packed devices with high membrane density and are obtained by stacking large area of active membrane into a relatively small volume, while preserving the efficiency of the system.

Four main module geometries are usually exploited such as (i) tubular, (ii) Plate-and-Frame, (iii) Spiral Wound and (iv) hollow fiber. On the basis of the different geometry the aforementioned modules have different properties. For example, the tubular module can hold up a high flow volume but are characterized by low packing density; on the other hand Hollow Fiber module cannot tolerate a high feed flow volume and has an excellent packing density. Last but not least Plate-and-Frame and Spiral Wound modules, these two modules are quite similar and their properties are halfway between the Tubular geometry and the Hollow Fiber one, but with low cleaning efficiency.

Many materials can be exploited to obtain membranes; among those polymers, ceramics, oxides and metals are the most used. Indeed, the materials for affinity membranes must satisfy some specific requirements (157) such as (i) hydrophilicity, (ii) large surface to volume ratio, (iii) availability of functional groups, (iv) biocompatibility and (v) chemical and physical stability. Hydrophilicity of the used materials is very important since it can prevent the phenomena of non-specific absorption of proteins, which take place through hydrophobic interactions. The used materials should be characterized by the presence of proper functional groups that will be exploited to obtain the bioconjugation necessary to selectively bind specific analytes while the large surface to volume ratio is necessary to enhance the

interaction between the ligand and the receptor, obtaining a better separation behavior. The material used for the SAM should be biocompatible in order to not compromise the biological activity of the target, once the latter is immobilized on the surface, and, in the mean time, it must be stable from the chemical and physical point of view, since some bioconjugation and functionalization steps might be performed under harsh condition and the material should be able to sustain them.

SAM can be obtained starting from an already fabricated membrane, exploiting the existing available functional groups to perform the bioconjugation. Alternatively, it can be obtained as composite membranes in which a functional polymer is grafted above a base membrane. This last architecture reaches a good compromise between the functions of the two different materials. Finally, it can be obtained by crosslinking a polymer in the presence of the analyte, which can be later removed, leaving a template structure capable to act as binding sites that are complementary in shape and functionality to the analyte.

The first approach, i.e. the functionalization of already existing membranes, is the most commonly pursued. Usually, this strategy involves the chemical functionalization to make the membranes suitable for the bioconjugation with biomacromolecules, such as proteins and antibodies, with polymers (158) or small molecule. In the case of bioconjugated membrane it should be took into account the poor stability of the used biomacromolecules that, during the process of functionalization and consequent conjugation, might be easily deactivated as a consequence of their 3D structure loss. To overcome this limitation it is sometimes preferred to use a pseudo-biospecific ligands, that mimic the 3D structure of a complete biomacromolecules but are smaller and physically and chemically stable. One example of this approach might be the Cibacron Blue F3GA (CB). This is a general affinity dye ligand that can bind a wide range of targets such as dehydrogenases, catalases and bovine serum albumin (BSA) (159). Some synthetic amino acids like tryptophan, histidine and poly(L-lysine) are employed, respectively, for the separation of bovine γ-globulin, human IgG from placenta and heparin from plasma (160).

As previously mentioned in order to achieve bioconjugation, the used membrane should possess the proper functional groups. The most commonly used functional groups are carboxyl (–COOH), primary amine (–NH2) and sulfhydryl (–SH) and carbonyl (RCOR) groups. Even though these groups are widely present in several polymers sometimes it is necessary to add them with a functionalization step. For instance, Sundberg and Porath activated an agarose polymer matrix with the 1,4 butanediol diglycidyl ether (161), Ramakrishna et al. used a sodium periodate mediated oxidation to obtain two terminal aldehyde groups on a regenerated cellulose surface (162) and sometimes phisycal treatment are

exploited to achieve the functionalization, as in the case of plasma activated polymeric surfaces (163). The last is of particular interesting since the functionalization can be successfully achieved without the use of toxic solvents, indeed it might be of great interest for industries and companies.

SAM should be characterized by a large surface to volume ratio and should be ideally biocompatible and easy to functionalize. In this context electrospun scaffolds might be great candidates as SAM since they possess all the necessary requirements. In fact, electrospun scaffolds, thanks to their micro and nano fibrous structure, are characterized by high functionalizable surfaces and furthermore they can be obtained using different polymers, according to the specific needs. Many examples can be found in literature of successful use of electrospun scaffolds as affinity membranes such as the work of Ma et al. that report the possibility to use regenerated cellulose (RC) nanofibrous mesh as affinity membrane for immunoglobulin G (IgG) purification. The authors demonstrated that the obtained SAM has a strong binding specificity towards IgG molecules, higher than current commercial products (162). Another interesting example is reported by Miyauchi ad coworkers, in this work they fabricated an electrospun cellulose scaffolds and functionalized it with a model specific affinity ligand, Cibacron Blue F3GA (CB). The produced SAM was successfully used to investigate bovine serum albumin (BSA) adsorption/desorption properties. In this work it was demonstrated that the BSA captured on CB immobilized SAM was bound with 5 time more efficacy compared to the used control (165).

The world of SAM represents a hot topic of the scientific community and much work still needs to be addressed. The great impact that this technology might have in our daily life makes it something to look up in the next future.

2 Materials and Methods

2.1 Materials

Solvents: methanol (MeOH), chloroform(CLF), dichloromethane (DCM), N,N-dimethyl-formamide (DMF), tetrahydrofuran (THF), hydrochloric acid (37% w/w in H_2O), toluene (anhydrous, 99.8%), chloroform (HPLC grade), *n*-hexane, chloroform-*d*, Hexafluoroisopropanol (HFIP), Milli-Q Millipore system was used for the purification of water (resistivity g18 MΩ).

Polymers and Monomers:

- α-ω-Hydroxyl-terminated poly(ε-caprolactone) (average M_n ≈ 10 000 g mol $^{-1}$ and average M_w ≈ 14000 g mol^{-1}), ε-Caprolactone (CL, 97%), Oxacyclotridecan-2-one (DDL, 98%), 16-Hexadecanolide (HDL, 97%), poly(ethylene glycol) methyl ether (M_n = 2000 Da, MeO-PEG-OH), Gelatin from porcine skin, poly(vinyl alcohol) (PVA, M_w = 30,000–70,000, 87–89% hydrolyzed) were purchased from Sigma-Aldrich.
- *p*-Dioxanone (DO, ≥99%) was purchased from Leap Labchem Scientific Co. (China).
- Poly(L-lactic acid) (Lacea H.100-E) (M_w = 129 × 10^3 g mol^{-1}) was supplied by Mitsui Fine Chemicals.
- Poly(ethylene oxide terephthalate)-co-poly(butylene terephthalate) 30:70 (PEOT average M_w ≈ 1000 g mol^{-1}, 70wt% PBT and 30wt% PEOT); Poly(ethylene oxide terephthalate)-co-poly(butylene terephthalate) 70:30 (PEOT average M_w ≈ 1000 g mol^{-1}, 30wt% PBT and 70wt% PEOT) were purchased from Polyvation (Groningen, The Netherlands).
- Poly(lactic-co-glycolic acid) 50:50, Poly(lactic-co-glycolic acid) 75:25 were purchased from Evonik Nutrition & Care GmbH

Reagents: 4-morpholineethane-sulfonic acid (MES) 99.5%, FITC isomer I (90.0% (HPLC) powder), 1-ethyl-3-[3-dimethylaminopropyl] carbodiimide (EDC), hydroxysulfosuccinimide (sNHS) (98.0% (HPLC) powder), 1,4-diaminobutane 99% (DAB), NaOH, monoclonal Anti-MME antibody produced in mouse (anti-CD10), anti- Mouse IgG-FITC antibody (Ab-FITC), bovine serum albumin (BSA), 3-(triethox- ysilyl)propyl

isocyanate (ICPTS), immobilized *Candida antarctica* Lipase B (CALB) supported on acrylic resin (Novozym 435), genipin, K_2HPO_4, Rhodamine B base (>98%),

Drugs and particles: Chlorine-Tetracycline Hydrochloride (CTC), Diclofenac Potassium (DK), Luminescent core shell silica NPs have been produced by Prof. Nelsi Zaccheroni and co workers at Chemistry department "G.Ciamician".

2.2 Scaffolds fabrication

2.2.1 Electrospinning apparatus

All scaffolds have been fabricated by starting from different polymeric solutions and by using an home made apparatus made of: a high-voltage power supply (Spellman SL 50 P 10/CE/230), a syringe pump (KD Scientific 200 series), a glass syringe, a stainless steel blunt-ended needle (inner diameter variable from 0.31 mm to 0.80mm) and a grounded aluminum drum-type collector (diameter 2 to 10 cm), rotating from 100 rpm to 6500rpm. Polymer solutions were dispensed through a PTFE tube to the needle, which was placed vertically on the collecting drum at variable distances. The electrospun scaffolds were produced at room temperature (RT) and at relative humidity (RH) from 30% to 80%. All the obtained scaffolds have been stored overnight under vacuum to remove all the remaining solvents.

2.2.2 Electrospinning conditions

Plain electrospinning solutions have been prepared by dissolving the right amount of polymer into the selected solvent mixture and stirring until clear viscous solutions were obtained, after that the solutions were transferred into a glass syringe and electrospun by mean of the apparatus described in paragraph 2.2.1. The operative electrospinning conditions as well as the used polymer concentration and solvent mixture are reported in Table 5. All the loaded electrospun mats (DK and NPs loaded) were prepared by applying a pre-solubilization step in which the specific loaded molecule/particles have been solubilized before starting the process of polymer solubilization. In particular NPs loaded scaffolds have been prepared by stirring for 24h the NPs into the amount of DMF that was used to prepare the final electrospun mixture. DK loaded scaffolds have been prepared first by dissolving the molecules into HFIP and DMF respectively and then using the obtained solutions to prepare the relative electrospinning mixture.

Table 5. Electrospinning condition used for the scaffold fabrication

Polymer	Concentration (% w/v)	loading (%w/w)[a]	Solution composition	Flow rate (mL/h)	Voltage (kV)	Distance (cm)
PLLA	13	n.a	DCM:DMF 65:35	1.2	20	20
PLGA5050[b]	35	n.a	DMF:DCM=70:30	0.8	18	20
PLGA5050+NPs [b]	35	2	DMF:DCM=70:30	0.8	18	20
PLGA7525 [b]	25	n.a	DMF:DCM=70:30	0.8	18	20
PLGA7525+NPs [b]	25	2	DMF:DCM=70:30	0.8	18	20
HMW-ABA	25	n.a	DMF:DCM=65:35	1.2	20	20
PEOT30PBT70 PEOT70PBT30	20	n.a	HFIP	1.2	19	18
PEOT30PBT70+DK PEOT70PBT30+DK	20	5	HFIP	1.2	20	18
α,ω-triethoxysilane-terminated PCL	35	n.a	THF:DMF=80:20 +0,54% w/w H_2O +0,011% w/w HCl	0.6	17	25

[a] Drug concentration with respect to the dissolved polymer
[b] Electrospinning process performed at RH of 80%

2.2.3 Composite fabrication

The following operative instructions are related to the fabrication of plain and dual drug loaded composites made of PEOT30PBT70 and PEOT70PBT30 electrospun fibers embedded within a partially reticulated gelatin layer. The composites were designed to achieve a dual drug release with two different kinetics, a fast release of an anti-inflammatory drug and a sustained release of a model anticancer drug. Polymeric electrospun scaffolds have been selected due to the possibility to simultaneously sustain cellular proliferation while releasing the embedded drug. Gelatin was selected due to its hydrophilicity and tunable crosslinking density that allows to both control drug release and gelatin solubilization, making it possible to fast release the loaded drug while exposing the embedded fibrous structure. Gelatin is also exploited to act as a barrier layer allowing to slow down, by playing with its thickness and reticulation extent, the release kinetics of the drug embedded into the electrospun scaffolds.

The plain gelatin solution was prepared at concentration of 10% w/v in water and has been reticulated with 1% w/w of genipin in respect to the amount of used gelatin. The CTC loaded gelatin solution were prepared at 10% w/v in water and reticulated with 0,5% or 1% of genipin; both solutions have been loaded with 2% w/w of CTC with respect to the amount of used gelatin. Two different composites have been fabricated, here defined as mono and double layer composites.

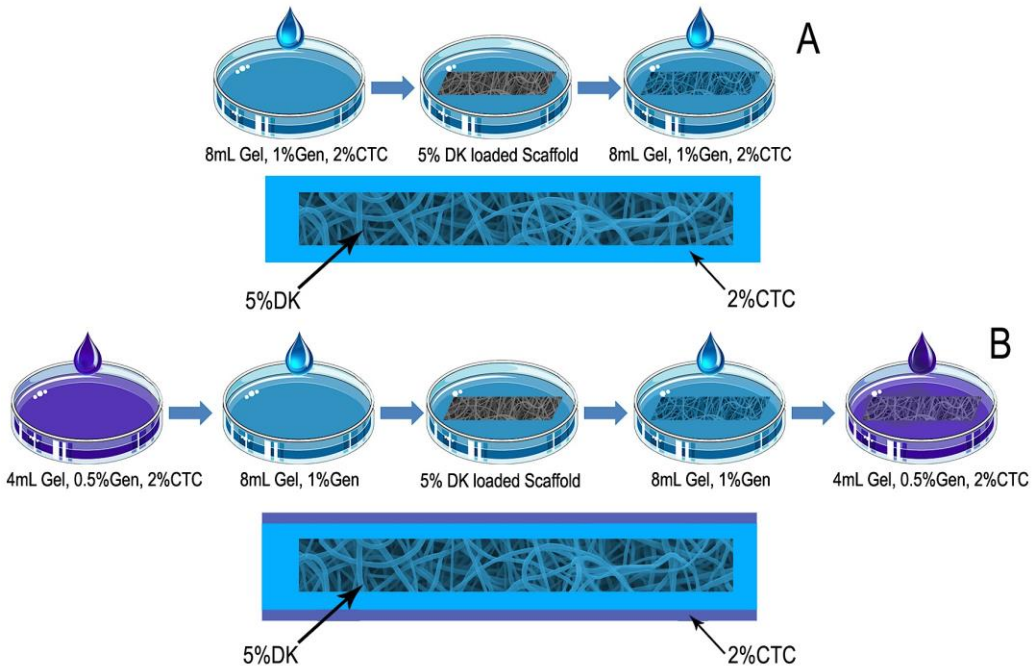

Figure 19. Schematic representation of the fabricated composites. (A) Mono-layer composites and (B) double-layer composite

Mono layer composites have been prepared as follows: after pouring 8 mL of CTC loaded gelatin with 1% of genipin into a 5 cm polystyrene petri, and let it solidify for about 30 minutes at 4°C, a DK loaded electrospun scaffold (0,5x4 cm) was laid over the obtained surface and left until wet. Later, 8 mL of the same gelatin mixture was poured over the electrospun scaffold obtaining the final mono-layer composite (Figure 19 A). Plain mono layer composites have been prepared as described above but without the addition of drugs. A double layer composite was prepared as follows: 4mL of CTC loaded gelatin solution with 0,5% of genipin were poured over a 5 cm polystyrene petri and let it solidify for about 30 minutes at 4°C. Later, 8 mL of gelatin with 1% of genipin were dropped over the previously prepared film and after 30 minutes at 4°C a DK loaded electrospun scaffold (0,5x4 cm) was laid over the obtained surface and left until wet. To complete the double layer composites the remaining gelatin layers were prepared according to the first two reported steps (Figure 19 B). Plain double layer composites have been prepared as above described but without the addition of drugs. The obtained composites were left in fridge at 4°C for 24 h and, afterwards, left for other 24 h under laminar flow fume hood to dry.

2.3 Scaffold surface modifications

2.3.1 PLLA electrospun scaffold functionalization

In order to perform the bioconjugation of PLLA electrospun scaffold it was necessary to perform a previous functionalization step to generate the proper functional group to be exploited. To achieve this result a chemical or physical functionalization were carried out as follow. PLLA scaffolds were fixed by means of CellCrown supports (Scaffdex, Tampere, Finland), in a 24-well plate and immersed in H_2O:EtOH 90:10 for 10 minutes and subsequently washed twice with distilled water, after they were incubate with sodium hydroxide (NaOH, 0,01M) solution for 5 minutes to generate the –COOH groups. Afterward, they were abundantly washed with distilled water. The –COOH groups were also obtained by mean of plasma treatment, performed by Prof. Colombo and collaborators at Industrial Engineering Department (DIN) of University of Bologna. The dielectric barrier discharge (DBD) plasma source, employed for the introduction of –COOH groups onto the surface of PLLA electrospun scaffolds, consisted of two aluminium parallel-plate electrodes; the upper electrode, having a surface of 13 × 8 cm and a thickness of 0,13 mm, was covered by a dielectric polyoxymethylene (POM-C) plate, having a surface of 15 × 11 cm and a thickness of 2,4 mm and was connected to the high voltage (HV) generator; while the lower electrode, with a surface of 13 × 9 cm and a thickness of 0,13 mm, was grounded. The plasma source was enclosed in a volume having a size of (21 × 17 × 3) cm^3 (L × W × H) to perform the treatment in a controlled atmosphere by introducing specific gases or gas mixtures. The gas mixtures used for the volume saturation and the plasma discharge generation are introduced from the top of the plasma reactor through a rilsan tube (diameter 6 mm) connected to the gas flow meter. A bleed port (1 cm diameter) was placed on a side wall of the plasma reactor for removing the air at the beginning of the process and for keeping a constant pressure inside the close volume during the process itself. The DBD plasma source was driven by a commercial pulsed DC generator (FID GmbH-FPG 20-1NMK) producing high-voltage pulses with a slew rate of 3–5 kV ns^{-1}, a pulse duration around 30 ns, a peak voltage (PV) of 7–20 kV, and an energy per pulse of 50 mJ at maximum voltage amplitude into a 100–200 V load impedance, with a maximum pulse repetition rate (RR) of 1000 Hz. During the plasma treatment, the scaffolds were placed onto the grounded electrode and directly subjected to the plasma discharge. The plasma was generated by fixing the gap between the rounded electrode and the POM-C plate at 0.5 mm and setting the PV and RR at 10,4 kV and 500 Hz, respectively. A treatment time of 5 minutes was adopted.

2.3.2 PLLA electrospun scaffold conjugation

PLLA mats carrying –COOH groups at their surface (functionalized) were activated with EDC/sNHS in 0,1 M MES (pH 5,0) buffer and incubated with Ab-FITC and at different concentrations, time, pH and temperature, as indicated in the results and discussion sections. As a negative control, the reaction was performed on PLLA hydrolyzed or PLLA plasma-treated without EDC/sNHS activation to evaluate non-specific binding of Ab-FITC to the fiber surface. The data are shown after the subtraction of the negative control. Anti-CD10 was also conjugated to the –COOH functionalized PLLA scaffold. Briefly, the anti-CD10 antibody was conjugated onto the previously activated –COOH at three different concentrations (1, 5, 10 μg ml−1) in 0,1 M PBS overnight at 4 °C. In order to verify the anti-CD10 antibody immobilization, Ab-FITC at 1:200 dilution in 0,1 M PBS (2 h at RT) was used.

In order to evaluate the amount of COOH group generated during the functionalization step the PLLA scaffold has been conjugated with FITC as follow. Briefly, functionalized PLLA scaffolds were fixed by means of CellCrown supports and activated by incubation with 10 mM EDC and 10 mM sNHS in 0,1 M MES buffer (pH 5) for 30 min at RT. The solution was removed and the mats were incubated with diaminobutane (0,01 M) in 0,1 M carbonate buffer (pH 9.8) for 1h at RT and rinsed three times for 5 min with carbonate buffer. Finally, the mats were incubated with 10^{-4} M FITC in carbonate buffer for 2h at RT and rinsed three times in phosphate buffer saline (PBS) solution for 5 min. Negative control was obtained by omitting the presence of reactive reagents (EDC and sNHS) in the above described procedure in order to evaluate non-specific binding of FITC to the fiber surface. The mean intensity fluorescence is shown after the subtraction of the negative control.

2.4 Poly(L-lactic acid)-poly(propylene azelate-co-propylene sebacate)-poly(L-lactic acid), (HMW-ABA) synthesis

The synthesis of the high molecular weight triblock copolymer poly(L-lactic acid)-poly(propylene azelate-co- propylene sebacate)-poly(L-lactic acid) [PLLA- P(PAz60PSeb40)- PLLA], herein defined HMW-ABA, involved three steps, as outlined in Scheme 1. Prof. Nadia Lotti and co-workers synthesized the obtained polymer at Department of Civil, Chemical, Environmental, and Materials Engineering (DICAM) of University of Bologna trying to achieve the thermal properties suggested by Prof. M. L. Focarete and co-workers in order to obtain a shape memory polymer with a transition temperature around human body temperature.

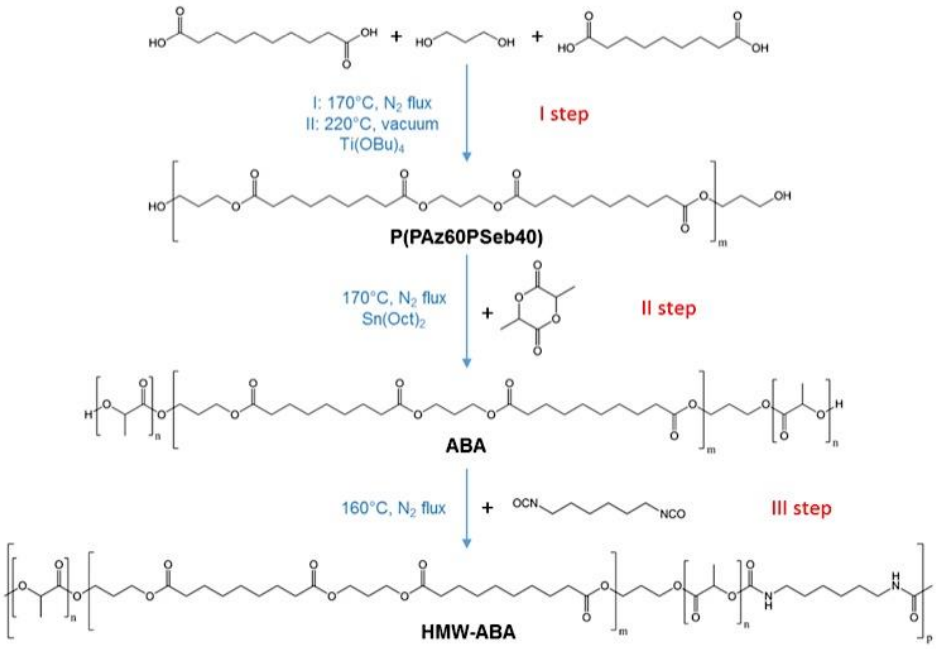

Scheme 1. Reaction Scheme for the Synthesis of the HMW-ABA Copolymer.
Reprinted with permission from Biomacromolecules, 2017, 18 (8), pp 2499–2508.

Random hydroxyl-terminated poly(propylene azelate-co-propylene sebacate) (60/40), P(PAz60PSeb40), herein defined B block, was synthesized by reacting 1,3-propanediol with a mixture of the two dicarboxylic acids: 60 mol % azelaic and 40 mol % sebacic (Scheme 1, I step). To obtain an OH-terminated prepolymer, an excess (60%) of 1,3-propanediol with respect to the dicarboxylic acids was employed. The reaction was carried out in bulk according to the standard melt polycondensation procedure by employing Ti(OBu) as catalyst (about 150 ppm of Ti/g of polymer). The first part was run at 170 °C under nitrogen flux until over 90% of the theoretical water distilled off (about 70 min). In the second part, the temperature was increased to 220 °C and the pressure was gradually reduced to 0,01 mbar to aid the removal of the excess of glycol. The reaction was stopped after additional 120 min. The obtained B block was purified by dissolution in chloroform and reprecipitation in methanol and was dried at room temperature (RT) under vacuum for at least 7 days prior to further use.

The PLLA-P(PAz60PSeb40)-PLLA triblock copolymer (ABA) was synthesized by ring-opening polymerization (ROP) of L-lactide, by using P(PAz60PSeb40) prepolymer as initiator (L-lactide: P-(PAz60PSeb40) ratio equal to 4:6 by weight) and Sn(Oct) (100 ppm/g of polymer) as catalyst (Scheme 1, II step). The reaction was carried out in the melt at 170 °C under nitrogen flux. To further increase the molecular weight of the triblock copolymer, HDI has been used as chain extender, thus, leading to the

formation of urethane bonds. An equimolar amount of HDI with respect to the OH-terminal groups of P(PAz60PSeb40), as measured by NMR,was added to the reaction mixture after about 3 h (Scheme 1, III step). The temperature was set to 160 °C and the reaction was allowed to continue for another 45 min. The chain extended ABA copolymer, hereafter referred to as HMW-ABA, was purified by dissolution in chloroform and reprecipitation in methanol and was dried at RT under vacuum for at least 7 days prior to further characterization.

2.5 PEG-poly(CL/DDL/HDL-co-DO) synthesis and nanoparticles preparations

Three different reaction sets containing DO, MeO-PEG-OH, N435 (5 wt % vs total substrate) and CL, DDL, HDL respectively were magnetically stirred in toluene (200 wt % vs total substrate) at 70 °C under nitrogen (1 atm) for 25 h. At the end of the reactions, the product mixtures were added to n-hexane and stirred for 45 minutes to precipitate the formed copolymers. The copolymers were then dissolved in chloroform, and filtered to remove the catalyst particles. The filtrate were concentrated and dropwise added to a stirring solution of n-hexane to reprecipitate the copolymers. Finally, after washing with fresh n-hexane, the purified copolymers were dried under 1.0 mmHg at 40 °C for 18 h.

NPs were fabricated by using a modified emulsion technique. Briefly, 25 mg of copolymers were dissolved in 500 µL of DCM. CL and HDL based copolymer solutions were dropwise added to a PVA aqueous solution (4 mL, 1 wt/v%) while DDL based copolymer solutions were dropwise added to 4 mL of distilled water, all under vortex. The obtained emulsions were sonicated 3x10” at 0 °C. CL and DDL based copolymers emulsion were poured into a beaker containing 15 mL of deionized water, stirred for 1 minute and subsequently connected to a rotary evaporator for 15 min to remove the residue DCM. HDL based copolymers emulsion were poured into a beaker containing 25 mL of deionized water and stirred overnight. CL and HDL based NPs were washed by mean of centrifuge at 12K rpm, 15’x3 removing each time the supernatant and adding fresh water. HDL based NPs were filtered with 0,22 µm syringe filter to remove aggregates (higher than 400-500nm).

2.6 Drug release studies

2.6.1 Diclofenac Potassium and Chlorotetracycline-hydrocloride release

DK and CTC cumulative release from mono and double-layer composites, as well as from DK loaded electrospun scaffolds, have been evaluated in-vitro. Release studies have been carried out on rectangular stripes (0,9x3cm) placed inside test tubes filled with 10 mL of PBS buffer (pH 7,4) and left shaking into a SW22 Julabo shaking water bath at 37°C, 50 rpm for a maximum period of 15 days. At regular intervals, the supernatant was completely removed, analyzed by means of HPLC, and replaced with fresh buffer. The loading efficacy evaluation of each sample was performed as follow. A small amount of material representative of the sample was dissolved it in the proper solvents and the extracted mixture was analyzed by mean of HPLC. The amount of drug determined analyzing the extracted mixture was used to calculate the exact amount of drug embedded into each sample. This step was necessary in order to correctly calculate the cumulative drug release % over time. HPLC analysis have been performed in collaboration with Prof. Nadia Passerini at department of pharmacy of University of Bologna.

2.6.2 Core shell silica nanoparticles release

Two rectangular samples (≈ 100 mg) of PLGA5050 and PLGA7525 electrospun mats loaded with 2% w/w of NPs in respect to the polymer were wetted under vacuum and immersed in 20 mL of PB solution (pH=7,4). The solution was left stirring on a SW22 Julabo shaking water bath at 37°C and 50 rpm for 50 days. At fixed time all the PB solution was removed, analyzed, and replaced with fresh one. Photophysical measurements were performed in order to determine the amount of NPs dissolved into the PB solution at each time. Fluorescence spectra were recorded with an Edinburgh FLS920 instrument equipped with a Hamamatsu R928P photomultiplier. Quartz cuvettes with an optical path length of 1 cm were used. Fluorescence spectra were recorded from 550nm to 750 nm after 530 nm irradiation. Fluorescence calibration curve was obtained by mean of NPs solution at known concentration. The loading efficiency evaluation of each sample has been performed by dissolving it in the proper solvents the NPs loaded scaffold thus extracting the loaded drugs and analyzing the obtained solution by mean of fluorescence spectra.

2.7 Characterization methods

Fiber morphology was observed with a Philips 515 scanning electron microscope (SEM) at an accelerating voltage of 15 kV. Prior to SEM analysis, samples were sputter-coated with gold. The distribution of fiber diameters was determined through the measurement of about 250 fibers by means of an acquisition and image analysis software (EDAX Genesis) and the results were given as the average diameter ± standard deviation (SD).

Static water contact angle (WCA) measurements were performed at RT by using an optical contact angle and surface tension meter KSV's CAM 100 (KSV, Espoo, Finland), by recording the side profiles of Milli-Q water drops for image analysis. The water drop profile images were collected in a time range of 0–60 s, by recording an 10 images every 1 s. Results were averaged on at least five measurements obtained in different areas of the sample.

Polymer molecular weight data were obtained by gel permeation chromatography (GPC) at 33 °C using a KNAUER Advance Instruments system equipped with three columns (Agilent) connected in series as follow: two PLgel minimix C (PM range from 200–2 000 000 g mol^{-1}, 250 mm/4,6 mm length/i.d.) and a PLgel minimix E (PM range up to 30 000 g mol^{-1}, 250 mm/4,6 mm length/i.d.). Polystyrene standards in the range of molecular weight 2000–100 000 g mol^{-1} were used and a refractive index detector was employed. Chloroform was used as eluent with a 0,3 ml min^{-1} flow and sample concentration of about 10 mg ml^{-1} was applied.

Fluorescence characterization has been performed using a Nikon eclipse E600 microscope (Nikon, Italy) equipped with digital CCD camera Q Imaging Retiga 20002V (Q Imaging, Surry, BC, Canada). All images were taken with a 10x objective (10× /0.50 NIKON Plan Fluor). The images were analyzed using Imaging NIS Elements software. Images from at least five different fields for each sample were analyzed in order to obtain the mean fluorescence intensity. Furthermore for each of these fields the average intensity of eight different areas has been calculated. Data were expressed as mean ± SD.

Thermal characterization of the electrospun mat was carried out by means of differential scanning calorimetry (DSC Q100; TA Instruments), on about 5 mg sample. The DSC traces allowed to evaluate the glass transition temperature, T_g, the T_c, as the exothermal peak temperature of the cooling run, and the Tm, as the peak of the endothermal peak; from this latter curve also, the heat of fusion (ΔH_m) was determined, and the crystallinity content was evaluated by considering the ΔH_m of the 100% crystalline polymer.

Thermogravimetric analyzer Q500 (TA Instruments, New Castle, Delaware, USA) was used to perform thermal degradation tests (TGA). The analyses were carried out on samples of 5-10 mg, under nitrogen flow. The program involved heating from room temperature to 700 °C, with a temperature ramp of 10° C / min.

^{1}H and ^{13}C NMR spectra were recorded on an Agilent 500 spectrometer.

The following table summarizes the characterization methods used for each experimental work.

	SEM	DSC	TGA	WCA	GPC	NMR	Fluorescence microscopy
Shape memory PCL	✓	✓	✓				
Shape memory HMW-ABA	✓	✓			✓	✓	
Luminescent NPs release	✓	✓	✓		✓		
Dual drug release composites	✓	✓	✓	✓			
Anti CD-10 conjugated PLLA	✓			✓			✓
PEG-poly(CL/DDL/HDL-co-DO) NPs	✓				✓	✓	

2.7.1 Shape memory evaluation

Thermo-mechanical cycles were carried out on the thermally treated material to investigate one-way shape memory behavior of SM PCL and SM ABA scaffolds. The tests were carried out using DMA Q800 (TA Instruments, New Castle, Delaware, U.S.A.) in tensile configuration on rectangular strips (average overall length: 20 mm; average gauge length: 7 mm; average cross-section: 0,5 mm^2). A traditional shape memory cyclic history was adopted, consisting in the following steps: (i) heating the specimen above transition temperature (T_{trans}), i.e. above the polymer T_m; (ii) deforming the specimen above T_{trans} up to a given level of strain, ε_{appl}, (iii) cooling the specimen under T_{trans} in fixed strain condition, and then unloading; (iv) monitoring the strain recovery during a heating ramp at 3°C min^{-1} to above T_{trans}. During the heating step (i) and recovery step (iv) the specimen was maintained under a constant load of 0,005 N. This load was necessary to maintain the specimen in tension during the heating ramps, to monitor its quasi stress-free strain changes and to avoid buckling and wrinkles. Concerning the SM ABA scaffolds, beside the normal above described one-way shape memory cycle, in some experiments, thermal annealing was applied to the sample after the fixing step. Briefly, at the end of the programming step, the sample was quenched to −60 °C, equilibrated at the annealing temperature (either 15 or 30 °C) for 180 min and cooled down to −60 °C. The recovering step was then performed as described above.

The one-way shape memory capabilities were described in terms of strain fixity, which quantifies the amount of the applied strain fixed at the end of the cooling step, and strain recovery, representing the

amount of applied strain recovered by the specimen by heating up to above T_{trans}, and thus the ability to recover to its pristine strain. These parameters are evaluated as follows:

$$Strain\ Fixity\ (\%) = R_f = (\varepsilon_{unload} / \varepsilon_{applied}) x100$$

where $\varepsilon_{applied}$ is the applied deformation (end of step ii) and ε_{unload} is the strain after load removal (end of step iii).

$$Strain\ Recovery\ (\%) = R_r = [(\varepsilon_{applied} - \varepsilon_{rec})/(\varepsilon_{applied} - \varepsilon_0)] x100$$

where ε_{rec} is the residual strain measured after the heating ramp (end of step iv), and ε_0 is the pre-strain measured before deformation (end of step i).

2.7.2 PEG-poly(CL/DDL/HDL-co-DO) nanoparticle characterizations

The particle size, size distribution and Z potential of the obtained NPs were measured by dynamic light scattering (DLS) using a Malvern Nano ZS instrument (Malvern Instruments Ltd, Malvern, UK) equipped with a 633 nm laser diode. Measurements were performed in deionized water at 25°C. Storage stability were investigated by measuring the size distribution variation after freezing, freeze-drying and after keeping the NPs at constant temperature of 4°C (DDL and HDL based copolymers) and 37°C (CL based copolymer) for 4 days.

3 Results and discussion

3.1 Smart scaffolds for tissue engineering

3.1.1 Electrospun shape memory PCL

A polymeric material in order to show a shape memory behavior should be characterized by the presence of a proper network formed by switching phase and net-points. The first are necessary to recall the permanent shape at the end of a thermomechanical cycle while the latter enable to fix the temporary shape at the end of the fixing step of a thermomechanical cycle (166). PCL is characterized by a switching phase, the crystalline phase, but it lacks of a proper net point structure that in this work, was achieved by exploiting the reactive terminals of a previously synthesized α-ω triethoxysilane-terminated PCL to perform a sol gel crosslinking reaction. The density of the reactive terminals is directly correlated to the molecular weight of the starting material, and a more crosslinked system can be more easily achieved by starting from a low molecular weight α-ω triethoxysilane-terminated PCL rather than from a high molecular weight one. On the other hand it is well known that an efficient electrospinning process is usually obtained with high molecular weight polymers. Considering these two opposite aspects a α-ω triethoxysilane-terminated PCL with M_n of about 10 000 g mol^{-1} was used. This polymer was selected on the basis of its M_w, it was the one with the highest molecular weight among the previously synthesized (167), and shape memory performance after sol–gel crosslinking, in fact this polymer exhibited a promising SM behavior in bulk state, i.e. the number of reactive terminals of the polymer was high enough to create a covalent net-point network featuring shape memory capabilities. Preliminary experiments to produce non-woven fibrous mats consisted in electrospinning solutions of not crosslinked α-ω triethoxysilane-terminated PCL in THF:DMF=80:20 (v/v) at increasing polymer concentration. All the performed experiments resulted in the collection of polymeric beads rather than fibers (see Figure 20 A as an example).

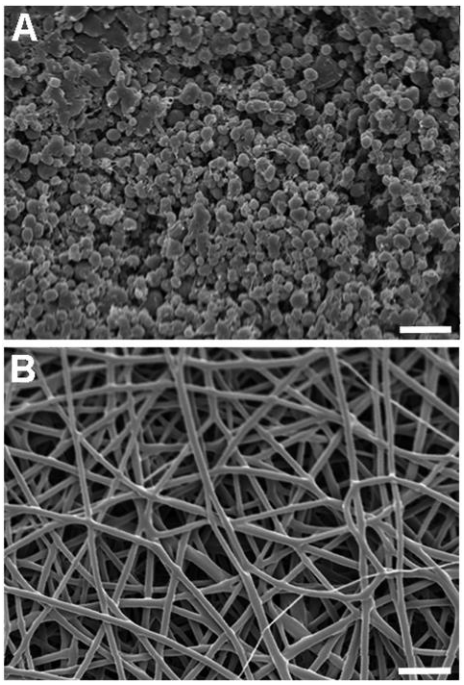

Figure 20. SEM images of the electrospun meshes obtained from (A) 35% w/v α,ω-triethoxysilane-terminated PCL solution in THF : DMF = 80 : 20 (v/v) and (B) 35% w/v α,ω-triethoxysilane-terminated PCL solution in THF : DMF = 80 : 20 (v/v) with the addition of H_2O and HCl (sol–gel solution). Scale bars = 20 μm.

It is well known that solution viscosity, determined by polymer molecular weight and polymer concentration, is the key parameter that defines polymer processability into continuous fibers through electrospinning. Indeed, it was demonstrated that chain entanglement concentration is the main parameter that influence fiber formation during electrospinning (168) for a specific polymer with a defined molecular weight, and the minimum concentration at which a polymer can produce uniform fibers is related to the entanglement density of the polymer solution (168,170,171). In the presence of elastically deformable entanglement network obtained above a critical polymer concentration and/or polymer molecular weight, viscoelastic forces are high enough to allow the generation of continuous fibers and the polymer is collected in the form of bead-free fibers. In the case of our polymeric system, with the aim of increasing entanglement density and hence solution viscosity, the reactive triethoxysilane terminal groups have been activated by adding to the polymer solution water and HCl. The resultant sol–gel solution of α-ω triethoxysilane terminated PCL was electrospun and continuous bead-free fibers were obtained (Figure 20 B). It is worth noting that by further increasing the amount of water and HCl the polymer solution turned into a gel after few hours of stirring and electrospinning was not possible. The dramatic change of morphology, from polymer beads into continuous fibers achieved by the addition of a

low amount of water and acid can be explained by the occurrence, in the sol–gel solution, of a partial crosslinking reaction before electrospinning process (herein defined pre-crosslinking), schematically represented in Figure 21 A.The pre-crosslinking led to the formation of Si–O–Si linkages between polymer chains, as a consequence of hydrolysis of the triethoxysilane terminal groups and their condensation, and therefore to an increase of PCL molecular weight, thus obtaining an electrospinnable solution (Figure 21 B) that provided bead free fibers (Figure 20 B).

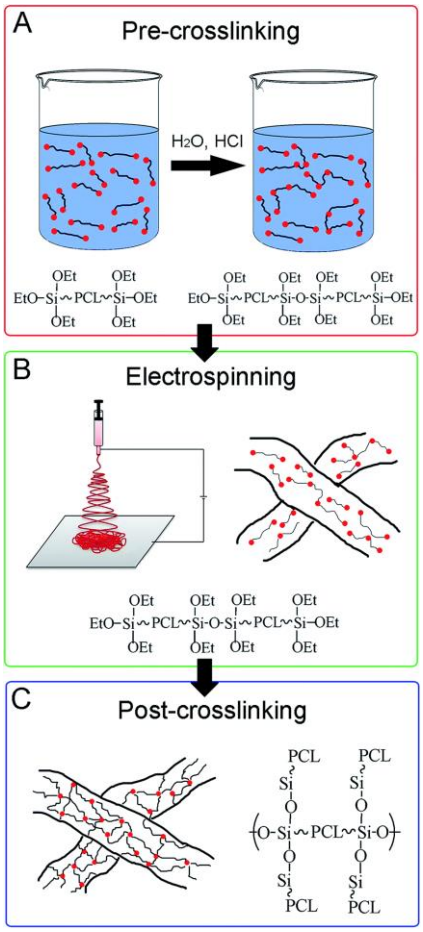

Figure 21. (A) Pre-crosslinking: α,ω-triethoxysilane-terminated PCL solution was subjected to a partial sol–gel reaction to increase polymer molecular weight, due to the formation of Si–O–Si crosslink points. (B) Electrospinning: the pre-crosslinked solution was electrospun to obtain partially crosslinked fibers. (C) Post-crosslinking: the attained electrospun mat was subsequently thermally post-crosslinked achieving a semicrystalline crosslinked electrospun shape memory polymer.

Rheological analysis was performed to verify that the change of electrospun polymer morphology from beads to defect-free fibers was related to a change of solution viscosity. The viscosity of the formulation that led to bead-free fibers after several hours of stirring was monitored at different times after solution

preparation (Figure 22). The viscosity of the solution, initially too low to provide bead-free fibers, slightly increased during the first hour of stirring at RT (from 0,032 Pa s to 0,034Pa s, Figure 22, curve A and B) and rapidly increased after 2 hours (0,065 Pa s, Figure 22, curve D), reaching a value of 0,11 Pa s after 17hours of stirring (Figure 22 curve E) when an electrospinnable solution, that led to a bead-free electrospun mat, was obtained.

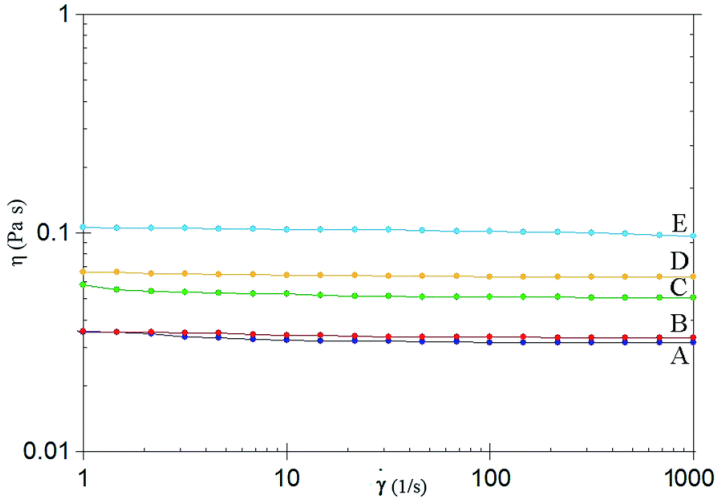

Figure 22. Flow curves of 35% w/v α,ω-triethoxysilane-terminated PCL in THF : DMF = 80 : 20 sol–gel solution acquired during the partial pre-crosslinking treatment at different times at RT. (A) t = 0' (B) t = 60' (C) t = 100' (D) t = 120' (E) t = 17 h.

As already mentioned, by increasing the water and acid concentration, the solution turned into a not electrospinnable gel in few hours. Therefore, the use of small amounts of $H_2O$and HCl activated only a fraction of triethoxysilane reactive terminals for the generation of a limited number of Si–O–Si covalent bond. The α-ω triethoxysilane-terminated PCL electrospun mat was thus subjected to a post-crosslinking treatment (Figure 21 C) in order to increase the net-points density between the macromolecular chains. The post-crosslinking treatment was performed by exposing the mats to acid aqueous vapors that induced the formation of further Si–O–Si covalent bonds to generate a 3D network of PCL macromolecules. It is well known that increasing the temperature it is possible to accelerate condensation reactions. However, for not compromising the morphology of the obtained fibers the post crosslinking treatment had to be carried out at a temperature below polymer T_m. DSC analysis of the partially crosslinked electrospun α-ω triethoxysilane-terminated PCL showed a T_g around -60°C and a broad endotherm in the temperature range 40–70 °C, with a maximum peak around 55 °C (T_m). Electrospun mats were kept at different temperatures (below PCL T_m) in order to determine the highest one that enables the maintenance of fiber morphology for the successive post crosslinking treatments. In

Figure 23 SEM images of the electrospun PCL samples stored at different temperatures (45°C and 50°C) for 1 h are reported, revealing that both the investigated temperatures caused a small increase of fibers diameter from around 1,8 µm to around 2,2 µm.

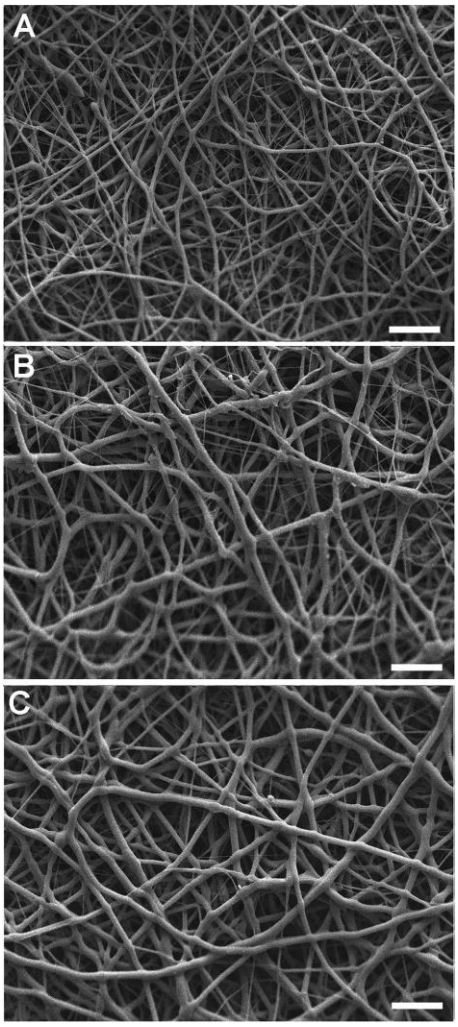

Figure 23. SEM images of the electrospun PCL mat at (A) RT, (B) after 1 h at 45 °C and (C) after 1 h at 50 °C. Scale bars = 20 µm.

Furthermore it is pointed out that the mat stored at 50 °C underwent a small macroscopic shrinkage due to the melting of a small fraction of polymer crystal phase (in accordance with DSC results), thus no higher temperatures were tested and 50 °C was selected as the operating temperature for the post-crosslinking treatments. Post-crosslinking was carried out by keeping the electrospun samples at 50°C either for 3 h or 72 h, in order to achieve two different crosslinking degrees (PCL-low and PCL-high) that were subsequently quantified in terms of degree of swelling (Q) in THF and gel content (G) according to following equations:

$$Q = \frac{V_s}{V_d} = 1 + \frac{\rho_2}{\rho_1}\left(\frac{m_s}{m_d} - 1\right)$$

$$G = \frac{m_d}{m_0} \times 100$$

Were V_s is the volume of the swollen mat, V_d is the volume of the dried mat, ρ_1 is the THF density (0,889 g cm^{-3}), ρ_2 is the PCL density (1,094 g cm^{-3}) and M_s and M_d are the swollen and dried PCL mass respectively. Q and G of the starting electrospun mat were also determined for comparison. The mats immersed in THF are expected to swell to a certain extent, according to their crosslink density. Concomitantly, the macromolecular chains not involved in the molecular network dissolve in THF. Therefore, with the increase of crosslinking degree the Q value is expected to decrease while the G value is expected to increase. The values reported in Table 6 confirm the expected increase of crosslinking density after post-crosslinking treatments. Indeed, after 3 h and 72 h at 50°C, the G value of the as-spun PCL mat increased from 33,4% to 60% and 81,4%, respectively, while Q values decreased from 44 v/v to 5 v/v and 1,54 v/v**,** respectively.

Table 6. Degree of swelling (Q) and gel content (G) of the as spun and prost-crosslinked PCL mats

Sample	Q (v/v)	G (%)
As-spun PCL	44 ± 5	33.4 ± 0.6
PCL-low	5.0 ± 0.3	60.0 ± 0.4
PCL-high	1.54 ± 0.06	81.4 ± 0.2

The thermal properties of the post-crosslinked electrospun mats with two different crosslinking degrees were investigated through DSC test. Both PCL-low and PCL-high showed a T_g located at-60°C, T_m at 55°C and a T_c at 31°C; further, a high crystallinity content of about 41% was estimated from the heat of fusion of the second heating scan, accordingly with the previously obtained results in bulk state starting from PCL precursors with the same molecular weight (172). The dynamic mechanical response of the mats, investigated in DMA tests from RT to above T_m, is reported in terms of the storage modulus trace in Figure 24 A.

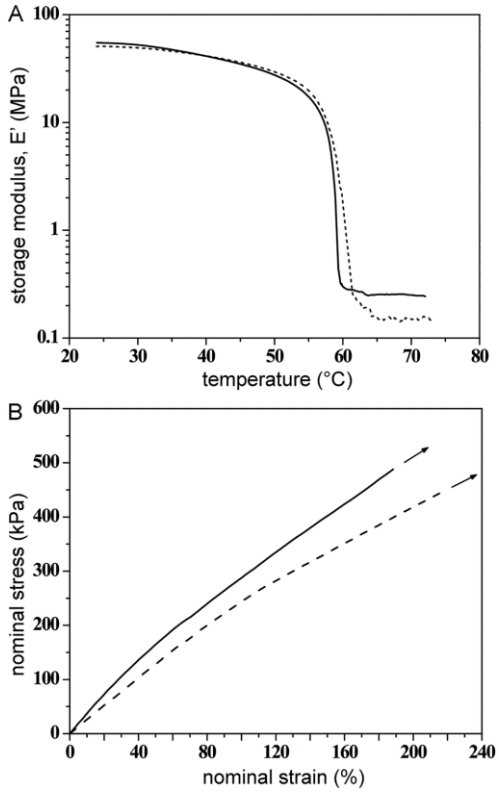

Figure 24. Thermo-mechanical properties in terms of storage modulus trace as a function of temperature (A) and of stress vs. strain curves above Tm (B) for PCL-high (continuous line) and for PCL-low (dashed line); the arrows are reported to indicate that the specimens did not break and may be further deformed.

The electrospun mats with two different crosslinking degrees show a very similar behaviour, with storage modulus values in the order of tens of MPa at RT, and approaching a drop of about two orders of magnitude when crossing the T_m. At higher temperatures, thanks to the crosslinked structure, a plateau is approached, at about 200 kPa for PCL-high and, as expected, at a slightly lower value for PCL-low. The mechanical behaviour in the rubbery plateau region was investigated in tensile tests performed at 80°C. The stress vs. strain relationship measured at this temperature was needed to evaluate the material behaviour in the deformation ramp of the shape memory cycle, and more specifically to evaluate the maximum strain that can be applied in a shape memory test. The results are reported in Figure 24 B. A tensile modulus of (320±30) kPa was measured for PCL-high and (200±40) kPa for PCL-low. A highly ductile behavior was shown by both mats, and when subjected to deformations of about 200% the specimen never displayed failure. The evolution of the microstructure with strain, for a deformation carried out in the rubbery-like region, was investigated, on PCL-high, by means of an ex situ SEM analysis of specimens deformed at various strain levels and fixed at the applied strain ε_{appl}, by means of cooling

below T_c under fixed strain conditions. The good fixing capabilities, as it will be discussed later, allow to refer to the actual specimen strain practically as to the applied strain value. The results are reported in Figure 6,comparing the morphology of an undeformed specimen (Figure 25 A) with that of various levels of strain (25%; 50%; 100%;185%; Figure 25 B–E, respectively).

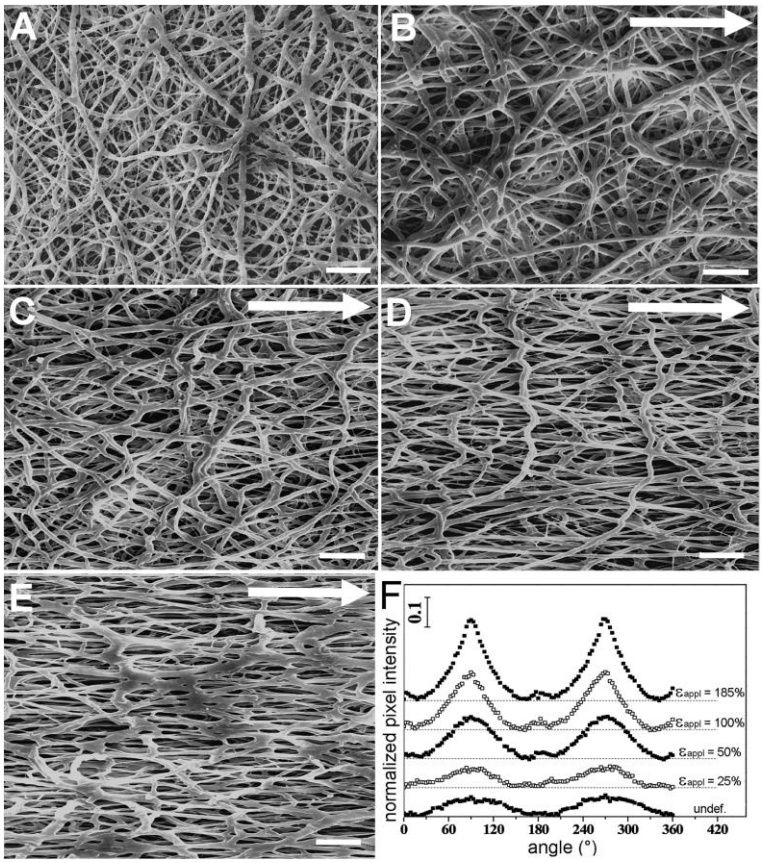

Figure 25. Images from the ex situ SEM analysis carried out on PCL-high. Figure refer to an undeformed specimen (A) and deformed at progressively higher strain levels ((B) 25%; (C) 50%; (D) 100%; (E) 185%), the strain direction (indicated by the arrow) being parallel with the major length of the image; (F) 2-D FFT frequency distributions of the corresponding SEM images (curves vertically shifted of an arbitrary quantity to improve readability). Scale bars = 20 µm.

A significant evolution of fiber architecture with the applied strain is highlighted, mainly consisting in a more pronounced alignment along the deformation direction as the strain increases. In particular, for strain levels above 50% the fibers show to be highly stretched and aligned along strain direction. To better highlight the alignment degree the images are accompanied by 2-D fast Fourier transform (2-D FFT) plots (Figure 25 F), representing the normalized intensity of the pixel along specific direction (0° representing a direction perpendicular to that of deformation). The curve of the undeformed specimen,

which shows two broad peaks can be considered as a reference curve for the pristine randomly oriented state. The more pronounced fibers alignment is clearly evidenced by the peaks at 90° and 270° which become more intense and narrower for strain levels above 25%. The progressive orientation along the strain direction occurs at first prevalently through rotational/flexural rearrangements of the fibers (Figure 25 B and C), which start to be effectively stretched at nominal strain above 50% (Figure 25 D and E). At the highest level of nominal strain explored (Figure 25 E) the stretching of the fiber networks becomes particularly relevant, as testified by the highly deformed appearance of the region on which the fibers overlap, as already shown in highly stretched non-woven membranes (173). This latter image indicates a significant fiber–fiber cohesion, presumably achieved during the processing and thermal history of the specimen, through post-crosslinking or local melting (174). Further it is shown that, on a micro mechanical point of view, the mats undergo important morphological changes with strain, evolving from the structure of a material governed by the fiber rearrangements to practically that of a highly porous material. The shape memory performances of the electrospun mats were investigated by means of a conventional one-way cyclic shape memory testing methodology, and a representation of the cycle is displayed in Figure 26 in terms of a strain–stress temperature curve for an applied strain ε_{ppl} =102% on PCL-high. The specimen is first "programmed" to set a temporary shape, and this part of the cycle consists in heating the material at a deformation temperature, T_{def}, above T_m (step i, Figure 26 A and B; the pre-strain level, 30, is attained), deforming the material at a given level of applied strain, ε_{ppl} (step ii; Figure 26 B and C) and cooling under fixed strain, after which the load is finally removed (step iii; Figure 26 C and D); no reliable values of the stress were measured in the cooling step, and for this reason in Figure 26 this part of the curve is represented as a dashed line.

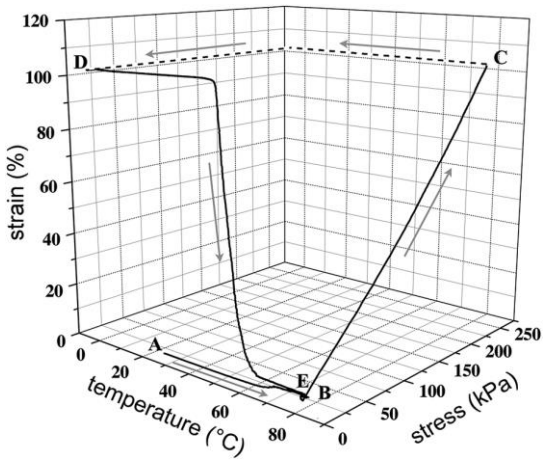

Figure 26. Thermo-mechanical history for a one-way shape memory cycle for ε_{appl} = 102% ((A and B) heating; (B and C) deformation; (C and D) cooling under fixed strain and unloading; (D and E) quasi stress-free recovery); cycle carried out on PCL-high.

After stress removal the residual strain at unloading (ε_{unload}) is measured and the strain reduction is further monitored during a heating ramp to temperatures above melting, until a final value of residual stress, ε_{rec}, is attained (step iv, D and E). On the values of ε_{unload} it was possible to evaluate the strain fixity, while on those of ε_{rec} the strain recovery capabilities were determined. In the cycle of Figure 7 a high percentage of both strain fixity values (100% of the applied strain is permanently set after load removal) and strain recovery (98% of the applied strain is recovered through heating induced actuation) are found. The recovery process was mainly localized in proximity of T_m, showing its steepest decrease at about 52°Cand an overall extent of the sigmoidal trend on a region between 50°C and 65°C. The shape memory response was investigated also at further levels of strain and for more subsequent cycles. The results for PCL-high are summarized in terms of strain fixity and recovery in Table 7 and represented in terms of strain evolution in Figure 27 A, which reports the strain recovery for various ε_{appl}, and in Figure 27 B, which reports the strain recovery for five consecutive cycles in case of ε_{appl} =106%.

Table 7. Strain fixity and strain recovery capabilities of different values of applied strain and after various shape memory cycles applied to PCL-high.

ε_{appl} (%)	1st cycle		2nd cycle		5th cycle	
	R_f (%)	R_r (%)	R_f (%)	R_r (%)	R_f (%)	R_r (%)
24	100	100	100	100	—	—
55	100	98	100	98	—	—
106	100	98	100	99	100	99

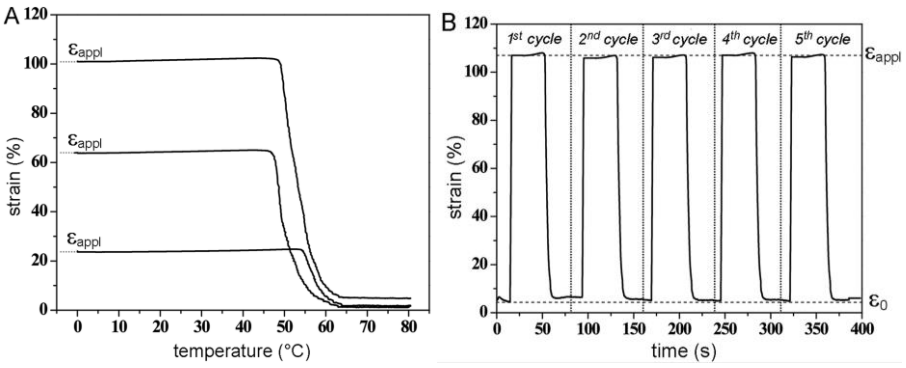

Figure 27. Strain evolution in a one-way shape memory cycle for various levels of applied strain (A) and within a five-fold cyclic history at ε_{appl} = 106% (B); cycles carried out on PCL-high; the dashed segments in (A) represent the values of deformation applied before unloading (ε_{appl}).

An overall similar recovery response is found for this material, independently from the strain level explored and the number of applied cycles. The shape memory response of PCL-low was investigated on single shape memory cycles at various strain levels, in order to verify if the reduction in crosslinking density compromises the shape memory response. The thermo-mechanical response is practically the same as that of PCL-high, and the results are reported in Table 8 in terms of strain fixity and strain recovery. High fixation and recovery capabilities are found at all the levels of strain explored, and only at the highest strain applied (225%) a slight reduction of the strain recovery to about 96% was found.

Table 8. Strain fixity and recovery capabilities in the case of PCL-low.

ε_{appl} (%)	Strain fixity (1st cycle) (%)	Strain recovery (1st cycle) (%)
45	100	100
60	100	100
125	100	100
225	100	96

The results show that also after this less extensive post-crosslinking treatment, the network structure developed is sufficient to still sustain large recovery capabilities. Other electrospun mats exploiting the T_{trans} of PCL reported in the literature (176- 178) display very interesting shape memory properties, with good strain fixity and strain recovery values that, however, are overall lower than those reported in Table 7 and Table 8 of the present work. For instance, the electrospun PDLCL fabrics described by Matsumoto and coworkers (177) exhibited good shape-memory properties with strain recovery of 89–95% and strain fixity of 82–83% after the 2nd cycle, when small deformations were applied at 60°C. The UV-crosslinked PCL mat fabricated by Gong et al. (178) exhibited shape recover of 90%and shape fixity of 74,5%, after the 1st cycle, that were increased up to 92% and 83.7%, respectively, by the addition of MWNTs coated with Fe_3O_4. The SM mat described by Chen et al.(176) had a shape fixing of (99,1±0.4)% and a shape recovery of (81.3±0.8)% in the three cycles of the stretching-recovery test. SEM analysis was carried out on PCL-high subjected to a single and five-fold shape memory cycle (Figure 28 A and B, respectively) at an applied strain of about 100% to evaluate changes in the fiber architecture after thermal activated recovery. The images show that shape recovery is accompanied by a recovery of the randomly oriented structures, also after the significant fiber alignment promoted by the applied strain (see Figure 25 D and F), and this finding is further confirmed by the close similarity of the 2-FFT plot of the recovered samples with that of the undeformed one, as shown in Figure 28 C.

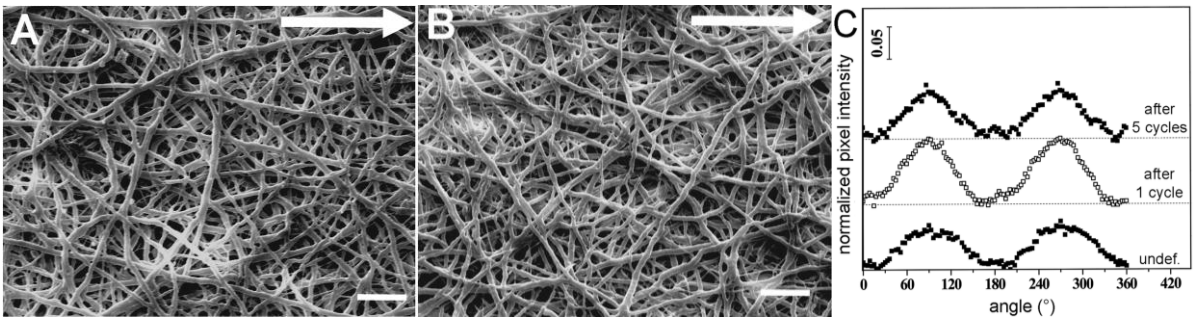

Figure 28. SEM images of PCL-high subjected to a single (A) and five-fold (B) shape memory cycle at $\varepsilon_{appl} \simeq 100\%$ (the arrow indicates the strain direction); (C) comparison of the 2-D FFT plot of the undeformed and recovered specimens. Scale bars = 20 µm.

In conclusion partially crosslinked α-ω triethoxysilane-terminated PCL solutions were successfully electrospun, allowing obtaining bead free fibrous non-woven mats. The viscosity of the electrospinnable solution was optimized by controlling the hydrolysis/condensation reaction time activated by water and HCl, while the crosslinking degree of PCL fibers was controlled by varying the exposure time of non-woven mats to acidic vapors. The mechanical properties (storage modulus and tensile modulus) in the rubbery plateau region were consequently governed by the crosslinking degree of PCL. The evolution of fiber architecture within the non-woven mat with the applied strain was observed: the fibers underwent rotational/flexural motions, reorienting as the strain increases and, for strain values higher than 50% the fibers became highly stretched and aligned along the direction of strain. All the prepared electrospun non-woven mats exhibited very good one-way shape memory properties as evidenced by high fixation and recovery capabilities, almost independently on the applied strain and the crosslinking degree of PCL fibers. These results were obtained through a straightforward and facile process, without any need of polymeric template or more complex approaches, obtaining a material with controllable ad adjustable crosslinking content.

3.1.2 Shape memory PLLA-based triblock copolymer (HMW-ABA)

In the current study, the molecular structure of the new high molecular weight ABA (HMW-ABA) triblock copolymer was specifically designed to display the thermal and mechanical properties requested to obtain a material with shape memory performance in the physiological temperature range. In particular, the P(PAz60Seb40) block (B block) was chosen as the switching segment, and based on the results of

previous work(182,183), it was synthesized with a chemical composition able to guarantee a crystal phase melting in the range of the physiological temperature. Poly(l-lactic acid), which melts at higher temperature than P(PAz60Seb40), (184,185) was chosen as a hard segment to provide the physical net-point. Prof. Nadia Lotti and co-workers synthesized the obtained polymer at DICAM department of the university of Bologna.

The chemical structure of the B block, evaluated by ^{1}H NMR (not shown), was consistent with the expected structure and the actual composition was very close to the feed, that is, 62,5% and 37,5% of PAz and PSeb co-units, respectively. ^{1}H NMR has been also employed for the determination of the molecular weight of the prepolymer. The calculated value (M_n = 11200 g/mol) is comparable to that obtained by GPC (M_n = 12500 g/mol, PDI = 2,2). It might be worth highlighting that the prepolymer synthesis procedure has been optimized to achieve a quite high molecular weight, while preserving a high amount of OH-terminal groups, needed for the ring-opening of the lactide monomer. Accordingly, titration experiments demonstrated a very low concentration of carboxylic terminal groups $(36 \pm 6) \times 10^{-3}$ mmol NaOH/g.

The HMW-ABA copolymer was obtained, as described in the Experimental Section and outlined in Scheme 1, by in situ ring opening polymerization of l-lactide, starting from P(PAz60PSeb40) prepolymer as initiator, and successive chain extension process through HDI addition, to increase triblock copolymer molecular weight. No unreacted HDI was detected by ^{1}H NMR after the purification process. The ^{1}H NMR spectrum of HMW-ABA is reported in Figure 29, together with the resonance assignments. The HMW-ABA copolymer is composed for the 62,7 mol % of A and for the 36,1 mol % of B. Moreover, 1,2 mol % of HDI has been incorporated into the polymer. GPC experiments evidenced that a high molecular weight was achieved and a good control over the whole polymerization process was maintained (M_n = 40000 g/mol, PDI = 2,2).

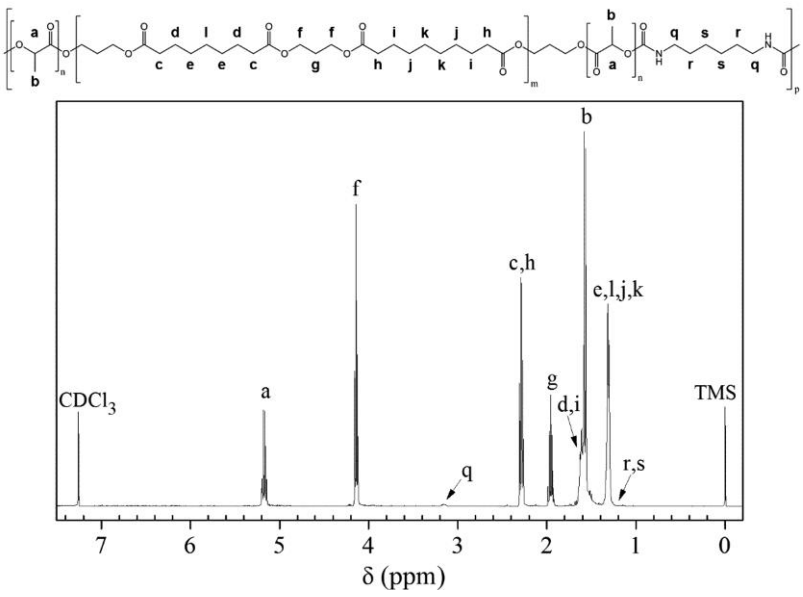

Figure 29. *^{1}H NMR spectrum of HMW-ABA with resonance assignments.*

Thermogravimetric analysis was carried out on the HMW-ABA copolymer, in order to evaluate its thermal stability, and on the plain B block for the sake of comparison (data not shown). Thermal degradation occurred in two distinct weight loss steps whose entity closely reflects copolymer composition, as calculated by ^{1}H NMR. The step at lower temperature (T_{max} = 272 °C) is attributed to the degradation of PLLA (A blocks), while that at higher T (T_{max} = 416 °C) to the decomposition of the B block, as confirmed by the TGA curve of the plain B block (T_{max} = 417 °C).

Figure 2 shows the calorimetric curves of the synthesized HMW-ABA triblock copolymer and of the B block for the sake of comparison, whereas the corresponding calorimetric data are reported in Table 1. The triblock copolymer (Figure 30 A) is semicrystalline and it is characterized by the thermal transitions of both the A and B blocks. The T_g at around −60 °C, and the multipeak melting endotherm in the temperature range 0–50 °C, can be ascribed to the softening of the glassy phase and to the melting of the crystal phase of the B block, respectively, on the basis of the calorimetric scan of B block (Figure 30 B). The high-temperature melting endotherm (T_m around 150 °C) is associated with the melting of PLLA block crystal phase while the PLLA T_g, which is assumed to be in the range 30–50 °C, is not observable due to the melting endotherm of the B block. The lower cold crystallization enthalpy value (ΔH_{cc}) compared to the melting enthalpy one (ΔH_m) in the second heating scan of the HMW-ABA copolymer (Table 9), demonstrates that the PLLA block partially crystallize during quenching from the melt.

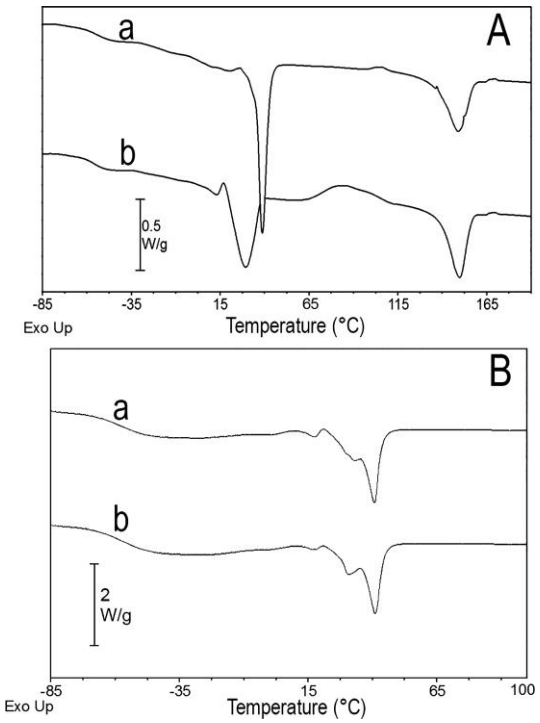

Figure 30. DSC scans of (A) HMW-ABA and (B) B block (a: first scan; b: second scan after quench).

Table 9. Thermal characterization of the HMW-ABA copolymer and of the B block

	B block				A block			
	T_g^a (°C)	ΔC_p^a (J/g °C)	T_m^a (°C)	ΔH_m^a (J/g)	T_{cc}^b (°C)	ΔH_{cc}^b (J/g)	T_m^b (°C)	ΔH_m^b (J/g)
HMW-ABA (1st scan)	–54	0.25	39	28	106	0.75	149	16
HMW-ABA (2nd scan)	–56	0.25	13; 29	19	86	12	150	17
B block (1st scan)	–57	1.48	17; 32; 41	48				
B block (2nd scan)	–57	1.64	17; 30; 41	47				

The HMW-ABA copolymer was successfully processed to obtain electrospun scaffolds made of randomly arranged bead-free fibers with a mean diameter distribution of 1,1 ± 0,2 µm (Figure 31 A,B). After the electrospinning process the polymer still displayed the characteristic thermal properties of the pristine material (see DSC scan in Figure 31 C): the low-melting crystal phase of the B block and the high-melting crystal phase of the A block. It is worth noting that the PLLA block is capable to partially crystallize during the electrospinning process, as demonstrated by the melting endotherm in Figure 31 C and by the absence of a significant cold crystallization exotherm. However, it is widely accepted that PLLA is a slowly

crystallizable polymer compared to many conventional thermoplastics (186) and as-electrospun PLLA fibers are known to be completely amorphous just after the process (187). The capability of the PLLA block to crystallize in our polymeric system can be reasonably related to its low molecular weight (estimated to be 4000 g/mol) that determines a shift of PLLA "crystallization window" to lower temperatures compared to the high molecular weight PLLA. This hypothesis is confirmed by both the not detectable PLLA T_g and the relatively low T_m (around 150 °C) of the PLLA segment. The enhanced mobility of the PLLA segment in this particular polymeric architecture leads to a faster crystallization kinetics and, therefore, to the development of a crystal phase during the electrospinning process. This is of primary importance for the designed material, since the presence of PLLA crystal phase is necessary for the scaffold to exhibit shape memory properties.

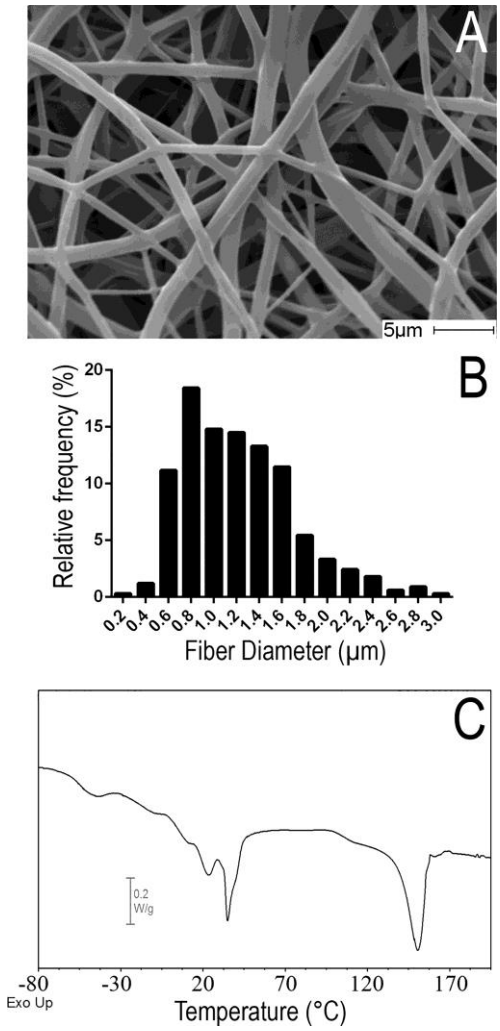

Figure 31. (A) SEM micrograph, (B) fiber diameter distribution, and (C) DSC (first scan) of electrospun HMW-ABA.

A thermomechanical cycle, as described in the Experimental Section, was used to characterize the shape memory properties of the electrospun copolymer. On the basis of the calorimetric results the cycle was planned by exploiting the B block crystal phase as molecular switch and the A block crystal phase as the physical network of the polymer chains. The material was (i) heated at 50 °C, to completely melt the switching block and to allow relaxation of macromolecular orientation related to stretching and elongation of the polymer network in the electrospinning process; (ii) cooled to 30 °C, that is, below PLLA T_g, and (iii) deformed to confer the temporary shape that was subsequently fixed by cooling the sample at −60°. By applying the programming step at a T below PLLA T_g it is expected that the deformation was only applied to the switching phase (B block) component. Then, during the cooling, the applied strain was fixed thanks to the formation of B block crystal phase. To recover the permanent shape, and thus completing the thermomechanical cycle, the material was heated again above B block T_m (Figure 32 A,B). Strain recovery as a function of temperature is reported in Figure 32 C. The recovery of the permanent shape takes place starting from around −20 °C (Figure 32 C-b) reaching a value of around 10% at 20 °C. The recovery becomes more evident in the range 20–30 °C where the scaffold recovers about 90% of the initial strain (Figure 32 C-a). Such recovery behavior, spanning a wide temperature range (from around −20 °C to around 30 °C), can be ascribable both to the multipeak melting endotherm of P(PAz60Seb40) crystals and to the broad melting region that starts well below RT (see DSC curve in Figure 31). Table 10 reports R_f and R_r calculated according to eq 1 and 2, respectively. It is worth pointing out that at the end of the thermomechanical cycle, after the scaffold completely recovered its macroscopic permanent shape, the microscopic fibrous structure is maintained thanks to the presence of the high-melting phase of PLLA (Figure 32 D).

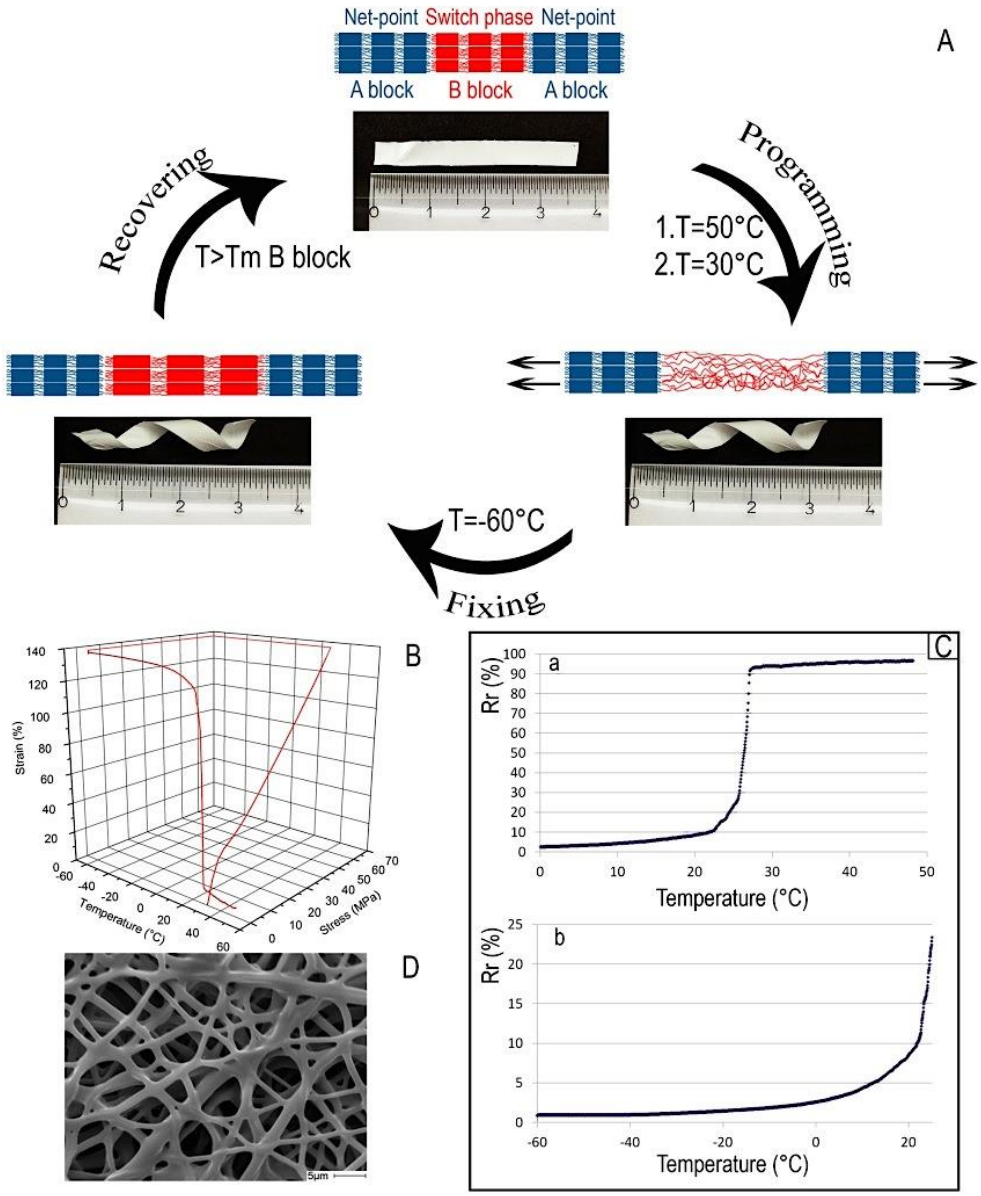

Figure 32. (A) Schematic representation of the mechanism of shape-memory for HMW-ABA; (B) 3D representation of the applied thermomechanical cycle; (C) strain recovery evolution over temperature in the range 0–50 °C (a) and from −60 to 25 °C (b); (D) SEM micrograph of the electrospun scaffold after the application of the thermomechanical cycle.

Table 10. Applied strain (ε_{app}), shape fixity ration(R_f) and shape recovery ratio (R_r) of as spun HMW-ABA and annealed electrospun HMW-ABA at 15 and 30°C

sample	ε_{app} (%)	R_f (%)	R_r (%)
HMW-ABA as-spun	140	99	96
HMW-ABA annealed at 15 °C	110	98	98
HMW-ABA annealed at 30 °C	150	99	99

As reported above, the broad melting region of the B block results in a recovery of the permanent shape that starts at around −20 °C (Figure 32 C-b) and about 10% of the strain is recovered close to the RT range, thus entailing a partial loss of the fixed temporary shape when the material is used at RT. In order to overcome this limitation and optimize the shape memory behavior, different annealing treatments were applied to narrow the broad and multiple melting endotherm of the B block. As a preliminary investigation, Temperature Modulated DSC (TMDSC) was performed on electrospun HMW-ABA scaffold in order to identify the proper annealing temperature. In fact, TMDSC allows to separate the concomitant phenomena of cold crystallization and melting of the B block, which are overlapped in a conventional DSC measurement. The resulting calorimetric curves are shown in Figure 33 A, where the nonreversing heat flow component displays a multipeak crystallization occurring between T_g and T_m of the B block (Figure 33 A-a). On the basis of TMDSC, the annealing was carried out by maintaining the sample mounted in the DMTA either at 15 or 30 °C for 3 h, after the programming and the fixing step, as described in the Experimental Section. To verify the effectiveness of the annealing, the samples were then analyzed through TMDSC in the temperature range of the switching segment melting, and the results are reported in Figure 33 B together with the not annealed sample. As expected, the annealing had the effect of partially eliminating the low melting crystal phase, by increasing the amount of crystals that melt at T > $T_{annealing}$ and by shifting the T_{onset} of the B block melting endotherm at higher temperature compared to the as-spun scaffold.

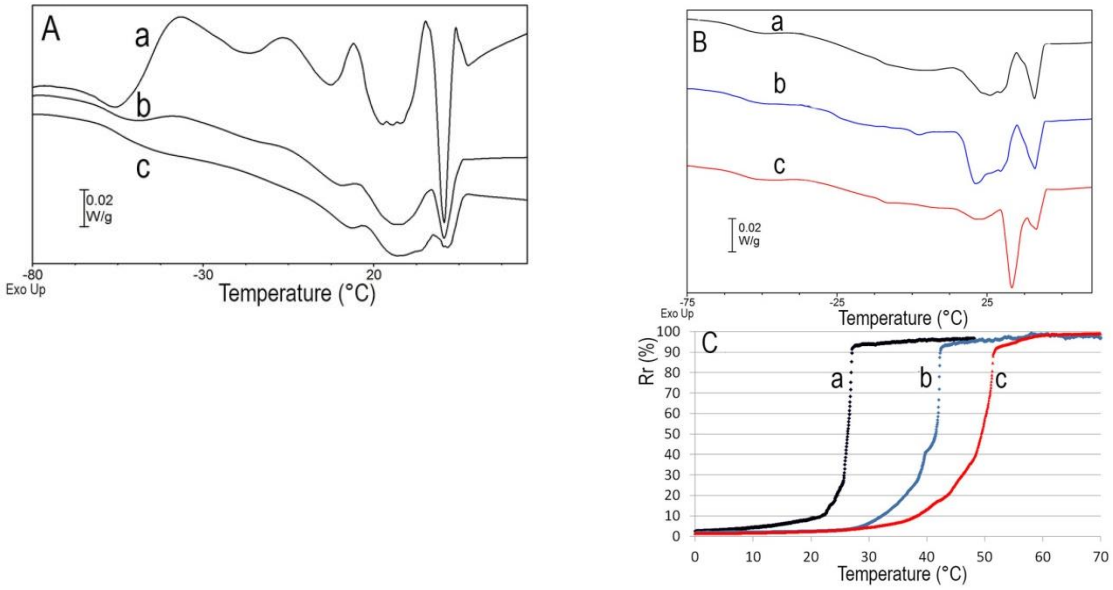

Figure 33. (A) TMDSC curves of electrospun HMW-ABA: (a) nonreversing heat flow, (b) reversing heat flow, and (c) total heat flow. (B) TMDSC curves (total heat flow) of (a) not annealed sample, (b) sample annealed at 15 °C, (c) sample annealed at 30 °C. (C) Strain recovery evolution over temperature in the range 0–60 °C for samples: (a) not annealed, (b) annealed at 15 °C, and (c) annealed at 30 °C.

The effect of the annealing treatment on the scaffold shape memory behavior, in terms of strain recovery as a function of temperature, is shown in Figure 33 C. The curve of the as-spun sample (reported above in Figure 32 C) is also shown for comparison. All samples display a recovery process in a T range that depends on the annealing treatment. In particular, after the annealing at 15 °C the sample starts to recover the permanent shape at around 25 °C and completes the recovery at 40 °C. After the annealing treatment at 30 °C, the strain recovery starts around 35 °C and is completed at around 55 °C. It is worth noticing that for both samples obtained after the two annealing treatments (at 15 °C and at 30 °C), the R_r and R_f values were excellent, with recovery indexes even better than those obtained for the as-spun HMW-ABA sample (Table 10). This "annealing-controlled" shape memory behavior is strictly related to the structural perfection of the B block crystal phase and, hence, to the corresponding melting transition, that is dependent on the polymer thermal history. In particular, the annealing treatment applied in this work allows the decrease of the amount of low melting crystals by increasing the structural perfection of crystallites, moving the melting of the switching phase at higher temperatures (Figure 33 B). Since the recovery of the permanent shape occurs when the switching phase gains enough mobility to release the strain energy stored during shape fixing, the annealing has the effect of stabilizing the material at RT and of shifting the recovery temperature at higher values. These results demonstrate that, by applying a simple thermal treatment, the shape memory behavior and switching T of the HMW-ABA fibrous scaffold can be tuned without any change to the material composition. The obtained results suggest that a clever design of polymer microstructure and of thermal transitions might be a useful strategy to better exploit the potential of thermal responsive shape memory polymers.

In order to evaluate the biocompatibility of the new shape memory scaffolds, at 1 and 3 days NIH/3T3 fibroblast cells viability has been evaluated by MTS assay (Figure 34). Cells showed an optimal viability when seeded on the electrospun HMW-ABA scaffold, that increased with time. After 1 and 3 days of culture, phallodin and DAPI were used to observe cell morphology (Figure 34). Already after 1 day of culture, NIH/3T3 fibroblasts were well spread and showing the characteristic spindle morphology (elongated cytoplasm). Unaltered cell morphology was maintained and cell proliferation was adequate compared to the control.

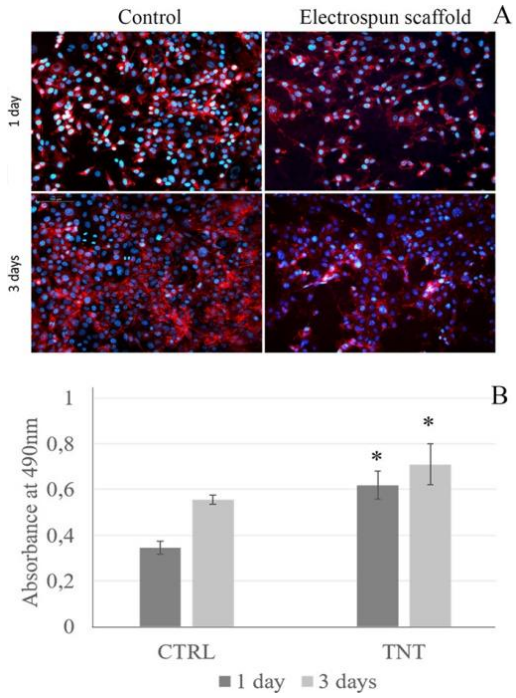

*Figure 34. (A) Phalloidin staining for cell morphology and (B) cell viability of NIH/3T3 seeded on HMW-ABA scaffold. Data are statistically significant with respect to control. * indicates p ≤ 0.05.*

These preliminary results are promising in view of the application of the shape memory electrospun devices as functional tissue engineering scaffolds, as recently demonstrated by Bao et al. (188) Such scaffolds combine the biomimicking characteristic of the fibrous structure with the shape memory effects to allow minimally invasive surgical implantation and to achieve an enhanced efficacy in tissue repair and regeneration by controlling the cell behavior through mechanical-biological stimuli.

In conclusion, a new linear PLLA-based triblock copolymer was proposed to fabricate a scaffold for tissue engineering applications, displaying a thermally induced shape-memory behavior around physiologically relevant temperature. The copolymer microstructure was designed to provide a low melting crystal phase acting as switching segment, with the capability to promptly fix the temporary shape of the SMP, and a high melting crystal phase acting as physical network. Remarkably, the monomers adopted for the copolymer synthesis, with the exception of a small amount of HDI used as chain extender, are characterized by a 100% biobased character, as being lactic acid, 1,3-propanediol, azelaic, and sebacic acids. The switching segment central block, that is, poly(propylene azelate-co-propylene sebacate) (60/40) random copolymer, is characterized by a chemical composition which guarantees a crystal phase melting in the range of the physiological temperature; the PLLA sequences provide the physical network. The copolymer was suitable to be processed through electrospinning to obtain a microporous scaffold

made of randomly arranged bead-free fibers. The shape memory properties of the scaffold were characterized through a thermomechanical cycle programmed on the basis of a throughout thermal characterization of the material. In particular, it was shown for the first time that a thermal annealing treatment, whose aim was to narrow the broad and multiple melting endotherm of the switching phase by increasing crystal phase perfection and melting temperature, was effective in controlling the shape-memory trigger temperature interval. It is worth pointing out that, at the end of the thermomechanical cycles, the scaffold completely recovered its macroscopic permanent shape, while well maintaining its microscopic fibrous structure. In conclusion, in this work we demonstrated that, by controlling the melting and recrystallization processes, it is possible to shift the shape recovery temperature range without the need of varying the copolymer's chemical structure. Hence, the annealing approach reported in this work turned out to be a smart tool to obtain a shape memory material with tunable recovery behavior. More generally, the approach here adopted can be considered a useful strategy to tailor the shape recovery temperature of a given polymer, thus providing a simple, yet powerful way of "ad hoc" programming the same material for different applications requiring different shape recovery temperatures. Biocompatibity of the proposed scaffold was demonstrated by using NIH/3T3 fibroblast cells. The attractive shape-memory behavior of the biomimetic microporous scaffold investigated in this work, combined with its biocompatibility make it suited for tissue regeneration, to allow minimally invasive surgical implantation and control of cell behavior through mechanical-biological stimuli.

3.2 Electrospun carriers to deliver nanoparticles, molecules and bioactive agents

3.2.1 Diclofenac Potassium and Chlorotetracycline-hydrocloride release from composites made of PEOT-PBT block copolymers and gelatin

The present work has been conducted in collaboration with Prof. Nadia Passerini and Co-workers at department of Pharmacy and Biotechnology and Prof. Silvia Panzavolta at department of Chemistry "G. Ciamician", UNIBO. The present work is currently under finalization and submission.

The use of composites materials capable to deliver simultaneously more than one drug in a controlled and predictable way has attracted considerable attention in the last decade in the biomedical field. Among the different composites that it is possible to use in this field probably the most interesting ones are the homogeneous composites. Homogeneous composites are obtained embedding an electrospun scaffold to a hydrogel solution during the gelation process, obtaining composites in which the electrospun scaffold is completely integrated in the hydrogel matrix. These kinds of composites are very appealing since they can be highly adapted to meet the specific applications by modifying the chemical

and physical properties of the used components. Among the possible applications one of the most interesting is the possibility to use them in the field of cancer therapy, where usually a multi-drug treatment is needed, especially after resection surgical intervention, that usually does not assure the complete removal of all cancer cells. In this case it is necessary to prevent the disease relapse by getting rid of all the remaining cancerous cells, slowing down the inflammatory response and promoting the growth of health tissue. To match these specifics medical requirements it was decided to fabricate a dual drug loaded composite material made of gelatin and electrospun fibrous scaffold. The obtained composites final aim was to prevent cancer relapse and promote growth of health tissue by (i) fast releasing a model anticancer drug (Chlorotetracycline-hydrocloride, CTC) in the first days after the surgical intervention and (ii) releasing an anti-inflammatory drug (Diclofenac Potassium,DK) over a more prolonged period while sustaining the health tissue proliferation with the polymeric 3D fibrous scaffold. In this work medical grade and bioresorbable multi-block copolymers made of poly(ethylene oxide terephthalate) (PEOT) and poly(butylene terephthalate) (PBT) (189), combined with genipine-crosslinked gelatin hydrogel have been used. The used multi-block copolymers are characterized by phase separation of the hydrophilic (PEOT) and hydrophobic (PBT) segments. Controlling the PEOT/PBT blocks ratio, it is possible to control the material hydrophilicity (190) and, in turn, the embedded drug release behavior. In the present work, multi-block copolymers characterized by different ratios of PEOT and PBT blocks have been used, in particular PEOT30PBT70 and PEOT70PBT30 (wt%). The model drugs were chosen to be hydrophobic and hydrophilic, in particular DK and CTC were selected respectively. CTC was loaded into a partially reticulated gelatin hydrogel while blend electrospinning technique was used to obtain DK loaded polymeric scaffolds.

The electrospinning process has been optimized in order to obtain bead free PEOT30PBT70 and PEOT70PBT30 electrospun scaffolds, both plain and DK loaded (Figure 35). Interestingly both DK loaded scaffolds were characterized by smaller and narrower fiber diameter distribution compared to the corresponding plain ones, with mean fiber diameter of about 0,5 µm and 0,9 µm for DK loaded and plain scaffolds, respectively. These results can be explained by taking into account the increase in the dielectric constant of the electrospinning solution due to the addition of DK salt, with a consequent better elongation process during the fiber formation that produced smaller fiber.

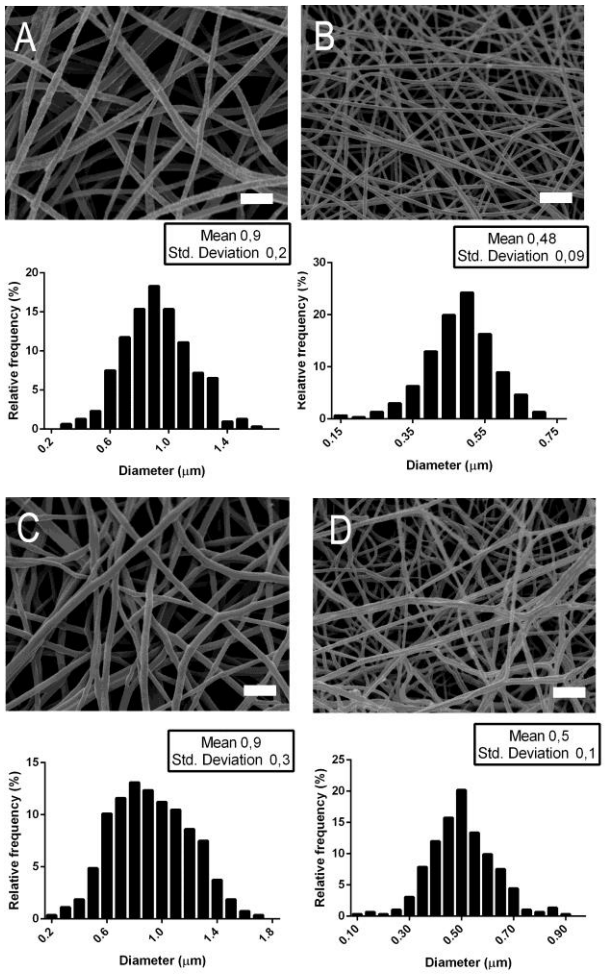

Figure 35. SEM images and fiber diameter distribution of plain (A-C) and DK loaded (B-D) PEOT30PBT70 (A-B) and PEOT70PBT30 (C-D) electrospun scaffolds. Scale bars = 5 μm.

Differential scanning calorimetry measurements have been performed on PEOT30PBT70 and PEOT70PBT30 scaffolds both plain and DK loaded, as well as on the raw block-copolymers. By analyzing the curves of the first scan of the PEOT30PBT70 samples (Figure 36 A) it is possible to assert that the PBT faction of raw copolymer, plain and DK loaded scaffolds is capable to crystalize during the electrospinning process and copolymer synthesis, leading to an evident endotherm peak around 210°C without the presences of any detectable cold crystallization. There is no evidence of PEOT crystallinity for all three samples, probably due to the low PEOT content, in this case just the PEOT T_g is detectable. The second scan (Figure 36 B) displays an evident endotherm peak around 210°C for all samples and the absence of any cold crystallization. This indicates the capability of the PBT fraction to crystalize during the quench. Furthermore, from the second scan it is possible to better evaluate a glass transition located around -40°C, compatible with the T_g of the PEOT block. In the second scan a more defined melting endotherm as

well as a slightly lower ΔH_m (J/g) is reported for DK loaded sample compared to the plain and raw copolymer, probably due to the DK presence that might inhibit the crystalline phase formation.

From the first scan of the DSC curves of PEOT70PBT30 samples (Figure 36 C) it is evident how this block copolymer is more hydrophilic than the previous one; the first scan of all samples are characterized by the presence of a broad endotherm from 25°C to around 120°C ascribable to the presence of water. This evidence is confirmed by the absence of any endotherm from 25°C to 120°C in the second scan after quench for all the samples (Figure 36 D). The presence of endotherm in the first and second scan around 150°C is ascribed to the melting of the PBT crystalline phase; unfortunately due to the presence of water it is not possible to determine its exact T_m and ΔH_m values in the first scan. The presence of adsorbed water in such a kind of hygroscopic polymer is favored in the nanofibrous samples compared to the powder sample by the high surface to volume ratio of the fibers. Analyzing the first scan of PEOT70PBT30 it is possible to notice that the PEOT blocks are basically amorphous for all copolymers and that in the case of the raw and as spun copolymers they are capable to crystalize during the first heating ramp (cold crystallization) while no evidence of crystallization is reported for the DK loaded sample, the presence of DK probably avoid the formation of such crystalline phase. From the second scan (Figure 36 D) it is more evident for all samples the presence of a glass transition around -48°C followed by a cold crystallization and a melting endotherm at -23°C and 10°C respectively. Those transitions can be ascribed to the PEOT blocks, while the endotherm around 150°C is ascribed to the PBT blocks that are still capable to crystalize during quench even at low amount (190). No significant impact on the calorimetric properties after quench can be reported after the DK loading into the scaffolds.

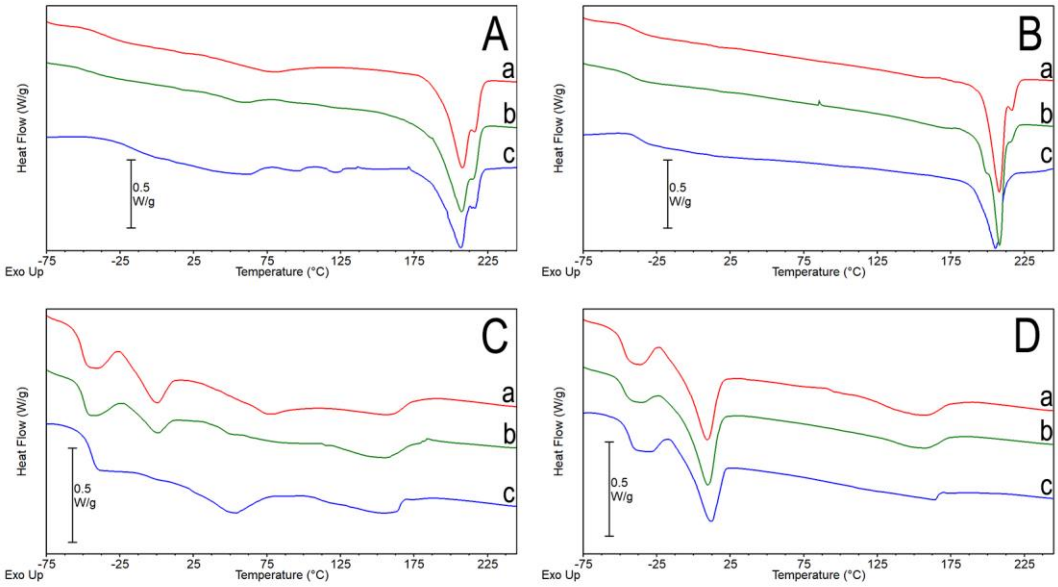

	First scan			Second scan			
	T_g (°C)	T_c (°C) ΔH_C (J/g)	T_m (°C) ΔH_m (J/g)	T_g (°C)	T_c (°C) ΔH_C (J/g)	T_m (°C) ΔH_m (J/g)	T_{m2} (°C) ΔH_{m2} (J/g)
PEOT30PBT70 raw	-36°C		207°C 37 J/g	-39°C		208°C 41 J/g	
PEOT30PBT70 as spun	-43°C		207°C 46 J/g	-40°C		208°C 43 J/g	
PEOT30PBT70+DK	-20°C		207°C 35 J/g	-37°C		207°C 35 J/g	
PEOT70PBT30 raw	-51°C	-25°C 4,8 J/g	-13°C 4,8 J/g	-48°C	-23°C 4,3 J/g	9°C 15,7 J/g	151°C 13,5 J/g
PEOT70PBT30 as spun	-50°C	-23°C 2,6 J/g	0,29°C 3,8 J/g	-48°C	-23°C 1,7 J/g	10°C 18,7 J/g	155°C 11 J/g
PEOT70PBT30+DK	-45°C			-48°C	-17°C 3,4 J/g	12°C 13,7 J/g	163°C 8 J/g

Figure 36. DSC curves and summary of relative calorimetric properties of PEOT30PBT70 (A-B) and PEOT70PBT30 (C-D), First scan (A-C) and second scan after quench (B-D). (a) Raw copolymers, (b) Plain scaffolds and (c) DK loaded scaffolds.

Thermogravimetric analyses have been performed on plain and DK loaded scaffolds as well as on pure DK (Figure 37). For both copolymers the plain scaffolds are characterized by a one-step degradation pathway, with a maximum at around 395°C, whereas the DK loaded scaffolds are characterized by a more complex degradation behavior, with a first weight loss from 260°C to 360°C followed by a prominent weight loss from 380°C with a maximum at 390°C. It is interesting to notice the presence of a small

weight loss around 100°C for both loaded copolymers, this behavior is attributed to water evaporation probably due to water absorption promoted by drug presences on the fiber surface; this hypothesis is in good agreement to the previously discussed DSC analysis. Comparing the weight loss of the DK loaded scaffolds and the pure DK is it possible to assert that the weight loss from 260°C to 360°C can be attributed mainly to the DK presence. However, the partial degradation overlap of the plain scaffolds and the pure DK makes not possible to determine the DK amount loaded into the scaffolds.

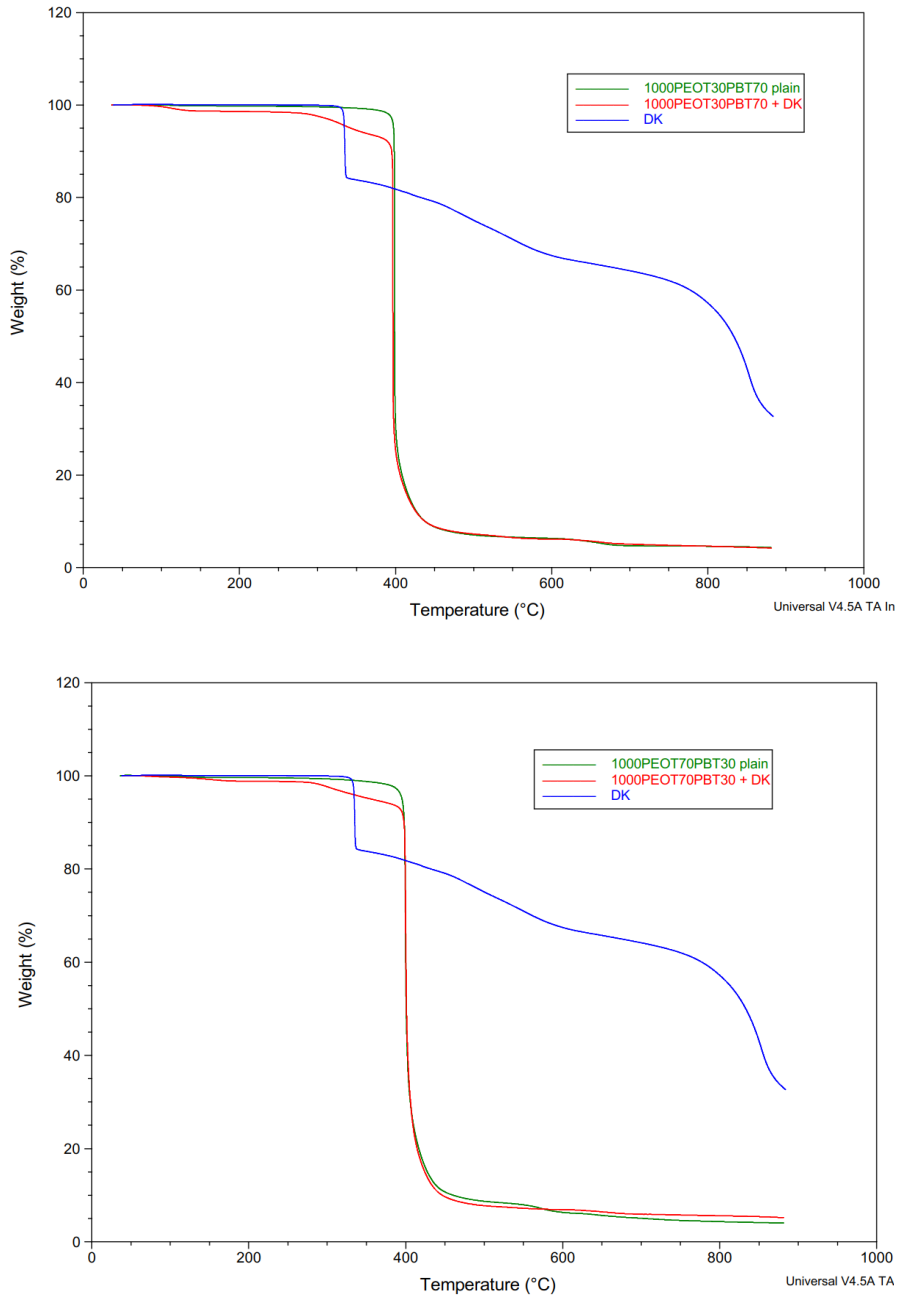

Figure 37. TGA curves of DK loaded PEOT30PBT70 scaffolds, PEOT30PBT70 plain scaffold, DK, DK loaded PEOT70PBT30 scaffolds and PEOT70PBT30 plain scaffold.

The evaluation of DK release from PEOT30PBT70 as well as from PEOT70PBT30 was investigated and the results are reported in Figure 38. DK release from both copolymers resulted in high burst release with about 80% of the drug released in the first hour and a complete drug release within 8 hours. This effect might be attributed to the drug distribution into the fibers, probably located closer to the fiber surface and not well embedded. This result persuaded us to proceed with the fabrication of the composites by using PEOT30PBT70 block copolymer as fibrous material since its slight higher hydrophobicity compared to PEOT70PBT30 (data not shown) might help to partially slow down drug diffusion once embedded into the final composites, thus leading to a more sustained DK release.

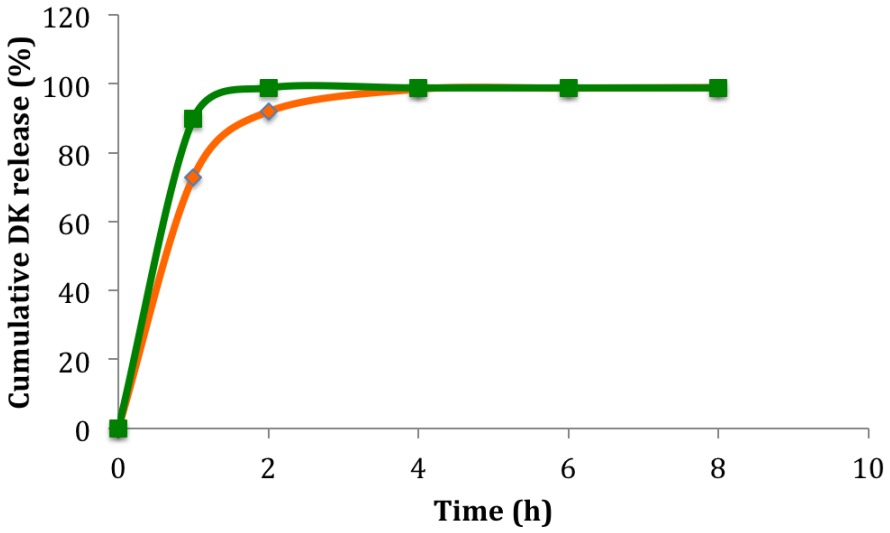

Figure 38. Cumulative release (%) from DK loaded electrospun mat of PEOT70PBT30 (green) and PEOT30PBT70 (orange)

The composites have been designed as reported In Figure 39 A and 5B and, in particular, two composites have been fabricated. The first one, here defined as mono-layer composite, was made of a 5% w/w DK loaded electrospun scaffold homogenously embedded into a 2%w/w CTC loaded gelatin layer, crosslinked with 1%w/w of genipin (Figure 39 A), whereas the second one, here defined as double-layer composite, was fabricated starting from the mono-layer architecture. In particular it was decided to lay a 2% w/w CTC loaded thin gelatin layer, reticulated with 0,5%w/w of genipin, at the top and at the bottom of a plain mono-layer composite containing a 5% w/w DK loaded electrospun scaffold, as reported in Figure 39 B.

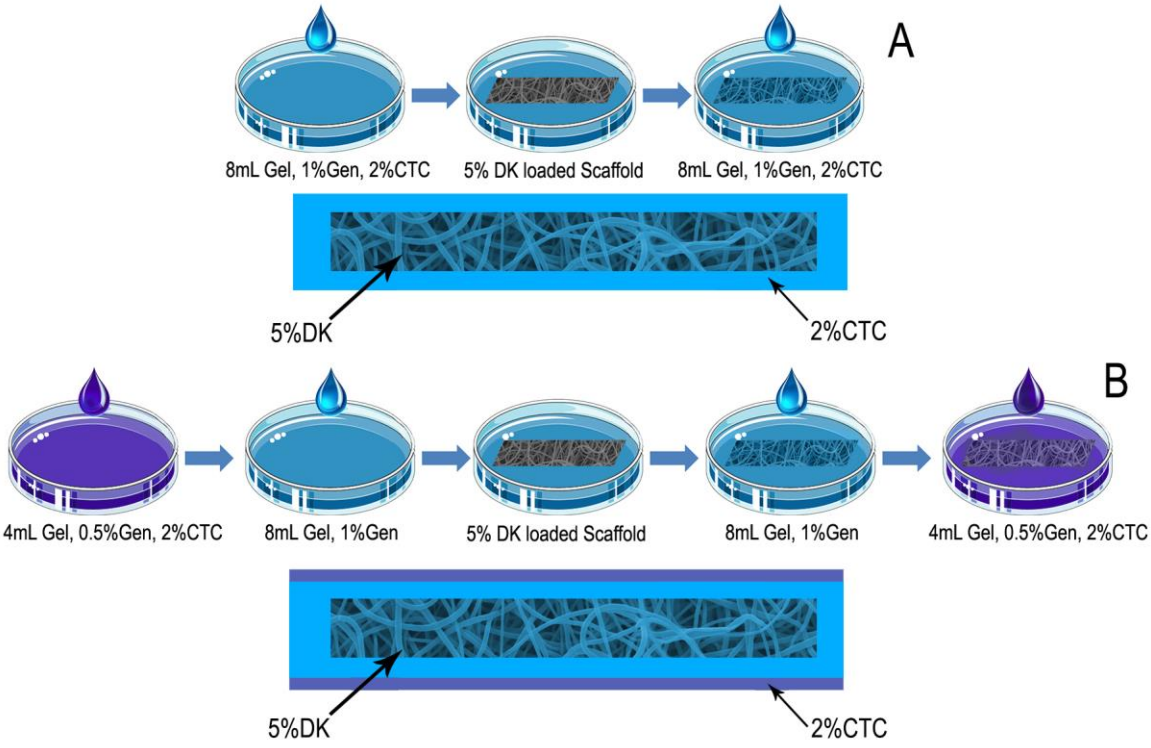

Figure 39. Schematic representation of the fabricated composites. (A) Mono-layer composites have been produced by immersing a DK loaded electrospun scaffolds into CTC loaded gelatin layer reticulated with genipine (B) A double-layer composite was prepared adding a reticulated CTC loaded gelatin thin layer at the top and bottom of a plain mono-layer composite containing a 5% w/w DK loaded electrospun scaffold.

The obtained composites have been investigated by means of a release study performed in PBS at 37°C up to 15 days. First the CTC release was evaluated demonstrating that the different design of the two composites, as expected, does not influence the release behavior of the CTC. Both for the mono and double layer composites the CTC was released within the first 7 hours, as reported in Figure 40.

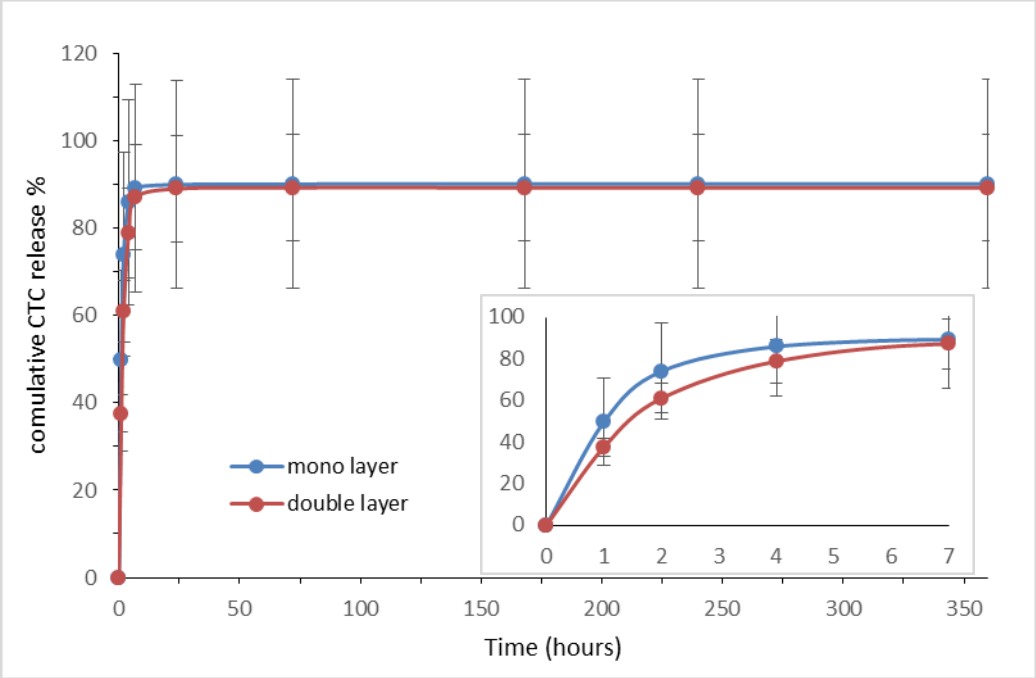

Figure 40. CTC release behavior from mono and double layer composites, blue and red respectively.

More interesting is the analysis of DK and CTC release behavior from the double layer composite (Figure 41). In this case, by modifying the architecture of the obtained composites it was possible to achieve the release of the two drugs in a controlled and distinct way. CTC was released by 90% within the first 8 hours (Figure 41) while DK was released by 83% in 7 days. Furthermore, it is interesting to notice that the presence of gelatin layer, acting as barrier layer, slow down the release of DK from 80% in few hours (Figure 38) to 83% in 7 days.

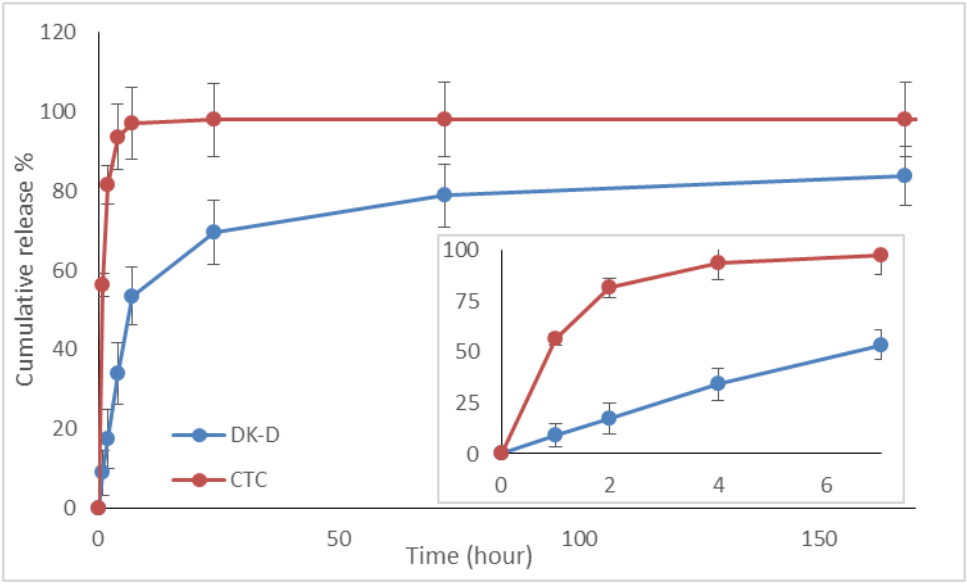

Figure 41. CTC and DK release behavior from double layer composited. Red and blue respectively.

Indeed the designed double layer composite might be considered as promising platform to perform in-situ dual drug release in cancer therapy, preventing the inflammatory response after surgical intervention and avoiding possible relapse.

At the moment biological tests to evaluate the biomedical performances of the obtained devices are under careful evaluation at Istituto Scientifico Romagnolo per lo Studio e la Cura dei Tumori (IRST institute, Meldola, Italy).

3.2.2 Luminescent core shell silica nanoparticles loaded PLGA5050 and PLGA7525 scaffolds

The present work has been conducted in collaboration with Prof. Nelsi Zaccheroni and co-workers at department of Chemistry "G. Ciamician", UNIBO. The present work is currently under finalization and submission.

The use of nanoscale objects, such as nanotubes and nanoparticles have gained great interest in the last decades in many field of research. Probably the most studied one is the biomedical field, in which nanoparticles (NPs) have been extensively studied as promising drug delivery system (191). On the contrary not as much effort has been put in the study of NPs as self-standing therapeutic material. In this case NPs might became active therapeutic devices and not just an inert carrier of drugs and molecules. In this respect an interesting application might be the *in-situ* sustained NPs release for particular treatments like photothermal therapies; in which specific NPs produce heat in an efficient manner when externally

excited, leading to irreversible damage to the surrounding cells (192). This concept might be applied to cancer therapy in which usually long-term treatments are required to prevent possible relapse.

When designing a material capable to achieve this result the ideal NPs carrier should be (i) biocompatible (ii) biodegradable and (iii) should be easily tunable to achieve different NPs release kinetics. In this context electrospinning represent a smart and versatile way to load specific NPs into a biodegradable non woven scaffolds made of biocompatible polymers; furthermore by carefully choosing the polymer composition it is possible to finely tune the degradation behavior of the scaffolds and in turn the embedded NPs release.

In the present proof of concept study, a polymeric fibrous scaffold, loaded with luminescent core shell silica NPs (193) have been produced and tested, using two different poly(lactide-co-glycolide) copolymers (PLGA5050 and PLGA7525). The aim of this work was to study the effect of the fibers composition, and thus their hydrolytic degradation behavior, on the NPs release. The used core shell silica NPs have been synthesized by Prof. Nelsi Zaccheroni and co-workers at department of Chemistry "G.Ciamician", they were made of silica core, in which Rhodamine (B) dye was covalently linked, and polymeric PlurionicF127 (PEG-PPG) shell. Rhodamine (B) has been used to study the amount of NPs released over time through spectrophotometric emission measurements. Size and morphology of the used NPs have been evaluated via TEM. NPs are round shape and characterized by a mean diameter of about 25 nm (Figure 42).

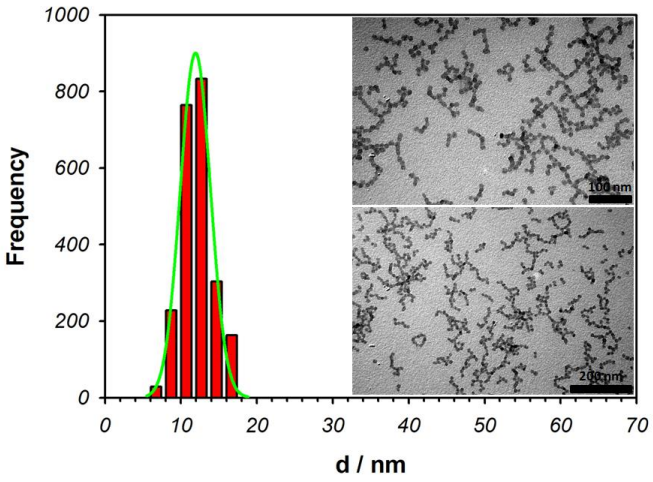

Figure 42. TEM images of core shell silica NPs and their relative dimensional frequency

PLGA50:50 and PLGA75:25 nanofibers loaded with 2% w/w of NPs have been produced and herein defined P1 and P2 respectively. The P1 and P2 fibers have been analyzed by means of SEM, confocal

microscopy and TEM to ensure the good dispersion of the loaded NPs as well as the good morphology of the obtained mats (Figure 43).

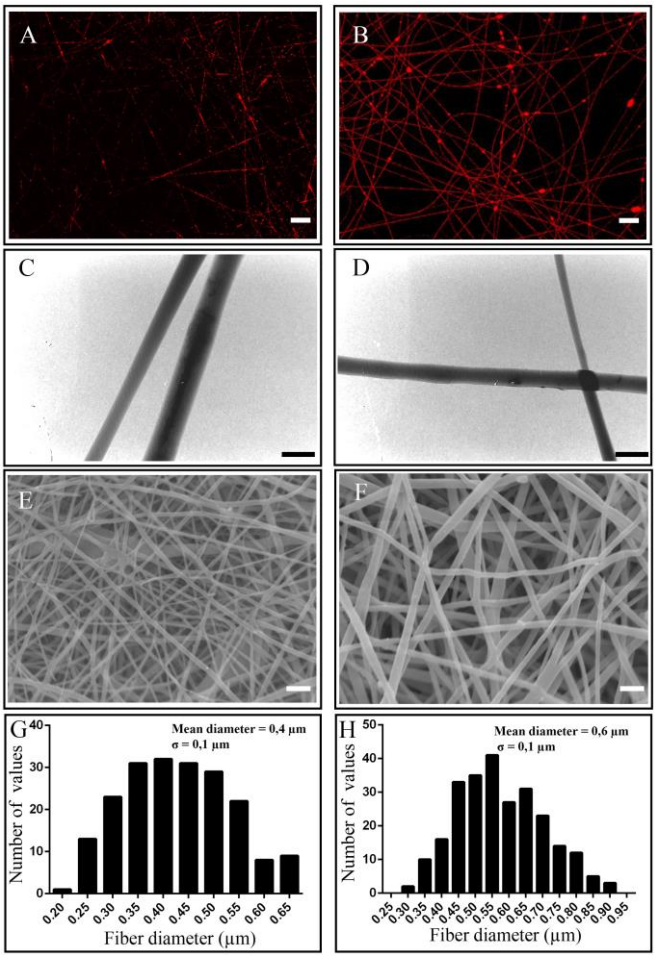

Figure 43. (A-B) Confocal images (scale bar 10 µm), (C-D) TEM images (scale bar 300 nm), (E-F) SEM images (4000x, scale bar 2 µm) and (G-H) fiber diameter distribution of electrospun P1 (A-C-E-G) and P2 (B-D-F-H)

SEM images of P1 and P2 exhibited bead free fiber morphology and a mean diameter of (0.4±0.1) µm and (0.6±0.1) µm respectively (Figure 43 E to H). To further study the NPs distribution into P1 and P2 fibrous matrix TEM and confocal microscopy studies have been performed demonstrating good NPs dispersion into the polymeric fiber (Figure 43 C-D). Results were confirmed also by the confocal images (Figure 43 A-B) that shows only few aggregates within P1 and P2 samples. Plain P1 and P2 electrospun mats have been also produced as reference and the obtained scaffolds were characterized by no significant changes in fiber diameter compared to the NPs loaded ones (data not shown). Hydrolytic degradation and NPs release studies have been performed on plain and NPs loaded P1 and P2 samples

over a period of 50 days; the materials degradation behavior was evaluated by mean of weight loss and M_w loss measurements at defined time points as well as with the use of SEM investigation (Figure 44 and Figure 45).

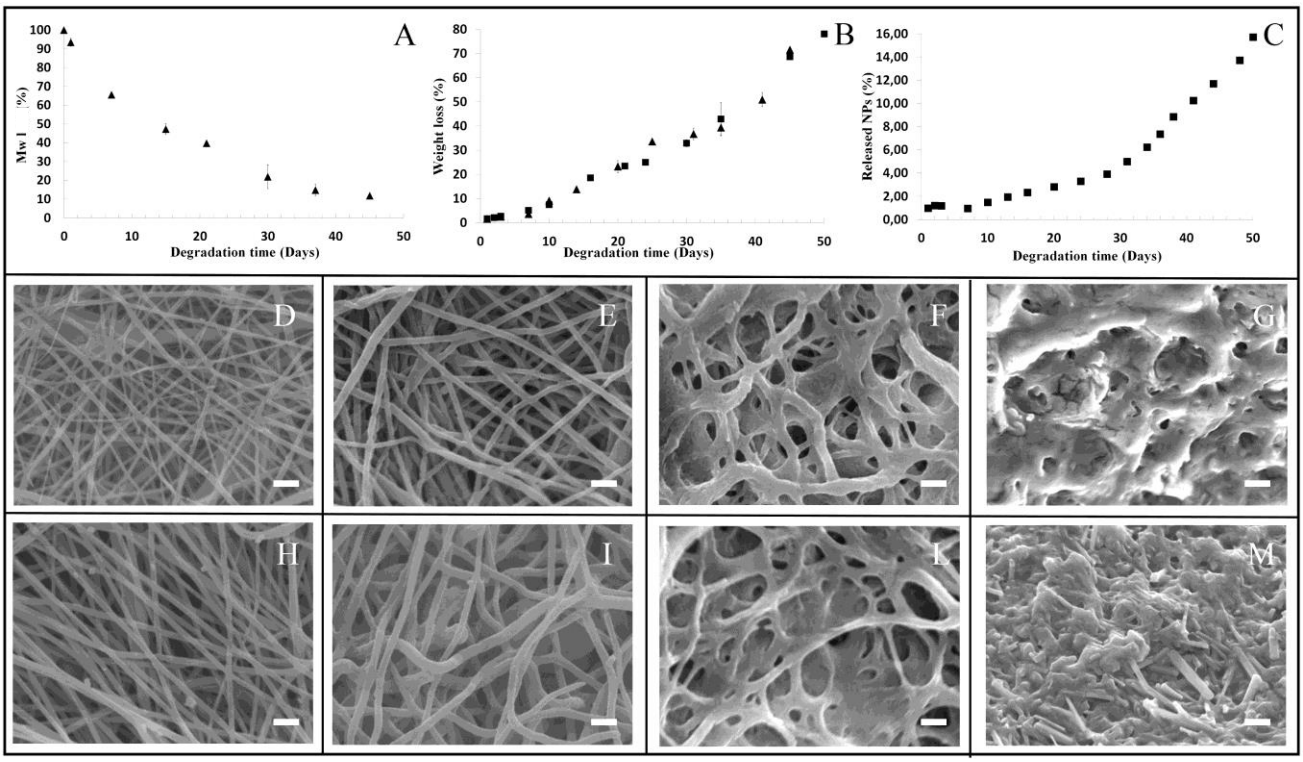

Figure 44. NPs loaded P1 mat (■). (D-M) SEM images (scale bar 2µm) of plain (H, I, L, M) and NPs loaded (D, E, F, G) hydrolytically degraded P2 mat after 0 (D,H), 20 (E,I), 35 (F,L) and 50 days (G,M).

The M_w loss over the period of 50 days of the P1 plain sample is about 90% (Figure 44 A) while the weight loss over the same period is about 75% (Figure 44 B). Similar results have been obtained for P1 NPs loaded samples, indicating that the presence of the NPs does not influence the degradation behavior of the obtained composites (Figure 44 B). SEM images acquired at different time confirm the results obtained in terms of weight loss %. The morphology of the P1 plain and loaded mats evolve in a similar way, displaying a progressive loss of fiber morphology starting from day 35 (Figure 44 F-L) to obtain a film like structure at day 50 (Figure 44 G-M). NPs release profile reported in Figure 44 C display a final NPs release of about 16% from sample P1. The release profile can be divided in two main sections, the first from 0 to 32 days and the second from 32 to 50 days. The first section is characterized by a slower NPs release compared to the latter. This peculiar trend is similar to that of the weight loss

underwent by P1. Therefore, it is possible to ascribe the release of the embedded NPs to the degradation of the polymeric mat.

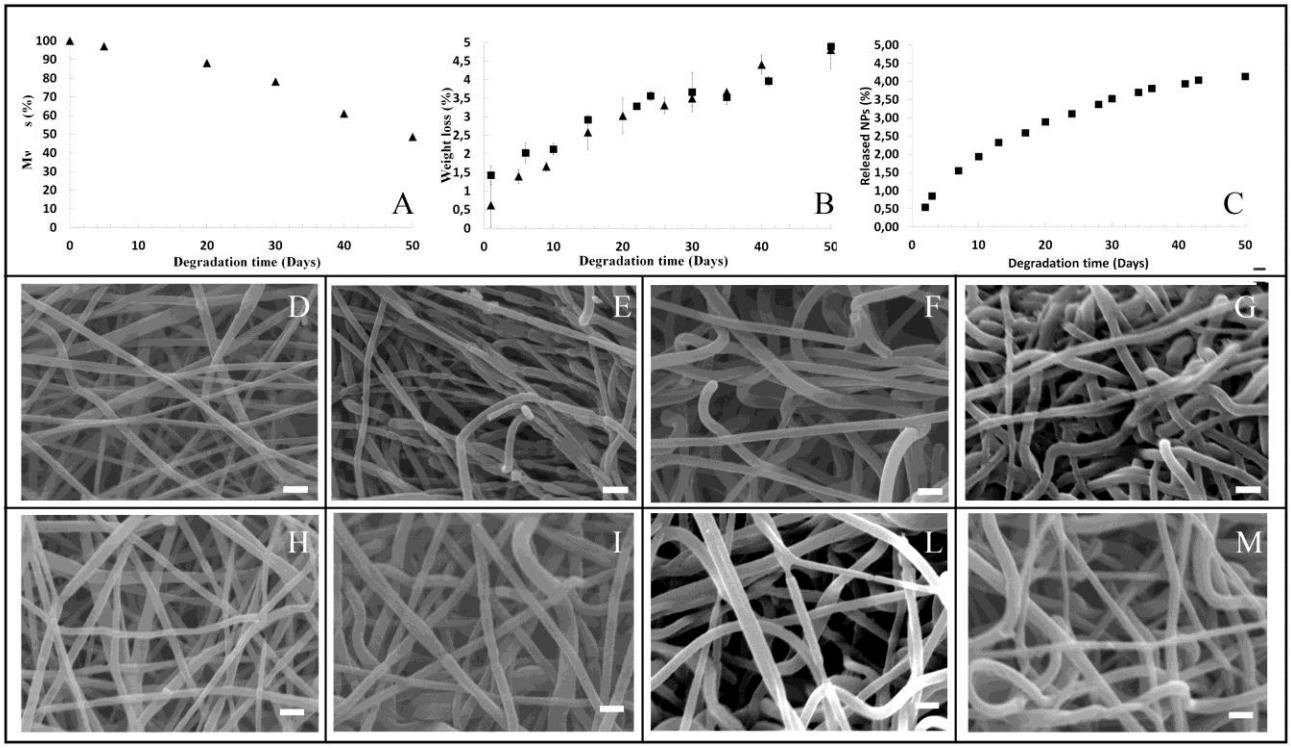

Figure 45. (A) Mw loss, (B) Weight loss percentage, (C) NPs release profile from 0 to 50th day of plain (▲) and NPs loaded P2 mat (■). (D-M) SEM images (scale bar 2µm) of plain (H, I, L, M) and NPs loaded (D, E, F, G) hydrolytically degraded P2 mat after 0 (D,H), 20 (E,I), 35 (F,L) and 50 days (G,M).

P2 plain and NPs loaded mats display a slower degradation behavior compared to the P1 mats with a Mw loss at 50 days of about 50% for the plain P1 mat (Figure 45 A) and a weight loss of about 5% for both plain and NPs loaded samples after 50 days (Figure 45 B). This behavior is related to the different chemical structure of the used copolymers. In fact it is well established that thehigher the content of glycolide units, the higher is the degradation rate, due to the more hydrophilic character of glycolide compared to the lactide. Interestingly the presence of the NPs into the mats does not influence the degradation behavior for both the used copolymers. The NPs release was also evaluated for P2 samples demonstrating that after 50 days only 4% of NPs have been released (Figure 45 C). Comparing the degradation pathway of the P2 loaded mats (Figure 45 B) and the NPs release profile (Figure 45 C) it is possible to assert that the NPs release and the degradation behavior follow the same route, thus the NPs release is mainly triggered by the polymeric matrix degradation. SEM evaluation at different times does not highlight significant morphology differences between the P2 plain and NPs loaded mats, both

maintaining a good fibrous morphology over the studied period (Figure 45 D to M). NPs release from both P1 and P2 loaded scaffolds seems to be directly related to the degradation behavior of the used polymer, indicating a strong NPs-polymeric interaction that inhibits the NPs release unless degradation occur. In both cases the final amount of the released NPs is at best of 16% while the degradation of the matrix is, at best, about 80%. The low release of NPs with respect of the polymer degradation can be explained by considering the chemistry of the used NPs, in particular of the shell. Hydroxyl-terminated PEG-PPG chains might interact with the carboxyl terminals of the hydrolyzed PLGA esters, via H-bond or via local esterification reaction, thus slowing down NPs release.

In parallel, a PLGA5050 electrospun mat loaded with free Rhodamine (B) was fabricated. The Rh(B) release profile was studied over a period of 12 days, during which almost no degradation of the matrix is reported (Figure 46 B-C). The release kinetics is characterized by a strong burst effect, about 35% of Rhodamine (B) is released during the first 7 hours, and the release at 12 hours is about 50%. Comparing this result with the degradation behavior of the P1 plain mat it is possible to assume that its degradation behavior does not influence the release of the embedded molecule. To further confirm this evidence the release profile was fitted with the Korsmeyer-Peppas model (Figure 46 C) obtaining a diffusion constant (n) of about 0.42 that is compatible with a Fickian diffusion mechanism, i.e. not related with the degradation of the used matrix.

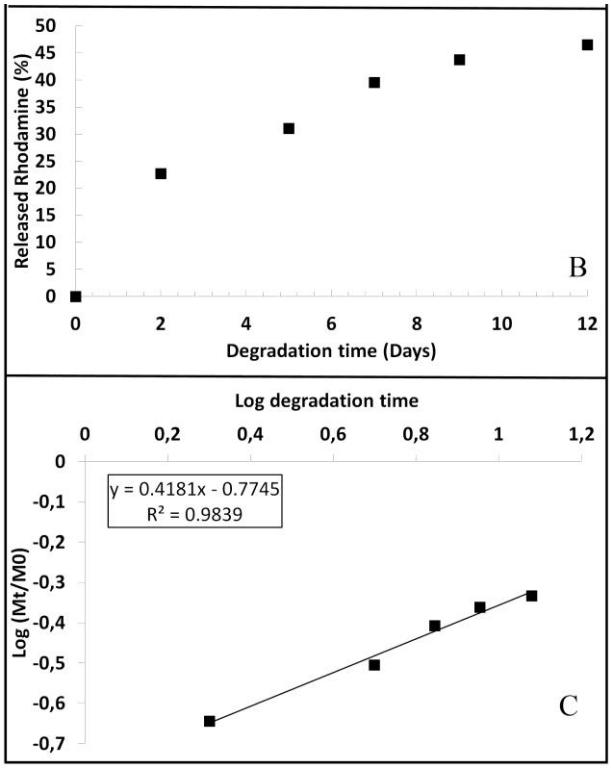

Figure 46. (B) Rhodamine B release profile from PLGA5050 mat and (C) Kinetic modeling of Rhodamine B release from PLGA5050 mat.

In conclusion, this work represents a first proof of concept to demonstrate that biodegradable and biocompatible electrospun polymeric fibrous system can be successfully employed not only as molecule carrier but also as nanoparticles carrier. Following this work, tests have been started trying to exploit the shell terminals of the used nanoparticles to perform bioconjugation with peptides capable to bind specific kind of cancer cells. The final aim of this work will be to obtain a device capable to in situ release a bioconjugated nanoparticle, being able to selectively treat just the diseased areas.

3.3 Anti CD-10 conjugated PLLA affinity membrane

https://doi.org/10.1088/0022-3727/49/27/274003

The present work reports the comparison between a conventional wet-chemical method and a non-equilibrium atmospheric pressure plasma process for the functionalization of poly(L-lactic acid) (PLLA) electrospun fibers with carboxylic groups, required for the subsequent chemical conjugation of an antibody onto the fibers surface.

PLLA nonwoven fibrous mats fabricated trough the electrospinning technology were chosen as substrate, since they are good candidates for numerous biomedical applications and are widely used as tissue engineering scaffolds, biosensors and membranes, given their high surface area and porosity (up to 90%).

The wet-chemical method was performed by means of alkaline hydrolysis at room temperature (RT), while the plasma process is carried out by means of a DBD operated at atmospheric pressure in a controlled atmosphere of a He/air mixture. After functionalization obtained by both methods, the physico-chemical and morphological properties of the electrospun PLLA fibers were evaluated and compared to those of the untreated fibers. The amount of –COOH functional groups, created at the fiber surface by both the wet chemical method and the plasma treatment, was assessed by means of fluorescence analysis after chemical derivatization with fluorescein isothiocyanate (FITC). In order to compare the efficiency of biomolecules immobilization for the chemically and the plasma treated surface functionalized fibers, the functionalization step was followed by the conjugation of an antibody (anti-CD10) to PLLA fibers surface by exploiting the carbodiimide chemistry, via 1-ethyl-3-[3-dimethylaminopropyl] carbodiimide (EDC) and hydroxysulfosuccinimide (sNHS). Finally, the presence of

the anti-CD10 antibody on the fibers surface was evaluated through a (FITC)-labeled secondary antibody by means of fluorescence intensity measurement.

The electrospinning process parameters were optimized in order to obtain PLLA defect-free fibers, randomly oriented, and characterized by a mean fiber diameter of 574 ± 190 nm, as shown in Figure 47.

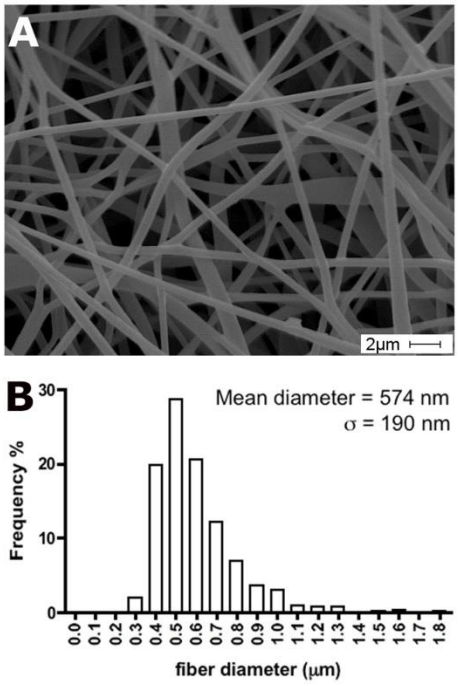

Figure 47. SEM micrograph and fiber diameter distribution of the obtained electrospun mats.

The chemical functionalization of the PLLA fibers was carried out using different alkaline hydrolysis conditions, by varying the hydrolysis time and the NaOH concentration, in order to achieve the highest density of carboxylic groups at the fiber surface while minimizing possible damage of the fibers caused by PLLA hydrolysis. PLLA fibers were treated with NaOH at concentrations of 0,01 M, 0,02 M and 0,05 M for treatment times of 5 and 10 min. In these experimental conditions, no modification of the fiber morphology was detected by SEM analysis, with respect to the as-spun, not-hydrolyzed mat. On the contrary, for concentrations of NaOH higher than 0,05 M, or for reaction times longer than 10 min, the nanofibers started collapsing and breaking (images not shown). The plasma functionalization of the PLLA fibers was performed according to the operating conditions reported in materials and methods by testing three different treatment times (5, 7,5 and 10 min). SEM analysis (Figure 48) highlighted that the treatment time of 5 min did not induce any morphological change or visible degradation to the electrospun mat. Conversely, both 7,5 min and 10 min of plasma exposure resulted in a partial loss of

the fibrous morphology and a macroscopic damage, i.e. the presence of little holes in the mat, probably due to the occurrence of polymer thermal degradation. Based on the obtained results, the 5 min plasma treatment was chosen as the optimal condition for the functionalization and the subsequent antibody conjugation step.

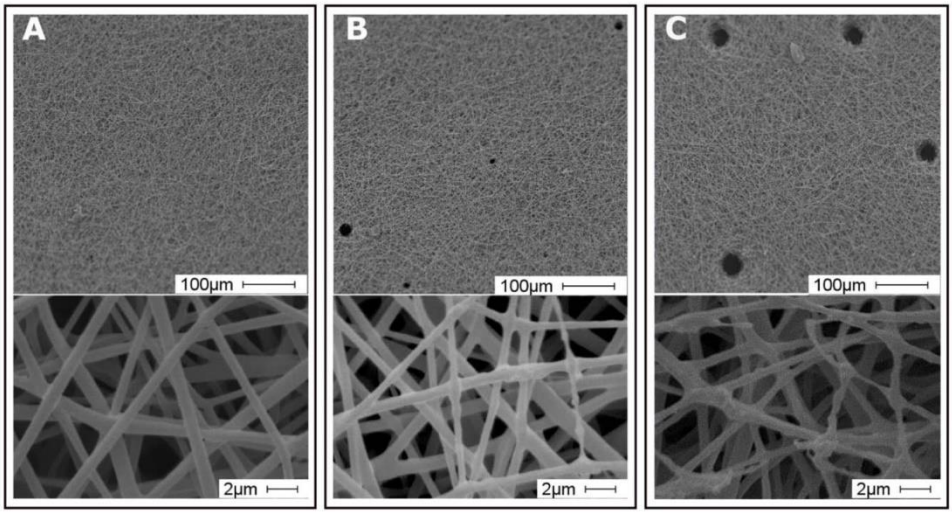

Figure 48. SEM images at two different magnifications of the plasma treated electrospun mats for 5 min (A), 7,5 min (B) and 10 min (C).

The presence of carboxyl groups onto PLLA fibers was assessed, for both the chemically and the plasma functionalized mats by means of conjugation reactions via the FITC fluorophore and measuring the –COOH-FITC mean fluorescence intensity (194). Results of the alkaline hydrolysis protocol are displayed in Figure 49 A, where the fluorescence intensity is reported as a function of NaOH concentration for the two different times investigated. As expected, the fluorescence intensity progressively increased as a function of NaOH concentration and incubation time. In light of the achieved results, the 10 min treatment with 0,05 M NaOH was selected as the optimal condition for the subsequent conjugation step.

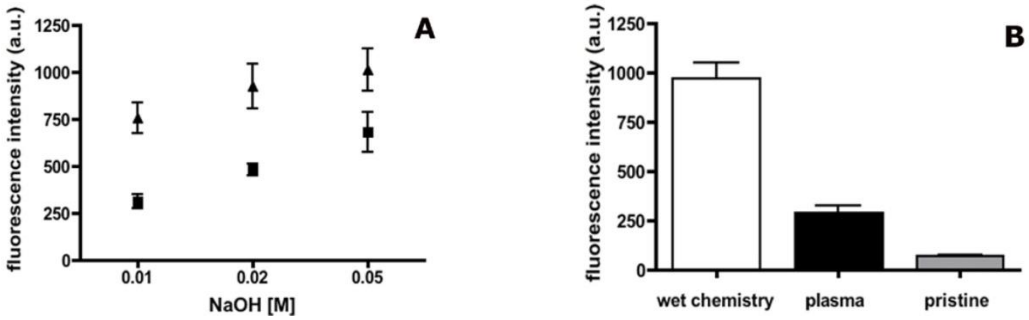

Figure 49. (A) –COOH-FITC mean fluorescence intensity response (after negative control subtraction) as a function of NaOH concentration for 5 min (■) and 10 min (▲) incubation time. (B) Comparison between –COOH-FITC mean fluorescence intensity of pristine, chemically hydrolyzed (0,05 M NaOH, 10 min) and plasma functionalized PLLA mats for 5 minutes.

Figure 49 B reports the comparison between the –COOH-FITC fluorescence intensities obtained for chemically and plasma functionalized mats, together with the results collected for the pristine PLLA mat. The fluorescence intensity of the mat after chemical hydrolysis increased more than five times if compared with that of untreated PLLA. Moreover, it can be observed that the optimal chemical hydrolysis conditions introduced a higher amount of carboxyl functionalities than the plasma treatment (Figure 49 B). Indeed, while the wet chemical method, performed by immersing samples in NaOH solution, affects all the fibers of the mat, the plasma treatment enables the effective functionalization only of the fibers directly exposed to the plasma. It is pointed out that, in order to evaluate any non-specific interactions, a control-reaction was performed on an electrospun PLLA mat without the EDC/sNHS reagents and the diaminobutane linker. In these conditions, i.e. in the absence of the conjugation reagents, the non-specific FITC fluorescence intensity resulted negligible. Electrospun mats functionalized by means of the two selected protocols—i.e. 0,05 M, 10 min NaOH hydrolysis and 5 min plasma treatment—were analyzed by GPC to evaluate the possible change in PLLA molecular weight that was expected due to hydrolysis and scission of the ester linkages of the PLLA backbone chain to generate carboxylic and hydroxyl end-groups on polymer chains. GPC measurements showed that polymer molecular weight did not change for the chemically treated mat (Mw = 129 × 103 g mol^{-1}), demonstrating that alkaline hydrolysis in the conditions applied in this work takes place mostly via a surface erosion mechanism in agreement with previous findings (195), whereas only a slight decrease was observed after the plasma treatment (M_w = 121 × 10^3 g mol^{-1}). Surface hydrophilicity of the functionalized PLLA mat was evaluated through WCA measurements and results are shown in Figure 50. A constant WCA value of 120° was obtained for pristine PLLA mat, indicating a hydrophobic behavior of the material. The carboxylic functionalization significantly lowered the WCA of the mats (compare the black square and the white square and circle in Figure 50) and increased mat wettability, allowing an almost instantaneous penetration of water. The reduction of WCA indicated that both the alkaline hydrolysis and the plasma treatment successfully improved the surface hydrophilicity.

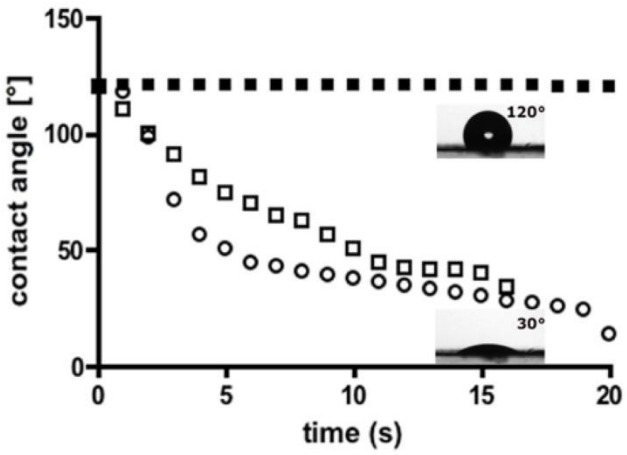

Figure 50. Contact angle behavior of pristine PLLA (■), PLLA after chemical treatment (O), PLLA after plasma treatment (□) and shape of water droplets on the electrospun mats

In order to define the suitable conditions for the antibody conjugation, a FITC labeled antibody (Ab-FITC) was used as a model compound. Ab-FITC was conjugated via EDC/sNHS to the surface of PLLA mat treated with NaOH 0,05 M for 10 min. Different conjugation conditions were tested in order to optimize the covalent binding efficiency and to minimize the non-specific interactions between the antibody and the PLLA fibers. In particular, temperature, pH, time of reaction and Ab-FITC concentration were varied. The antibody was tested at concentrations of 1 μg ml^{-1}, 5 μg ml^{-1} and 10 μg ml^{-1} in three different conditions: (I) carbonate buffer at pH 9,5 for 1 h at RT; (II) carbonate buffer at pH 9,5 for 4 h at 4 °C; (III) PBS buffer at pH 7,5 for 20 h at 4 °C. The data of the mean fluorescence intensity of the PLLA mats after Ab-FITC conjugation are highlighted in Figure 51. As a negative control the reaction was performed on NaOH hydrolyzed PLLA without EDC/sNHS to evaluate the non-specific binding of the Ab-FITC to the fiber surface.

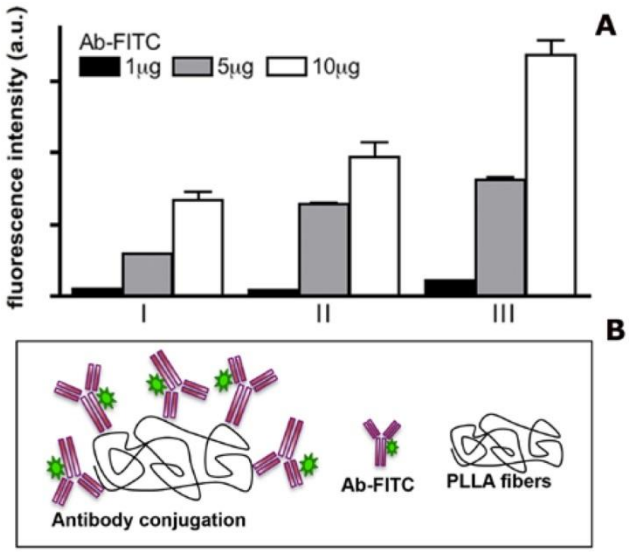

Figure 51. (A) Mean fluorescence intensity, after negative control subtraction, of Ab-FITC at the different conditions tested: (I) carbonate buffer, pH 9.5 for 1 h at RT; (II) carbonate buffer, pH 9,5 for 4 h at 4 °C; (III) PBS buffer, pH 7,5 for 20 h at 4 °C. (B) Scheme of the Ab-FITC conjugation.

As expected, the results showed an increase of fluorescence intensity as a function of Ab-FITC concentration (Figure 51). Moreover, among the tested conditions, the (III) reaction was revealed to be the most favorable for the antibody conjugation, probably due to the higher incubation time. As last step, the anti-CD10 antibody was covalently linked to the fiber surface of PLLA mats, both chemically and plasma functionalized, at the three different concentrations tested above, by using the selected optimal conjugation conditions (PBS at pH 7,5 for 20 h at 4 °C). Subsequently, in order to saturate the unreacted sites and to avoid unspecific interactions with the molecules of the Ab-FITC used to recognize the anti-CD10, the mats were incubated with BSA 2% in PBS 0,1 M pH7,5. As a negative control, the reaction was performed without primary anti-CD10 antibody in order to evaluate the unspecific interaction between Ab-FITC and the treated fibers. No significant fluorescence intensity was obtained. Figure 52 A shows the mean fluorescence intensity, after negative control subtraction, of the anti-CD10/Ab-FITC sandwich system as a function of anti-CD10 concentration. It is interesting to observe that, despite the different amount of –COOH groups introduced by the two functionalization methods, the chemically and the plasma treated PLLA mats displayed similar values of the mean fluorescence intensity due to anti-CD10 conjugation (Figure 52 A). This result suggests that the larger amount of –COOH groups, detected on the chemically functionalized mats with respect to the plasma treated ones (as shown in Figure 49 B), does not lead to a higher concentration of antibody conjugated onto the fibers.

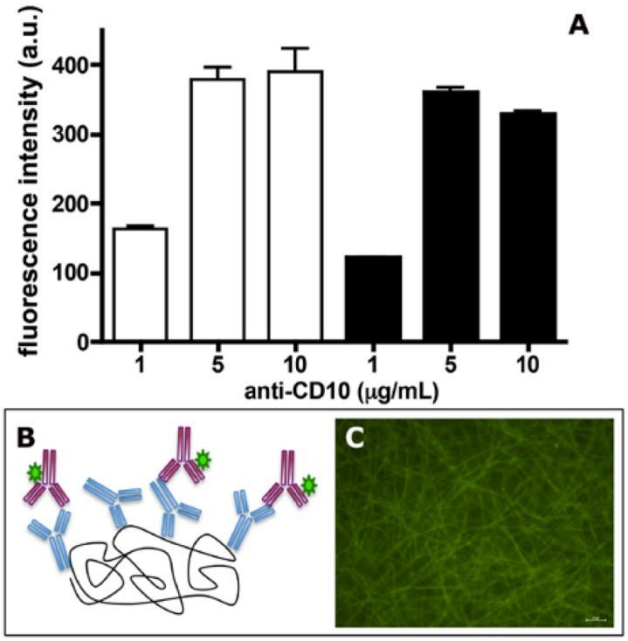

Figure 52. (A) Mean fluorescence intensity, after negative control subtraction, of the anti-CD10 conjugated at different concentrations onto the surface of PLLA mat (white bars = chemical functionalization; black bars = plasma treatment) and recognized by a (FITC)-labeled secondary antibody as schematized in (B). (C) Fluorescence microscope image of the PLLA fibers after anti-CD10 conjugation.

In conclusion, the efficacy of a non-equilibrium atmospheric pressure plasma process for the conjugation of biomolecules onto the surface of PLLA electrospun fibers has been demonstrated. The comparison between a conventional wet-chemical method and the proposed plasma assisted approach for covalently linking biomolecules was carried out through the conjugation of an artificial antibody onto chemically and plasma functionalized mats. The results clearly highlighted that a high concentration of antibody was linked to chemically and plasma functionalized mats with respect to pristine PLLA fibers and, more interestingly, no great differences in terms of antibody conjugation efficiency was detected by comparing the two functionalization approaches. The performed study brought out the possibility to replace chemical methods, usually toxic and time-consuming, with a highly flexible and eco-compatible non-equilibrium atmospheric plasma process for the effective immobilization of biomolecules onto biomaterials.

3.4 PEG-poly(CL/DDL/HDL-co-DO) synthesis, characterization and nanoparticles productions

The present work has been carried out in collaboration with Prof. Mark Saltzman and co-workers at School of Engineering and Applied Science, YALE, US.

PEG-poly(CL/DDL/HDL-*co*-DO) were synthesized via ring opening copolymerization (ROP) of CL/DDL/HDL and DO in the presence of MeO-PEG-OH as a macroinitiator. The composition (CL/DDL/HDL-DO unit ratio) of the copolymers can be controlled by adjusting the monomer ratio in the feeds (Table 11). Since the copolymer molecular weight can be significantly reduced by an excessive amount of water present in the reaction mixtures, the catalyst was dried prior to polymerization reactions, as reported in materials and methods section, and the ROP reactions were performed under nitrogen atmosphere. The obtained copolymers were characterized by GPC and NMR analyses to determine the molecular weights and structures of the products; the obtained results are reported in Table 11. For all copolymers, their PEG contents ranged from 35 to 40 wt% despite the initial feeds content of 35 wt% PEG vs total substrate (Table 11). This is primarily attributed to the incomplete conversion of DO monomer to the copolymer during the ROP reactions due to its thermodynamic constrain. All the reaction have been performed with yield (%) from 50% to 90%, lower yield have been obtained for the HDL based copolymer due to difficulties during the purification process due to the formation of waxy product.In the following paragraph the possibility to fabricate NPs from all the different obtained class of copolymers as well as their properties and stability will be discussed.

Table 11. PEG-poly(CL/DDL/HDL-co-DO) Copolymers Compositions [a]

Sample	M_w [b]	M_w/M_n [b]	DO Feed amount, mol%	DO Content, mol% [c]	PEG Content, wt% [d]	Yield [e] (%)
PEG-poly(CL-*co*-DO)-1	10300	1,6	60	55	39	65
PEG-poly(CL-*co*-DO)-2	10400	1,6	50	44	38	72
PEG-poly(CL-*co*-DO)-3	10900	1,7	40	36	38	66
PEG-poly(CL-*co*-DO)-4	11600	1,8	30	28	37	73
PEG-poly(CL-*co*-DO)-5	12100	1,8	20	19	36	82
PEG-poly(DDL-*co*-DO)-1	10800	1,6	65	57	40	61
PEG-poly(DDL-*co*-DO)-2	12500	1,6	50	43	37	73
PEG-poly(DDL-*co*-DO)-3	13600	1,7	35	29	36	74
PEG-poly(DDL-*co*-DO)-4	15200	1,8	20	17	35	90
PEG-poly(HDL-*co*-DO)-1	11800	1,6	65	54	39	59
PEG-poly(HDL-*co*-DO)-2	13100	1,8	50	38	38	51
PEG-poly(HDL-*co*-DO)-3	15000	1,9	35	30	36	46
PEG-poly(HDL-*co*-DO)-4	16200	1,9	20	16	35	54

a. The PEG blocks in the copolymers have a number average molecular weight of 2000 Da.

b. Measured by GPC using polystyrene standards.
c. Molar percentage of DO units vs (DO + CL/DDL/HDL) units in the polymer chains.
d. Weight percentage based on total polymer weight.
e. Yield was calculated on the basis of total monomer weight.

PEG-poly(CL-co-DO) NPs

All synthesized samples were successfully used to fabricate NPs via single emulsion technique using PVA as surfactant. The effect of DO content on the hydrodynamic NPs diameter, as well as on Z potential values, was evaluated (Table 12). NPs have been produced with size in the range from 43 to 60nm with Z potential values from -13 to -26mV. Interestingly DO content and the obtained NPs diameter are quasi inversely proportional.

Table 12. NPs size (nm) and Z potential (mV) of the NPs obtained starting from PEG-poly(CL-co-DO)-1-5

Samples	DO/(CL+DO) mol%	Diameter (nm)	Z pot (mV)
PEG-poly(CL-*co*-DO)-1	55	43	-21
PEG-poly(CL-*co*-DO)-2	44	49	-26
PEG-poly(CL-*co*-DO)-3	36	54	-25
PEG-poly(CL-*co*-DO)-4	28	59	-13
PEG-poly(CL-*co*-DO)-5	19	60	-13

The stability of the obtained NPs was tested by stirring them in water at 37°C up to 96 hours, the results are reported in Table 13 and Figure 53.

Table 13. Size (nm) evolution up to 96h for mild stirred NPs at 37°C. NPs obtained starting from PEG-poly(CL-co-DO)1-5.

		Mild stirring at 37°C (h)				
Samples	DO/(CL+DO) mol%	0	20	48	72	96
PEG-poly(CL-*co*-DO)-1	55	43	41	45	44	44
PEG-poly(CL-*co*-DO)-2	44	49	49	49	50	50
PEG-poly(CL-*co*-DO)-3	36	54	49	51	52	52
PEG-poly(CL-*co*-DO)-4	28	59	60	59	61	60
PEG-poly(CL-*co*-DO)-5	19	59	57	58	59	60

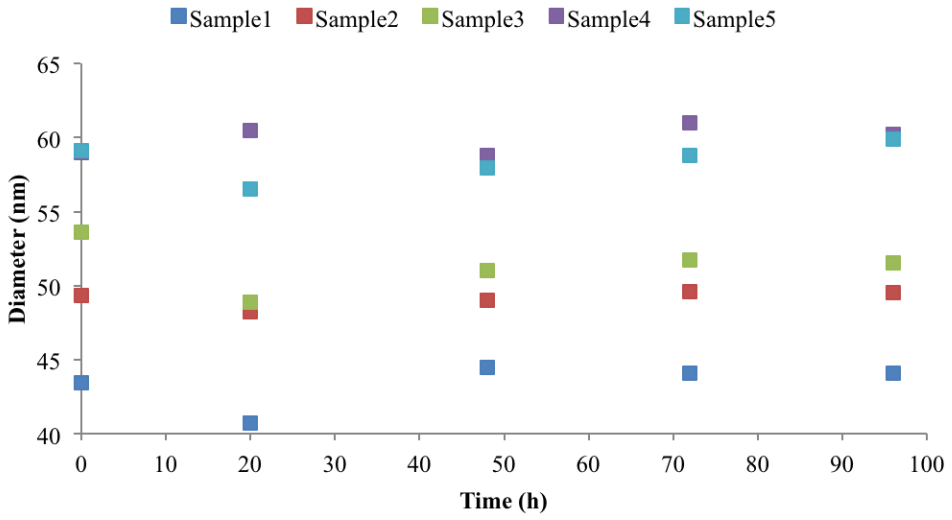

Figure 53. Size (nm) evolution up to 96h for mild stirred NPs at 37°C. NPs obtained starting from PEG-poly(CL-co-DO)1-5 (sample1-5).

As shown no significant changes of mean NPs diameter were observed during the experiment for all the samples, indicating that the PEG shell is crystalline enough to prevent the particles to stick together when solubilized. To further investigate the storage stability, the obtained NPs were (i) freeze at -20°C overnight and (ii) lyophilized. After freeze the samples were heated up to RT, shake with vortex, left stirring at 37°C for 1h and finally sonicated 3 minutes. The freeze-dried samples have been freeze at -75°C for 3h and then kept in the lyophilizer machine for 2 days. After completing the lyophilization process the samples have been resuspended in water (1 mg/mL), stirred with vortex and sonicated 5 minutes, left 37°C overnight and filtered via 0,22 µm syringe. All the obtained results, in comparison to the pristine NPs, are reported in Table 14 and Figure 54.

Table 14. Size (nm) and Z potential (mV) of pristine, freeze and freeze-dried NPs obtained starting from PEG-poly(CL-co-DO)1-5.

		Pristine		Freezing		Freeze dried [a]	
Samples	DO/(CL+DO) mol%	Size (nm)	Z potential (mV)	Size (nm)	Z potential (mV)	Size (nm)	Z potential (mV)
PEG-poly(CL-*co*-DO)-1	55	43	-21	68	-15	-	-
PEG-poly(CL-*co*-DO)-2	44	49	-26	56	-5	83	-22
PEG-poly(CL-*co*-DO)-3	36	54	-25	55	-13	47	-26
PEG-poly(CL-*co*-DO)-4	28	59	-13	61	-15	66	-28
PEG-poly(CL-*co*-DO)-5	19	59	-13	61	-	78	-28

[a] All samples (5mg/5mL) have been stirred with vortex and sonicated 5 minutes and left 37°C overnight and filtered via 0,22 µm syringe.

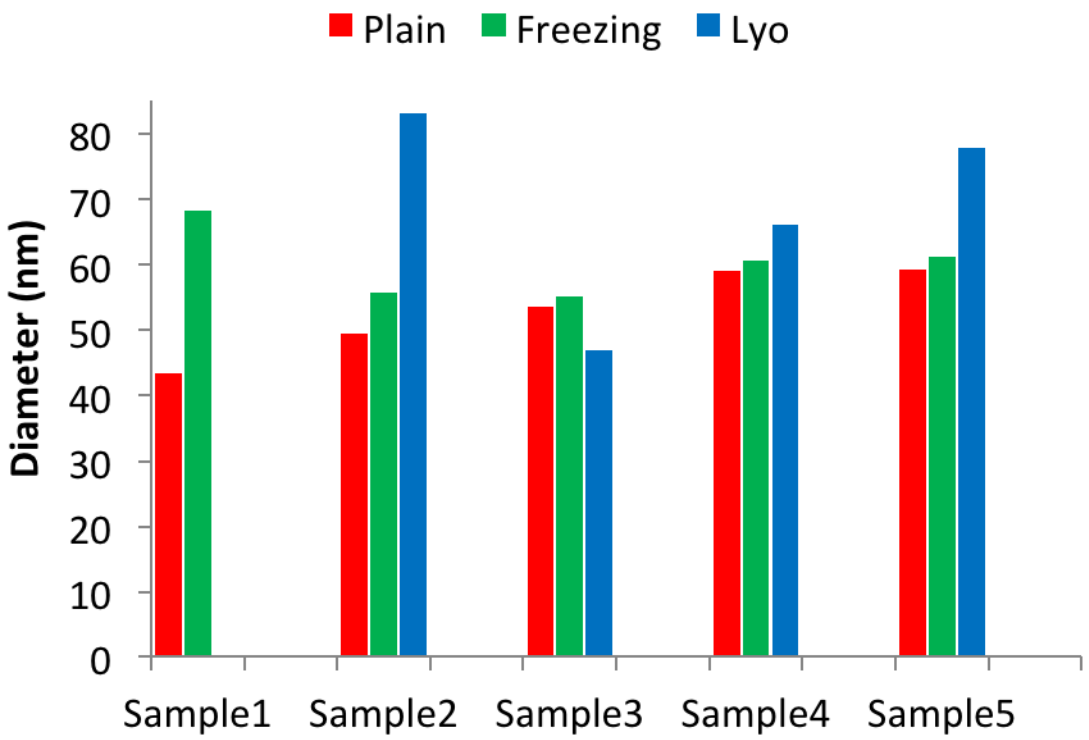

Figure 54. Size (nm) of pristine, freeze and freeze-dried NPs obtained starting from PEG-poly(CL-co-DO)1-5 (sample 1-5).

In the first experiment the NPs have been freeze and then heated to RT, left stirring at 37°C for 1h and finally sonicated 3 minutes. With this procedure it was possible to store the NPs without significantly affecting their mean diameter, except for PEG-poly(CL-co-DO)-1 (sample1, Figure 54) that after freeze showed aggregation. It is worth noticing that it was necessary to filtrate the Sample 1 and 2 with 0,22µm filters to remove some aggregate after freezing procedure. In the second experiments after lyophilization the NPs tend to stick together forming a "cotton-like" matrix that is difficult to resuspend in water. The possibility to use cryoprotectant (2:1 w/w trehalose in respect to the NPs content) was tested leading to no improvement (data not shown).

PEG-poly(DDL-co-DO) NPs

All synthesized samples were successfully used to fabricate NPs via single emulsion technique without using PVA as surfactant. The effect of DO content on the hydrodynamic NPs diameter, as well as on Z potential values, was evaluated (Table 15). NPs have been produced with size in the range from 49 to 82nm with Z potential values from -28 to -32mV.

Table 15. NPs size (nm) and Z potential (mV) of the NPs obtained starting from PEG-poly(DDL-co-DO)-1-4

Samples	DO/(CL+DO) mol%	Diameter (nm)	Z pot (mV)
PEG-poly(DDL-*co*-DO)-1	57	49	-28
PEG-poly(DDL-*co*-DO)-2	43	56	-28
PEG-poly(DDL-*co*-DO)-3	29	57	-28
PEG-poly(DDL-*co*-DO)-4	17	82	-32

To evaluate the storage stability of the obtained NPs freeze-thaw cycle, lyophilization and stability tests at 4°C have been conducted. NPs have been kept in fridge at 4°C for 4 days analyzing the diameter variation every 24h, results are reported in Table 16 and Figure 55.

Table 16. Size (nm) evolution up to 96h for NPs at 4°C. NPs obtained starting from PEG-poly(DDL-co-DO)-1-4.

Samples	DO/(CL+DO) mol%	Time at 4°C (h)				
		0	24	48	72	96
PEG-poly(DDL-*co*-DO)-1	57	49	51	52	55	55
PEG-poly(DDL-co-DO)-2	43	56	-	57	57	57
PEG-poly(DDL-co-DO)-3	29	57	57	58	58	57
PEG-poly(DDL-*co*-DO)-4	17	82	78	73	90	81

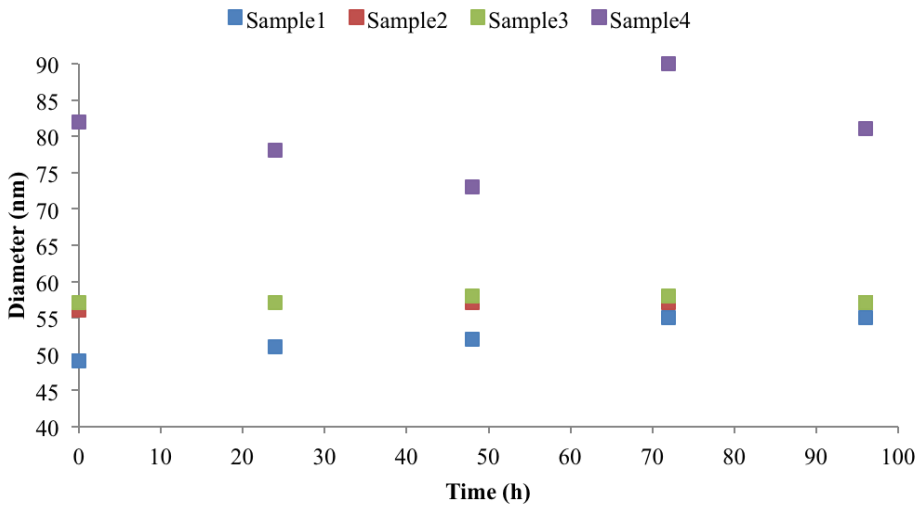

Figure 55. Size (nm) evolution up to 96h for NPs at 4°C. NPs obtained starting from PEG-poly(DDL-co-DO)-1-4.

During the tested period there was no significant change in NPs diameter for samples 1, 2 and 3 while a slight increase of NPs diameter was found for sample 4 after 72h (Table 16 and Figure 55). The possibility to store the obtained NPs as freeze aliquots or lyophilized powder have been explored. NPs obtained from samples 1 and 4 have been freeze and freeze-dried both pristine and using cryoprotectant (2:1 w/w trehalose in respect to the NPs content). The freeze samples have been kept overnight at -20°C and then let warm up at RT while the lyophilized samples have been freeze at -75°C for 3h and then kept in the lyophilizer machine for 3 days. After completing the lyophilization process the samples have been resuspended in water (1 mg/mL), vortex stirred and sonicated for 4 minutes. The resulting NPs solutions have been analyzed by mean of DLS and the results are reported in Table 17.

Table 17. Size (nm) of pristine, lyophilized and freeze-thaw NPs obtained starting from PEG-poly(DDL-co-DO) 1 and 4 with (cryo) and without (pristine) the use of cryoprotectant.

Samples	DO/(CL+DO) mol%	Pristine (nm)	Freeze-thaw pristine (nm)	Freeze-thaw cryo (nm)	Lyo Pristine (nm)	Lyo cryo (nm)
PEG-poly(DDL-*co*-DO)-1	57	49	110	105	388	221
PEG-poly(DDL-*co*-DO)-4	17	82	367	500	740	178

From the obtained results it is possible to conclude that the NPs obtained from PEG-poly(DDL-*co*-DO) are easily storable at 4°C up to 4 days while freeze the samples both with and without cryoprotectant leads to agglomerates. Lyophilization with the use of cryoprotectant lead to obtain better results compared to the pristine lyophilized samples but still some aggregations are present.

PEG-poly(HDL-co-DO) NPs

All synthesized samples were successfully used to fabricate NPs via single emulsion technique using PVA as surfactant. The effect of DO content on the hydrodynamic NPs diameter, as well as on Z potential values, was evaluated (Table 18). NPs have been produced with almost identical size in the range from 85 to 110nm with Z potential values from -12 to -24mV. It is possible to suppose that the centrifuge washing procedure influenced the obtained NPs diameters. During this procedure the centrifuge rpm was not high enough to avoid to the smaller NPs to remain in the supernatant fraction, and probably they were washed out, resulting in bigger NPs. The following results can still be considered as an interesting starting point to understand the behavior of the obtained NPs.

Table 18. Size (nm) and Z potential (mV) of the NPs obtained starting from PEG-poly(HDL-co-DO)-1-4

Samples	DO/(CL+DO) mol%	Diameter (nm)	Z pot (mV)
PEG-poly(HDL-*co*-DO)-1	54	85	-24
PEG-poly(HDL-*co*-DO)-2	38	93	-16
PEG-poly(HDL-*co*-DO)-3	30	110	-12
PEG-poly(HDL-*co*-DO)-4	16	90	-15

The NPs storage stability has been evaluated by mean of freeze-thaw cycle, lyophilization and stability tests at 4°C. NPs have been kept in fridge at 4°C for 4 days analyzing diameter variation every 24h, the results are reported in Table 19 and Figure 56.

Table 19. Size (nm) evolution up to 96h for NPs at 4°C. NPs obtained starting from PEG-poly(HDL-co-DO)-1-4.

Samples	DO/(CL+DO) mol%	4°C (h)				
		0	24	48	72	96
PEG-poly(HDL-*co*-DO)-1	54	85	84	85	82	82
PEG-poly(HDL-*co*-DO)-2	38	93	100	101	94	108
PEG-poly(HDL-*co*-DO)-3	30	110	112	104	103	106
PEG-poly(HDL-*co*-DO)-4	16	89	90	86	94	93

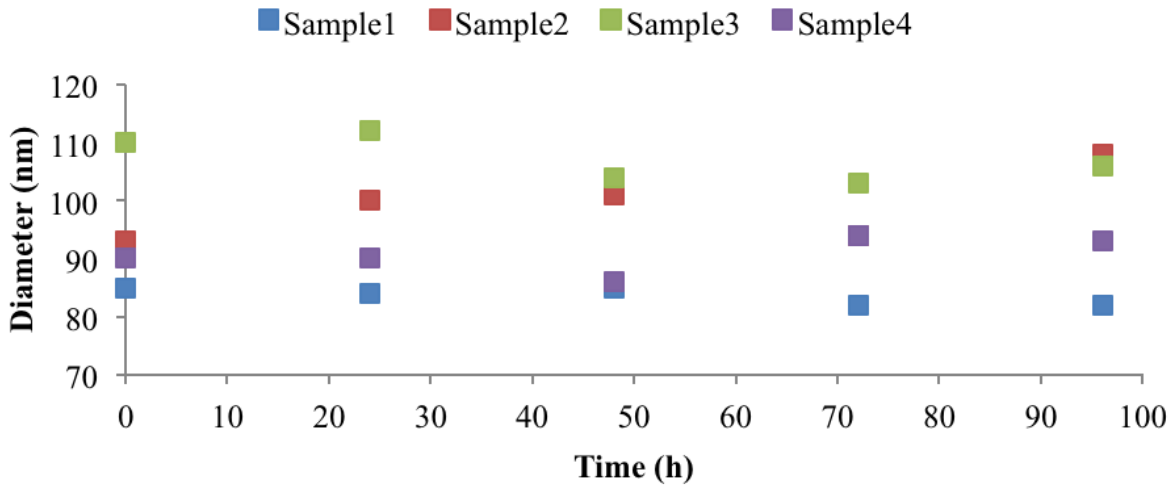

Figure 56. Size (nm) evolution up to 96h for NPs at 4°C. NPs obtained starting from PEG-poly(HDL-co-DO)-1-4

During the tested period there was no significant change in NPs diameter for all the analyzed samples. Freeze-thaw cycle as well as freeze-drying procedure have been applied to NPs obtained from samples 1 to 4. The freeze-thaw samples have been kept overnight at -20°C and then let warm up at RT while the lyophilized samples have been freeze at -75°C for 3h and then kept in the lyophilizer machine for 3 days. After completing the lyophilization process the samples have been resuspended in water (1 mg/mL), vortex stirred and sonicated for 4 minutes. The results are reported in Table 20 and Figure 57. In both cases no cryoprotectant was used and the samples were not filtered to remove possible agglomerates.

Table 20. Size (nm) of pristine, lyophilized and freeze-thaw NPs. NPs obtained starting from PEG-poly(HDL-co-DO)-1-4

Samples	DO/(CL+DO) mol%	Pristine (nm)	Freeze-thaw (nm)	Lyo (nm)
PEG-poly(HDL-*co*-DO)-1	54	85	83	308
PEG-poly(HDL-*co*-DO)-2	38	93	112	-[a]
PEG-poly(HDL-*co*-DO)-3	30	110	102	-[a]
PEG-poly(HDL-*co*-DO)-4	16	89	91	136

[a] Samples to diluted to perform a reliable tests.

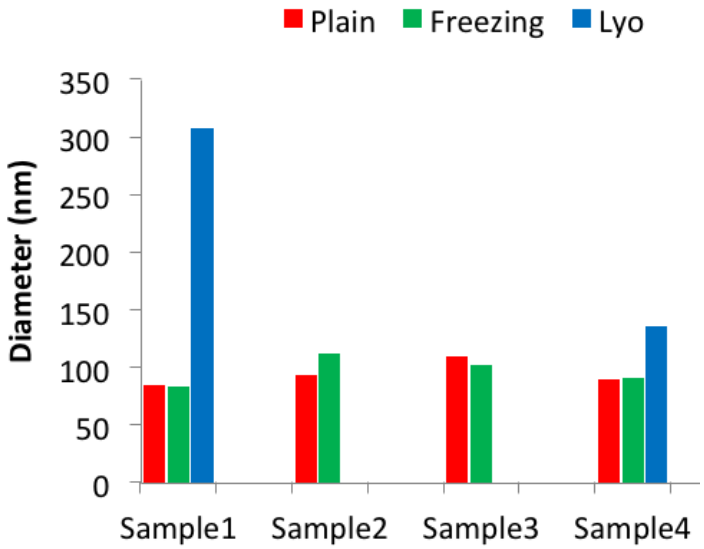

Figure 57. Size (nm) of pristine, freeze and lyophilized NPs. NPs obtained starting from PEG-poly(HDL-co-DO)-1-4

From the obtained results it is possible to conclude that the NPs obtained from PEG-poly(HDL-*co*-DO) are easily storable both at 4°C up to 4 days and as freeze aliquots without cryoprotectant avoiding NPs aggregation. Lyophilization lead to obtain some aggregate. It is possible to speculate that the good results

obtained for the freeze procedure can be related to the low concentration of the obtained NPs solution after centrifuge washing procedure.

In conclusion all the obtained copolymers have been tested and lead to NPs with diameters ranging from 40nm to 110nm. It was demonstrated that the NPs are effectively storable at least with one of the above described methods. Considering the reported data the obtained NPs have the potential of being used as drug delivery carrier, in particular in the field of brain cancer therapy. In fact NPs to be used in this field should be in the range of 20-100nm, i.e. small enough to cross the brain blood barrier (BBB) but not too small to avoid fast clearance effect. The work is proceeding, in collaboration with professor Mark Saltzman from Yale University, by evaluating the capacity of the obtained NPs to store drugs and evaluating the release behavior from the loaded particles. Once the *in vitro* tests will be finished the most promising NPs will be evaluated *in vivo*.

4 Conclusions

Much work has been done during this PhD concerning the use of polymeric materials in the biomedical fields and much still needs to be done. All the reported works, performed in collaboration with different research institution, universities and hospitals have been done with the idea to focus on the polymers structure-properties relation in order to always find the best match between the physical chemical polymeric characteristics and the specific final applications.

During this Thesis project different polymeric materials have been studied to achieve promising application in the biomedical fields, especially in drug delivery and tissue engineering.

Shape memory electrospun scaffolds, capable to switch from permanent to temporary shape at temperature comparable to human body temperature have been obtained starting from biocompatible and biodegradable polymers; their physical and chemical properties have been evaluated demonstrating excellent shape memory behavior.

In the field of drug delivery three different research lines have been explored (i) electrospun scaffolds as drug carrier (ii) electrospun scaffold as NPs carrier and (iii) composite material as dual drug delivery system. It was also studied the possibility to use electrospun scaffolds not only as drug carrier but also as suitable substrate for functionalization and bioconjugation of specific antibodies to achieve smart affinity membrane, in particular during this work It was possible to bioconjugated PLLA scaffolds by mean of chemical and physical approach, leading to antibody decorated fibrous structure. Electrospun scaffolds were also used as efficient core-shell silica NPs carrier obtaining a material capable to release the embedded NPs according to its degradation behavior avoiding the NPs release by diffusion. Finally electrospun polymeric carriers have been used to produce composites materials with partially reticulated gelatin; in this case the obtained homogeneous composites have been loaded with two different drugs, to be released with a controllable and distinct kinetics. This result was achieved by carefully selecting the properties of both polymeric carrier and gelatin layer, as well as evaluating the architecture of the fabricated composites.

During the abroad research activities, performed at Yale University as part of my PhD, the possibility to synthesize novel biodegradable copolymers has been investigated leading to the synthesis and purification of 13 new different copolymers. The obtained materials have been used to demonstrate the possibility to fabricate NPs in the nanometric range and the physical properties of the obtained samples have been studied as well as their storage stability.

The reported studies represent just a starting point and works have been planned for the near future in order to complete and improve the performed research activities. The obtained multi-drug delivery system will be further studied in collaboration with IRST institute (Istituto Scientifico Romagnolo per lo studio e la cura dei tumori) in order to evaluate its bioactivity; new composites will be fabricated with the use of different polymers and approaches, for example trying to obtain multi-layer devices, with the possibility to deliver in a controlled way even more than two drugs. The used luminescent core-shell silica NPs will be conjugated with peptides in order to be capable to detect specific cells once in-situ released and, finally, the newly synthesized biodegradable block-copolymers will be tested as nanoparticles drug carrier with the final aim to obtain a smart tool to treat Glioblastomas.

In conclusion, the biomedical field represents a vast sector that the scientific community has just started to study with novel technologies and knowledge. This Thesis work represents a small contribution, with the hope that one day some of the reported studies might be applied to make the life of patients somehow better.

5 References

1. Williams, David F. "On the nature of biomaterials." Biomaterials30.30 (2009): 5897-5909.
2. Jebakumar, A. Zechariah, Muhammad Idrees, and Hassan S. Nondo. “” "Journal of Science Health Sciences."
3. Luckachan, Gisha E., and C. K. S. Pillai. "Biodegradable polymers-a review on recent trends and emerging perspectives." Journal of Polymers and the Environment 19.3 (2011): 637-676.
4. Nair, Lakshmi S., and Cato T. Laurencin. "Biodegradable polymers as biomaterials." Progress in polymer science 32.8-9 (2007): 762-798.
5. Asghari, Fatemeh, et al. "Biodegradable and biocompatible polymers for tissue engineering application: a review." Artificial cells, nanomedicine, and biotechnology 45.2 (2017): 185-192.
6. Gomes, Manuela E., and R. L. Reis. "Biodegradable polymers and composites in biomedical applications: from catgut to tissue engineering. Part 1 Available systems and their properties." International materials reviews 49.5 (2004): 261-273.
7. Lee, Chi H., Anuj Singla, and Yugyung Lee. "Biomedical applications of collagen." International journal of pharmaceutics221.1-2 (2001): 1-22.
8. Gentile, Piergiorgio, et al. "An overview of poly (lactic-co-glycolic) acid (PLGA)-based biomaterials for bone tissue engineering." International journal of molecular sciences 15.3 (2014): 3640-3659.
9. Jayakumar, Rangasamy, et al. "Biomedical applications of chitin and chitosan based nanomaterials—A short review." Carbohydrate Polymers 82.2 (2010): 227-232.
10. Blum, Angela P., et al. "Stimuli-responsive nanomaterials for biomedical applications." Journal of the American Chemical Society 137.6 (2015): 2140-2154.
11. Calderón, Marcelo, et al. "Development of efficient acid cleavable multifunctional prodrugs derived from dendritic polyglycerol with a poly (ethylene glycol) shell." Journal of controlled release 151.3 (2011): 295-301.
12. Agasti, Sarit S., et al. "Photoregulated release of caged anticancer drugs from gold nanoparticles." Journal of the American Chemical Society 131.16 (2009): 5728-5729.
13. Place, Elsie S., et al. "Synthetic polymer scaffolds for tissue engineering." Chemical Society Reviews 38.4 (2009): 1139-1151.
14. Gu, Frank X., et al. "Targeted nanoparticles for cancer therapy." Nano today 2.3 (2007): 14-21
15. Singh, Rajesh, and James W. Lillard Jr. "Nanoparticle-based targeted drug delivery." Experimental and molecular pathology86.3 (2009): 215-223.
16. Greiner, Andreas, and Joachim H. Wendorff. "Electrospinning: a fascinating method for the preparation of ultrathin fibers." Angewandte Chemie International Edition 46.30 (2007): 5670-5703.

17. Ryan, C. N., K. L. Smith, and J. P. W. Stark. "The influence of geometry on the flow rate sensitivity to applied voltage within cone-jet mode electrospray." Journal of Applied Physics 112.11 (2012): 114510.
18. Mitchell, Geoffrey R., ed. Electrospinning: principles, practice and possibilities. Royal Society of Chemistry, 2015.
19. De Vrieze, Sander, et al. "The effect of temperature and humidity on electrospinning." Journal of materials science 44.5 (2009): 1357.
20. Wannatong, Ladawan, Anuvat Sirivat, and Pitt Supaphol. "Effects of solvents on electrospun polymeric fibers: preliminary study on polystyrene." Polymer International 53.11 (2004): 1851-1859.
21. Wool, Richard P. "Polymer entanglements." Macromolecules26.7 (1993): 1564-1569.
22. Shenoy, Suresh L., et al. "Role of chain entanglements on fiber formation during electrospinning of polymer solutions: good solvent, non-specific polymer–polymer interaction limit." Polymer46.10 (2005): 3372-3384.
23. Teo, Wee E., and Seeram Ramakrishna. "A review on electrospinning design and nanofibre assemblies." Nanotechnology 17.14 (2006): R89.
24. Mirjalili, Mohammad, and Salar Zohoori. "Review for application of electrospinning and electrospun nanofibers technology in textile industry." Journal of Nanostructure in Chemistry 6.3 (2016): 207-213.
25. Sundarrajan, Subramanian, et al. "Electrospun nanofibers for air filtration applications." Procedia Engineering 75 (2014): 159-163.
26. Suja, P. S., et al. "Electrospun nanofibrous membranes for water purification." Polymer Reviews 57.3 (2017): 467-504.
27. Structure and Properties of Composites (TW Chou ed.) VCH Weinheim, 1993, p. 625, Price DM 430,– ." Acta Polymerica 45.1 (1994): 56-57.
28. Formo, Eric, et al. "Functionalization of electrospun TiO2 nanofibers with Pt nanoparticles and nanowires for catalytic applications." Nano Letters 8.2 (2008): 668-672.
29. Stevens, Molly M., and Julian H. George. "Exploring and engineering the cell surface interface." Science 310.5751 (2005): 1135-1138.
30. Dahlin, Rebecca L., F. Kurtis Kasper, and Antonios G. Mikos. "Polymeric nanofibers in tissue engineering." Tissue Engineering Part B: Reviews 17.5 (2011): 349-364.
31. Tamayol, Ali, et al. "Fiber-based tissue engineering: Progress, challenges, and opportunities." Biotechnology advances 31.5 (2013): 669-687.
32. Hoffmann, Jan, et al. "Photopatterning of thermally sensitive hydrogels useful for microactuators." Sensors and Actuators A: Physical 77.2 (1999): 139-144.
33. Calderón, Marcelo, et al. "Development of efficient acid cleavable multifunctional prodrugs derived from dendritic polyglycerol with a poly (ethylene glycol) shell." Journal of controlled release 151.3 (2011): 295-301.
34. Du, Jin-Zhi, et al. "Tailor-made dual pH-sensitive polymer–doxorubicin nanoparticles for efficient anticancer drug delivery." Journal of the American Chemical Society 133.44 (2011): 17560-17563.
35. Gebhardt, Kay E., et al. "Rod-sphere transition in polybutadiene− poly (L-lysine) block copolymer assemblies." Langmuir 23.5 (2007): 2851-2856.

36. Liu, Guhuan, et al. "Self-immolative polymersomes for high-efficiency triggered release and programmed enzymatic reactions." Journal of the American Chemical Society 136.20 (2014): 7492-7497.
37. Phillips, Daniel J., et al. "Glutathione-triggered disassembly of isothermally responsive polymer nanoparticles obtained by nanoprecipitation of hydrophilic polymers." Polymer Chemistry5.1 (2014): 126-131.
38. Satchi, R., T. A. Connors, and R. Duncan. "PDEPT: polymer-directed enzyme prodrug therapy." British journal of cancer 85.7 (2001): 1070.
39. Vicent, María J., et al. "Polymer therapeutics designed for a combination therapy of hormone-dependent cancer." Angewandte Chemie International Edition 44.26 (2005): 4061-4066.
40. Chien, Miao-Ping, et al. "Programmable shape-shifting micelles." Angewandte Chemie International Edition 49.30 (2010): 5076-5080.
41. Ku, Ti-Hsuan, et al. "Controlling and switching the morphology of micellar nanoparticles with enzymes." Journal of the American Chemical Society 133.22 (2011): 8392-8395.
42. Yin, Xiangchun, Allan S. Hoffman, and Patrick S. Stayton. "Poly (N-isopropylacrylamide-co-propylacrylic acid) copolymers that respond sharply to temperature and pH." Biomacromolecules 7.5 (2006): 1381-1385.
43. Huang, Xiaonan, et al. "Acid-sensitive polymeric micelles based on thermoresponsive block copolymers with pendent cyclic orthoester groups." Macromolecules 42.3 (2009): 783-790.
44. MacKay, J. Andrew, et al. "Self-assembling chimeric polypeptide–doxorubicin conjugate nanoparticles that abolish tumours after a single injection." Nature materials 8.12 (2009): 993.
45. Moughton, Adam O., Joseph P. Patterson, and Rachel K. O'Reilly. "Reversible morphological switching of nanostructures in solution." Chemical Communications 47.1 (2011): 355-357.
46. Johnson, Jeremiah A., et al. "Core-clickable PEG-branch-azide bivalent-bottle-brush polymers by ROMP: grafting-through and clicking-to." Journal of the American Chemical Society 133.3 (2010): 559-566.
47. Muraoka, Takahiro, et al. "Light-triggered bioactivity in three dimensions." Angewandte Chemie 121.32 (2009): 6060-6063.
48. Du, Jin-Zhi, et al. "Micelle-to-vesicle morphological transition via light-induced rapid hydrophilic arm detachment from a star polymer." Chemical Communications 48.9 (2012): 1257-1259.
49. Wei, Menglian, et al. "Stimuli-responsive polymers and their applications." Polymer Chemistry 8.1 (2017): 127-143.
50. Chaterji, Somali, Il Keun Kwon, and Kinam Park. "Smart polymeric gels: redefining the limits of biomedical devices." Progress in polymer science 32.8-9 (2007): 1083-1122.
51. Palombo, M. S., Y. Singh, and P. J. Sinko. "Prodrug and conjugate drug delivery strategies for improving HIV/AIDS therapy." Journal of drug delivery science and technology 19.1 (2009): 3-14.
52. Wei, Menglian, et al. "Stimuli-responsive polymers and their applications." Polymer Chemistry 8.1 (2017): 127-143.
53. Kamada, Haruhiko, et al. "Design of a pH-sensitive polymeric carrier for drug release and its application in cancer therapy." Clinical Cancer Research 10.7 (2004): 2545-2550.
54. Rofstad, Einar K., et al. "Acidic extracellular pH promotes experimental metastasis of human melanoma cells in athymic nude mice." Cancer research 66.13 (2006): 6699-6707.

55. Liu, Yanhua, et al. "pH-sensitive polymeric micelles triggered drug release for extracellular and intracellular drug targeting delivery." asian journal of pharmaceutical sciences 8.3 (2013): 159-167.
56. Ohya, Shoji, et al. "The potential of poly (N-isopropylacrylamide)(PNIPAM)-grafted hyaluronan and PNIPAM-grafted gelatin in the control of post-surgical tissue adhesions." Biomaterials 26.6 (2005): 655-659.
57. Sosnik, Alejandro, and Daniel Cohn. "Ethoxysilane-capped PEO–PPO–PEO triblocks: a new family of reverse thermo-responsive polymers." Biomaterials 25.14 (2004): 2851-2858.
58. Suwa, Kazuo, et al. "Synthesis and functionalities of poly (N-vinylalkylamide). V. Control of a lower critical solution temperature of poly (N-vinylalkylamide)." Journal of Polymer Science Part A: Polymer Chemistry 35.15 (1997): 3087-3094.
59. Lendlein, Andreas, and Steffen Kelch. "Shape-memory polymers." Angewandte Chemie International Edition 41.12 (2002): 2034-2057.
60. Lendlein, Andreas, et al. "Light-induced shape-memory polymers." Nature 434.7035 (2005): 879-882.
61. Schmidt, Annette M. "Electromagnetic activation of shape memory polymer networks containing magnetic nanoparticles." Macromolecular Rapid Communications 27.14 (2006): 1168-1172.
62. Lendlein, Andreas, and Robert Langer. "Biodegradable, elastic shape-memory polymers for potential biomedical applications." Science 296.5573 (2002): 1673-1676.
63. Hu, Jinlian. Shape memory polymers and textiles. Elsevier, 2007.
64. Xie, Tao. "Recent advances in polymer shape memory." Polymer 52.22 (2011): 4985-5000.
65. Zhu, G., et al. "Shape-memory effects of radiation crosslinked poly (ϵ-caprolactone)." Journal of Applied Polymer Science 90.6 (2003): 1589-1595.
66. Mather, Patrick T., et al. "Crosslinked polycyclooctene." U.S. Patent No. 7,173,096. 6 Feb. 2007.
67. Muto, Koji, et al. "Polyethylene heat shrinkable tube." U.S. Patent No. 6,887,539. 3 May 2005.
68. Lendlein, Andreas, Annette M. Schmidt, and Robert Langer. "AB-polymer networks based on oligo (ε-caprolactone) segments showing shape-memory properties." Proceedings of the National Academy of Sciences 98.3 (2001): 842-847.
69. Alteheld, Armin, et al. "Biodegradable, amorphous copolyester-urethane networks having shape-memory properties." Angewandte Chemie International Edition 44.8 (2005): 1188-1192.
70. Chen, Wei, Chengye Zhu, and Xuerong Gu. "Thermosetting polyurethanes with water-swollen and shape memory properties." Journal of applied polymer science 84.8 (2002): 1504-1512.
71. Skákalová, Viera, Vladimír Lukeš, and Martin Breza. "Shape memory effect of dehydrochlorinated crosslinked poly (vinyl chloride)." Macromolecular Chemistry and Physics 198.10 (1997): 3161-3172.
72. Nagai, H., A. Ueda, and S. Isomura. "Shape-memory Norbornene Polymer Molded Products." Jpn. Pat 6080768 (1994).
73. Yang, Fuqian, Shengliang Zhang, and James CM Li. "Impression recovery of amorphous polymers." Journal of Electronic Materials 26.7 (1997): 859.
74. Kraft, Arno, and Gouher Rabani. "Thermally induced shape-memory effect in segmented copolymers containing polycaprolactone soft segments and aramid hard segments." Polymeric Materials Science and Engineering 90 (2004).
75. Min, Changchun, et al. "Biodegradable shape-memory polymer—polylactide-co-poly (glycolide-co-caprolactone) multiblock copolymer." Polymers for Advanced Technologies 16.8 (2005): 608-615.

76. Mather, P. T., et al. "Synthesis of nonionic telechelic polymers incorporating polyhedral oligosilsesquioxane and uses thereof." US. Pat 2004024098 (2004).
77. Behl, Marc, and Andreas Lendlein. "Shape-memory polymers." Materials today 10.4 (2007): 20-28.
78. Liu, C., H. Qin, and P. T. Mather. "Review of progress in shape-memory polymers." Journal of materials chemistry 17.16 (2007): 1543-1558.
79. Baer, Géraldine M., et al. "Thermomechanical properties, collapse pressure, and expansion of shape memory polymer neurovascular stent prototypes." Journal of Biomedical Materials Research Part B: Applied Biomaterials 90.1 (2009): 421-429.
80. Xue, Liang, Shiyao Dai, and Zhi Li. "Biodegradable shape-memory block co-polymers for fast self-expandable stents." Biomaterials 31.32 (2010): 8132-8140.
81. Lendlein, Andreas, and Robert Langer. "Biodegradable, elastic shape-memory polymers for potential biomedical applications." Science 296.5573 (2002): 1673-1676.
82. Wache, H. M., et al. "Development of a polymer stent with shape memory effect as a drug delivery system." Journal of Materials Science: Materials in Medicine 14.2 (2003): 109-112.
83. Zhang, Jing-Nan, et al. "Microfiber SMPU film affords quicker shape recovery than the bulk one." Materials Letters 65.23-24 (2011): 3639-3642.
84. Marcel Dekker. “Colloidal Drug Delivery Systems” , New York, (1994): 219 – 342
85. Fernández-Urrusuno, Rocío, et al. "Enhancement of nasal absorption of insulin using chitosan nanoparticles." Pharmaceutical research 16.10 (1999): 1576-1581.
86. Farrugia, claude a., and Michael J. Groves. "Gelatin behaviour in dilute aqueous solution: designing a nanoparticulate formulation." Journal of pharmacy and pharmacology 51.6 (1999): 643-649.
87. Wood, David A. "Biodegradable drug delivery systems." International Journal of pharmaceutics 7.1 (1980): 1-18.
88. Pitt, Colin G., et al. "Sustained drug delivery systems II: Factors affecting release rates from poly (ε-caprolactone) and related biodegradable polyesters." Journal of pharmaceutical sciences68.12 (1979): 1534-1538.
89. Nanjwade, Basavaraj K., et al. "Preparation and evaluation of carboplatin biodegradable polymeric nanoparticles." International journal of pharmaceutics 385.1-2 (2010): 176-180.
90. Rejinold, N. Sanoj, et al. "Biodegradable and thermo-sensitive chitosan-g-poly (N-vinylcaprolactam) nanoparticles as a 5-fluorouracil carrier." Carbohydrate polymers 83.2 (2011): 776-786.
91. Park, Jason, et al. "PEGylated PLGA nanoparticles for the improved delivery of doxorubicin." Nanomedicine: Nanotechnology, Biology and Medicine 5.4 (2009): 410-418.
92. Agnihotri, Sunil A., and Tejraj M. Aminabhavi. "Novel interpenetrating network chitosan-poly (ethylene oxide-g-acrylamide) hydrogel microspheres for the controlled release of capecitabine." International journal of pharmaceutics 324.2 (2006): 103-115.
93. Bilensoy, Erem, et al. "Intravesical cationic nanoparticles of chitosan and polycaprolactone for the delivery of Mitomycin C to bladder tumors." International journal of pharmaceutics 371.1-2 (2009): 170-176.
94. Saraogi, Gaurav Kant, et al. "Gelatin nanocarriers as potential vectors for effective management of tuberculosis." International journal of pharmaceutics 385.1-2 (2010): 143-149.
95. Lai, Jie, et al. "Pharmacokinetics and enhanced oral bioavailability in beagle dogs of cyclosporine A encapsulated in glyceryl monooleate/poloxamer 407 cubic nanoparticles." International journal of nanomedicine 5 (2010): 13.

96. Dev, Ashish, et al. "Preparation of poly (lactic acid)/chitosan nanoparticles for anti-HIV drug delivery applications." Carbohydrate polymers 80.3 (2010): 833-838.
97. Wilson, Barnabas, et al. "Chitosan nanoparticles as a new delivery system for the anti-Alzheimer drug tacrine." Nanomedicine: Nanotechnology, Biology and Medicine 6.1 (2010): 144-152.
98. Arayachukeat, Sunatda, Supason P. Wanichwecharungruang, and Thapakorn Tree-Udom. "Retinyl acetate-loaded nanoparticles: dermal penetration and release of the retinyl acetate." International journal of pharmaceutics 404.1-2 (2011): 281-288.
99. Turos, Edward, et al. "Antibiotic-conjugated polyacrylate nanoparticles: new opportunities for development of anti-MRSA agents." Bioorganic & medicinal chemistry letters 17.1 (2007): 53-56.
100. Pandey, Rajesh, et al. "Nano-encapsulation of azole antifungals: potential applications to improve oral drug delivery." International Journal of Pharmaceutics 301.1-2 (2005): 268-276.
101. Ueda, M., A. Iwara, and J. Kreuter. "Influence of the preparation methods on the drug release behaviour of loperamide-loaded nanoparticles." Journal of microencapsulation 15.3 (1998): 361-372.
102. Laurita, Romolo, et al. "Plasma Processing of Electrospun Li-Ion Battery Separators to Improve Electrolyte Uptake." Plasma Processes and Polymers 13.1 (2016): 124-133.
103. Sinha, Rajni, et al. "Nanotechnology in cancer therapeutics: bioconjugated nanoparticles for drug delivery." Molecular cancer therapeutics 5.8 (2006): 1909-1917.
104. Bennet, Devasier, and Sanghyo Kim. "Polymer nanoparticles for smart drug delivery." Application of Nanotechnology in Drug Delivery. InTech, 2014.
105. Sill, Travis J., and Horst A. von Recum. "Electrospinning: applications in drug delivery and tissue engineering." Biomaterials 29.13 (2008): 1989-2006.
106. Chou, Shih-Feng, Daniel Carson, and Kim A. Woodrow. "Current strategies for sustaining drug release from electrospun nanofibers." Journal of Controlled Release 220 (2015): 584-591.
107. Yoo, Hyuk Sang, Taek Gyoung Kim, and Tae Gwan Park. "Surface-functionalized electrospun nanofibers for tissue engineering and drug delivery." Advanced drug delivery reviews61.12 (2009): 1033-1042.
108. Ignatova, Milena, Iliya Rashkov, and Nevena Manolova. "Drug-loaded electrospun materials in wound-dressing applications and in local cancer treatment." Expert opinion on drug delivery 10.4 (2013): 469-483.
109. Huang, Hui-Hua, et al. "Preparation of core-shell biodegradable microfibers for long-term drug delivery." Journal of Biomedical Materials Research Part A: An Official Journal of The Society for Biomaterials, The Japanese Society for Biomaterials, and The Australian Society for Biomaterials and the Korean Society for Biomaterials 90.4 (2009): 1243-1251.
110. Li, Long, et al. "Controlled dual delivery of BMP-2 and dexamethasone by nanoparticle-embedded electrospun nanofibers for the efficient repair of critical-sized rat calvarial defect." Biomaterials 37 (2015): 218-229.
111. Kenawy, El-Refaie, et al. "Release of tetracycline hydrochloride from electrospun poly (ethylene-co-vinylacetate), poly (lactic acid), and a blend." Journal of controlled release 81.1-2 (2002): 57-64.
112. Zahedi, Payam, et al. "Preparation and performance evaluation of tetracycline hydrochloride loaded wound dressing mats based on electrospun nanofibrous poly (lactic acid)/poly (ϵ-caprolactone) blends." Journal of Applied Polymer Science 124.5 (2012): 4174-4183.
113. Cao, Haoqing, et al. "RNA interference by nanofiber-based siRNA delivery system." Journal of Controlled Release 144.2 (2010): 203-212.

114. Gilchrist, Samuel E., et al. "Fusidic acid and rifampicin co-loaded PLGA nanofibers for the prevention of orthopedic implant associated infections." Journal of controlled release 170.1 (2013): 64-73.
115. Huang, Li-Ya, et al. "Time-engineeringed biphasic drug release by electrospun nanofiber meshes." International journal of pharmaceutics 436.1-2 (2012): 88-96.
116. Jiang, Hongliang, et al. "Preparation and characterization of ibuprofen-loaded poly (lactide-co-glycolide)/poly (ethylene glycol)-g-chitosan electrospun membranes." Journal of Biomaterials Science, Polymer Edition 15.3 (2004): 279-296.
117. Kim, Kwangsok, et al. "Incorporation and controlled release of a hydrophilic antibiotic using poly (lactide-co-glycolide)-based electrospun nanofibrous scaffolds." Journal of Controlled Release 98.1 (2004): 47-56.
118. Kowalczyk, Tomasz, et al. "Electrospinning of bovine serum albumin. Optimization and the use for production of biosensors." Biomacromolecules 9.7 (2008): 2087-2090.
119. Lu, Tiancheng, et al. "Doxorubicin-loaded ultrafine PEG-PLA fiber mats against hepatocarcinoma." Journal of Applied Polymer Science 123.1 (2012): 209-217.
120. Luu, Y. K., et al. "Development of a nanostructured DNA delivery scaffold via electrospinning of PLGA and PLA–PEG block copolymers." Journal of controlled release 89.2 (2003): 341-353.
121. Mickova, Andrea, et al. "Core/shell nanofibers with embedded liposomes as a drug delivery system." Biomacromolecules 13.4 (2012): 952-962.
122. Ranganath, Sudhir H., and Chi-Hwa Wang. "Biodegradable microfiber implants delivering paclitaxel for post-surgical chemotherapy against malignant glioma." Biomaterials 29.20 (2008): 2996-3003.
123. Xie, Jingwei, Ruo Shan Tan, and Chi-Hwa Wang. "Biodegradable microparticles and fiber fabrics for sustained delivery of cisplatin to treat C6 glioma in vitro." Journal of Biomedical Materials Research Part A: An Official Journal of The Society for Biomaterials, The Japanese Society for Biomaterials, and The Australian Society for Biomaterials and the Korean Society for Biomaterials 85.4 (2008): 897-908.
124. Liu, Daxing, et al. "Necrosis of cervical carcinoma by dichloroacetate released from electrospun polylactide mats." Biomaterials 33.17 (2012): 4362-4369.
125. Xu, Xiuling, et al. "Preparation of core-sheath composite nanofibers by emulsion electrospinning." Macromolecular Rapid Communications 27.19 (2006): 1637-1642.
126. Chen, Mengxia, et al. "Antitumor efficacy of a PLGA composite nanofiber embedded with doxorubicin@ MSNs and hydroxycamptothecin@ HANPs." RSC Advances 4.95 (2014): 53344-53351.
127. Yohe, Stefan T., et al. "3D superhydrophobic electrospun meshes as reinforcement materials for sustained local drug delivery against colorectal cancer cells." Journal of controlled release 162.1 (2012): 92-101.
128. Ma, Yue, et al. "Local, combination chemotherapy in prevention of cervical cancer recurrence after surgery by using nanofibers co-loaded with cisplatin and curcumin." RSC Advances 5.129 (2015): 106325-106332
129. Chen, Shixuan, et al. "Emerging roles of electrospun nanofibers in cancer research." Advanced healthcare materials 7.6 (2018): 1701024
130. Balakrishnan, Preethi, et al. "Star poly (ε-caprolactone)-based electrospun fibers as biocompatible scaffold for doxorubicin with prolonged drug release activity." Colloids and Surfaces B: Biointerfaces 161 (2018): 488-496.
131. Norouzi, Mohammad. "Recent advances in brain tumor therapy: application of electrospun nanofibers." Drug discovery today23.4 (2018): 912-919.

132. Ramírez-Agudelo, Ricardo, et al. "Hybrid nanofibers based on poly-caprolactone/gelatin/hydroxyapatite nanoparticles-loaded Doxycycline: Effective anti-tumoral and antibacterial activity." Materials Science and Engineering: C 83 (2018): 25-34.
133. Song, Botao, Chengtie Wu, and Jiang Chang. "Dual drug release from electrospun poly (lactic-co-glycolic acid)/mesoporous silica nanoparticles composite mats with distinct release profiles." Acta biomaterialia 8.5 (2012): 1901-1907.
134. Xu, Jiqing, et al. "Controlled dual release of hydrophobic and hydrophilic drugs from electrospun poly (l-lactic acid) fiber mats loaded with chitosan microspheres." Materials letters 65.17-18 (2011): 2800-2803.
135. Song, Botao, Chengtie Wu, and Jiang Chang. "Dual drug release from electrospun poly (lactic-co-glycolic acid)/mesoporous silica nanoparticles composite mats with distinct release profiles." Acta biomaterialia 8.5 (2012): 1901-1907.
136. Eichhorn, Stephen J., and William W. Sampson. "Statistical geometry of pores and statistics of porous nanofibrous assemblies." Journal of the royal society Interface 2.4 (2005): 309-318.
137. Shin, M., et al. "Contractile cardiac grafts using a novel nanofibrous mesh." Biomaterials 25.17 (2004): 3717-3723.
138. Anseth KS, Bowman CN, Brannon-Peppas L. Biomaterials. 1996 Sep;17(17):1647-57.
139. Stammen, Jason A., et al. "Mechanical properties of a novel PVA hydrogel in shear and unconfined compression." Biomaterials22.8 (2001): 799-806.
140. Jeon, Oju, et al. "Mechanical properties and degradation behaviors of hyaluronic acid hydrogels cross-linked at various cross-linking densities." Carbohydrate polymers 70.3 (2007): 251-257.
141. Chou, Shih-Feng, Daniel Carson, and Kim A. Woodrow. "Current strategies for sustaining drug release from electrospun nanofibers." Journal of Controlled Release 220 (2015): 584-591.
142. Sill, Travis J., and Horst A. von Recum. "Electrospinning: applications in drug delivery and tissue engineering." Biomaterials 29.13 (2008): 1989-2006.
143. Gulsen, Derya, and Anuj Chauhan. "Dispersion of microemulsion drops in HEMA hydrogel: a potential ophthalmic drug delivery vehicle." International Journal of Pharmaceutics 292.1-2 (2005): 95-117.
144. Hoare, Todd R., and Daniel S. Kohane. "Hydrogels in drug delivery: Progress and challenges." Polymer 49.8 (2008): 1993-2007.
145. Burger, Christian, Benjamin S. Hsiao, and Benjamin Chu. "Nanofibrous materials and their applications." Annu. Rev. Mater. Res. 36 (2006): 333-368.
146. Xu, Shuxin, et al. "Composites of electrospun-fibers and hydrogels: A potential solution to current challenges in biological and biomedical field." Journal of Biomedical Materials Research Part B: Applied Biomaterials 104.3 (2016): 640-656.
147. Xu, Weijie, Junyu Ma, and Esmaiel Jabbari. "Material properties and osteogenic differentiation of marrow stromal cells on fiber-reinforced laminated hydrogel nanocomposites." Acta biomaterialia 6.6 (2010): 1992-2002.
148. Ekaputra, Andrew K., et al. "Combining electrospun scaffolds with electrosprayed hydrogels leads to three-dimensional cellularization of hybrid constructs." Biomacromolecules 9.8 (2008): 2097-2103.
149. Hong, Yi, et al. "Mechanical properties and in vivo behavior of a biodegradable synthetic polymer microfiber–extracellular matrix hydrogel biohybrid scaffold." Biomaterials 32.13 (2011): 3387-3394.

150. Ekaputra, Andrew K., et al. "The three-dimensional vascularization of growth factor-releasing hybrid scaffold of poly (ε-caprolactone)/collagen fibers and hyaluronic acid hydrogel." Biomaterials 32.32 (2011): 8108-8117.
151. Kim, Choo-Won, et al. "Structural studies of electrospun cellulose nanofibers." Polymer 47.14 (2006): 5097-5107.
152. Cui, Zhanwu, et al. "Poly (d-lactide)/poly (caprolactone) nanofiber-thermogelling chitosan gel composite scaffolds for osteochondral tissue regeneration in a rat model." Journal of Bioactive and Compatible Polymers 28.2 (2013): 115-125.
153. Han, Ning, et al. "Hydrogel–electrospun fiber composite materials for hydrophilic protein release." Journal of controlled release 158.1 (2012): 165-170.
154. Lee, Hyun Jong, Young Ha Park, and Won-Gun Koh. "Fabrication of nanofiber microarchitectures localized within hydrogel microparticles and their application to protein delivery and cell encapsulation." Advanced Functional Materials 23.5 (2013): 591-597.
155. Ma, Zuwei, M. Kotaki, and S. Ramakrishna. "Electrospun cellulose nanofiber as affinity membrane." Journal of membrane science 265.1-2 (2005): 115-123.
156. Kastritis, Panagiotis L., and Alexandre MJJ Bonvin. "On the binding affinity of macromolecular interactions: daring to ask why proteins interact." Journal of The Royal Society Interface 10.79 (2013): 20120835.
157. Ulbricht, Mathias. "Advanced functional polymer membranes." Polymer 47.7 (2006): 2217-2262..
158. Xiao, Li, et al. "Polymerization and functionalization of membrane pores for water related applications." Industrial & engineering chemistry research 54.16 (2015): 4174-4182.
159. Ma, Zuwei, Kotaki Masaya, and Seeram Ramakrishna. "Immobilization of Cibacron blue F3GA on electrospun polysulphone ultra-fine fiber surfaces towards developing an affinity membrane for albumin adsorption." Journal of membrane science 282.1-2 (2006): 237-244.
160. Poole, Colin. Handbook of methods and instrumentation in separation science. Vol. 1. Academic Press, 2009.
161. Sundberg, Lars, and Jerker Porath. "Preparation of adsorbents for biospecific affinity chromatography: I. Attachment of group-containing ligands to insoluble polymers by means of bifunctional oxiranes." Journal of Chromatography A 90.1 (1974): 87-98.
162. Ma, Zuwei, and Seeram Ramakrishna. "Electrospun regenerated cellulose nanofiber affinity membrane functionalized with protein A/G for IgG purification." Journal of Membrane Science 319.1-2 (2008): 23-28.
163. Schröder, K., et al. "Plasma-induced surface functionalization of polymeric biomaterials in ammonia plasma." Contributions to Plasma Physics 41.6 (2001): 562-572.
164. Ma, Zuwei, and Seeram Ramakrishna. "Electrospun regenerated cellulose nanofiber affinity membrane functionalized with protein A/G for IgG purification." Journal of Membrane Science 319.1-2 (2008): 23-28.
165. Miyauchi, M., et al. "Flexible electrospun cellulose fibers as an affinity packing material for the separation of bovine serum albumin." J. Chromatogr. Sep. Tech 2.2 (2011): 110.
166. Lendlein, Andreas, and Steffen Kelch. "Shape-memory polymers." Angewandte Chemie International Edition 41.12 (2002): 2034-2057.
167. Paderni, Katia, et al. "Shape-memory polymer networks from sol–gel cross-linked alkoxysilane-terminated poly (ε-caprolactone)." Journal of Materials Science 47.10 (2012): 4354-4362.

168. Shenoy, Suresh L., et al. "Role of chain entanglements on fiber formation during electrospinning of polymer solutions: good solvent, non-specific polymer–polymer interaction limit." Polymer46.10 (2005): 3372-3384.
169. McKee, Matthew G., et al. "Correlations of solution rheology with electrospun fiber formation of linear and branched polyesters." Macromolecules 37.5 (2004): 1760-1767.
170. Colby, Ralph H., et al. "Effects of concentration and thermodynamic interaction on the viscoelastic properties of polymer solutions." Macromolecules 24.13 (1991): 3873-3882.
171. Shenoy, Suresh L., W. Douglas Bates, and Gary Wnek. "Correlations between electrospinnability and physical gelation." Polymer 46.21 (2005): 8990-9004.
172. Pandini, S., et al. "One-way and two-way shape memory behaviour of semi-crystalline networks based on sol–gel cross-linked poly (ε-caprolactone)." Polymer 54.16 (2013): 4253-4265.
173. Inai, R., M. Kotaki, and S. Ramakrishna. "Deformation behavior of electrospun poly (L-lactide-co-ε-caprolactone) nonwoven membranes under uniaxial tensile loading." Journal of Polymer Science Part B: Polymer Physics 43.22 (2005): 3205-3212.
174. Wei, Xiaofan, et al. "Modelling of mechanical properties of electrospun nanofibre network." International Journal of Experimental and Computational Biomechanics 1.1 (2009): 45-57.
175. Zhang, Fenghua, et al. "Shape memory properties of electrospun Nafion nanofibers." Fibers and Polymers 15.3 (2014): 534-539.
176. Chen, Huiling, et al. "Electrospun shape memory film with reversible fibrous structure." Journal of Materials Chemistry22.42 (2012): 22387-22391.
177. Matsumoto, Hidetoshi, et al. "Shape-memory properties of electrospun non-woven fabrics prepared from degradable polyesterurethanes containing poly (ω-pentadecalactone) hard segments." European Polymer Journal 48.11 (2012): 1866-1874.
178. Gong, Tao, et al. "Remotely actuated shape memory effect of electrospun composite nanofibers." Acta biomaterialia 8.3 (2012): 1248-1259.
179. Matsumoto, Hidetoshi, et al. "Shape-memory properties of electrospun non-woven fabrics prepared from degradable polyesterurethanes containing poly (ω-pentadecalactone) hard segments." European Polymer Journal 48.11 (2012): 1866-1874.
180. Gong, Tao, et al. "Remotely actuated shape memory effect of electrospun composite nanofibers." Acta biomaterialia 8.3 (2012): 1248-1259.
181. Chen, Huiling, et al. "Electrospun shape memory film with reversible fibrous structure." Journal of Materials Chemistry22.42 (2012): 22387-22391.
182. Soccio, M., et al. "Neopenthyl glycol containing poly (propylene azelate) s: Synthesis and thermal properties." European polymer journal 43.8 (2007): 3301-3313
183. Soccio, M., et al. "Aliphatic poly (propylene dicarboxylate) s: Effect of chain length on thermal properties and crystallization kinetics." Polymer 48.11 (2007): 3125-3136.
184. Celli, Annamaria, and Mariastella Scandola. "Thermal properties and physical ageing of poly (L-lactic acid)." Polymer 33.13 (1992): 2699-2703.
185. Fabbri, Martina, et al. "New fully bio-based PLLA triblock copoly (ester urethane) s as potential candidates for soft tissue engineering." Polymer Degradation and Stability 132 (2016): 169-180.
186. Garlotta, Donald. "A literature review of poly (lactic acid)." Journal of Polymers and the Environment 9.2 (2001): 63-84.

187. Gualandi, Chiara, et al. "Ethanol disinfection affects physical properties and cell response of electrospun poly (l-lactic acid) scaffolds." European Polymer Journal 48.12 (2012): 2008-2018.
188. Bao, Min, et al. "Electrospun biomimetic fibrous scaffold from shape memory polymer of PDLLA-co-TMC for bone tissue engineering." ACS applied materials & interfaces 6.4 (2014): 2611-2621.
189. Deschamps, A. A., et al. "In vivo and in vitro degradation of poly (ether ester) block copolymers based on poly (ethylene glycol) and poly (butylene terephthalate)." Biomaterials 25.2 (2004): 247-258.
190. Deschamps, Audrey A., Dirk W. Grijpma, and Jan Feijen. "Poly (ethylene oxide)/poly (butylene terephthalate) segmented block copolymers: the effect of copolymer composition on physical properties and degradation behavior." Polymer 42.23 (2001): 9335-9345.
191. De Jong, Wim H., and Paul JA Borm. "Drug delivery and nanoparticles: applications and hazards." International journal of nanomedicine 3.2 (2008): 133-149.
192. Jaque, D., et al. "Nanoparticles for photothermal therapies." nanoscale 6.16 (2014): 9494-9530.
193. Bonacchi, Sara, et al. "Luminescent silica nanoparticles: extending the frontiers of brightness." Angewandte Chemie International Edition 50.18 (2011): 4056-4066.
194. Dolci, Luisa Stella, et al. "Carboxyl Surface Functionalization of Poly (l-lactic acid) Electrospun Nanofibers through Atmospheric Non-Thermal Plasma Affects Fibroblast Morphology." Plasma Processes and Polymers 11.3 (2014): 203-213.
195. Tsuji, Hideto, and Kazumasa Nakahara. "Poly (L-lactide). IX. Hydrolysis in acid media." Journal of Applied Polymer Science 86.1 (2002): 186-194.